QATAR UNIVERSITY

COLLEGE OF ENGINEERING

POLYMER NANOCOMPOSITE BASED HUMIDITY SENSORS

BY

SHOAIB ALAM MALLICK

A Dissertation Submitted to

the College of Engineering

in Partial Fulfillment of the Requirements for the Degree of

Doctor of Philosophy in Electrical Engineering

January   2021

COMMITTEE PAGE

The members of the Committee approve the Dissertation of

Shoaib Alam Mallick defended on 12/06/2020.

_____

Prof. Farid Touati

Thesis/Dissertation Supervisor

_____

Dr. Zubair Ahmad

Thesis/Dissertation Co-Supervisor

_____

Prof. Imaddin Al-Omari

Committee Member

_____

Prof. Aboubakr Mostafa Abdullah

Committee Member

_____

Dr. Dong Suk ("Shane") Han

Committee Member

Approved:

_____

Khalid Kamal Naji, Dean, College of Engineering

ABSTRACT

MALLICK,SHOAIB,ALAM, Doctorate : January : 2021,

Doctorate of Philosophy in Electrical Engineering

Title: Polymer nanocomposite based humidity sensor

Supervisor of Dissertation: Farid, Touati.

Co-Supervisor of Dissertation: Zubair, Ahmad.

Controlling and monitoring humidity levels are paramount in industrial and manufacturing processes such as food packaging, electronic and optical device fabrications, quality control in textile industry, and oil & gas industry. It is essential to measure the moisture content to control or remove the unwanted moisture subsequently. Therefore, accurate and reliable monitoring of the water content and its composition is very important. Different types of humidity sensing techniques have been used for humidity sensing applications which include chilled mirror hygrometer, capacitive, resistive and Quartz microbalance (QCM). Capacitive and resistive type sensors are easy to make and can be fabricated using low-cost materials. The operating principles of capacitive humidity sensors are based on the change in dielectric constant of the sensing film with a change in a humidity level. Similarly, in resistive type humidity sensors the conductivity of the sensing film changes with alteration in humidity levels. Despite their significant characteristics, polymer-based capacitive and resistive humidity sensors have critical limitations, including low sensitivity, nonlinear response at higher humidity levels, high hysteresis loss and the known polymeric sensing film deformation with time. Therefore, the electrical response of polymer-based humidity

sensors is not stable. This increases the need for developing a humidity sensor that shows higher thermal stability, linear response at higher humidity levels, shorter response and recovery time, and low hysteresis loss.

In this dissertation, polymer-based humidity sensors are investigated for humidity sensing applications. We develop both capacitive and impedance-based humidity sensors and investigate different polymeric nanocomposites films to improve sensors' characteristics. We investigated the incorporation of hydrophilic and piezoelectric nanoparticles within the polymer matrix to improve the morphology and sensing characteristics such as linearity, response and recovery time and hysteresis loss. Results show that the optimised capacitive sensor shows 2.5% maximum hysteresis loss and response and recovery achieved is 40 sec and 25 sec. Also, we used the polymer blending technique to improve the resistive humidity sensor's sensitivity. The impedance response of the sensing film showed that as the concentration of SPEEK increases the sensitivity of the sensing film increases at lower humidity levels (10 %RH to 90 %RH). In addition, we have investigated the effect of conducting polymer and inorganic nanoparticle hybridization for impedance humidity sensing applications. Result shows that sensor hysteresis is around 4.5% with response and recovery time optimized to 30 sec and 35 sec, respectively. Moreover, we prepared the graphene quantum dots through graphite waste and evaluated potential applications for resistive humidity measurement. we achieved maximum hysteresis is around 2.2% at 30 %RH.

The above results are deemed having valuable scientific merit in the area of humidity sensing and related areas, and hence expected to impact the sensing industry at large.

DEDICATION

To my family, who supported me throughout the duration of my studies.

ACKNOWLEDGMENTS

encouragement. They help me and supported me every time.

LIST OF TABLES

LIST OF FIGURES

TABLE OF CONTENT

CHAPTER 1: INTRODUCTION

Humidity plays a critical role in industrial processing and monitoring of environmental conditions. For fabricating highly sophisticated integrated microelectronics circuits in the semiconductor industry and wafer processing, humidity or moisture levels are considered essential factors and are monitored continuously [1, 2]. Textile based humidity sensors developed to control the humidity level for the development of products [3]. In electronic and optical device fabrication, monitoring of humidity levels is essential [4, 5]. Moisture is an unwanted contaminant that exists in industrial gases and the atmosphere. It can penetrate virtually any surface, including such metals as copper, bronze, and carbon steel, which cause low product quality, cause corrosion in the gas pipeline, and lead to ice formation at low temperatures. Corrosion is one of the gas industry's major problems since it requires considerable resources for pipeline inspection, repairing, and replacement [6]. Therefore, it is essential to measure the moisture content to control or remove the unwanted moisture subsequently. Therefore, accurate and reliable monitoring of the water content and its composition is very important. Technologies that are commonly used in industry to measure moisture content are capacitive humidity sensor [7] and impedance humidity sensor [8], Quartz crystal microbalance (QCM) sensor [9], fiber optic hygrometer [10], and chilled mirror hygrometer [11].

1.1.   Chilled mirror hygrometers:

The humidity sensing in natural gas flow through the chilled mirror method includes estimating the gas's dew or frost point. Today, the most chilled mirror hygrometers have

constant condensation, which immediately reads the dew and frost point, as seen in Figure 1-1. The reading is predicated on a control system with an electro-optic control. The mirror is lit by a collimated light source (high intensity LED light), and a photodetector emits a photocurrent. When water condenses or precipitates on the mirror surface during the cooling process, most of the incident light is spread, decreasing the amount of light the photodetectors produce. The literature indicates the deposition of particulate or reactive pollutants on the mirror surface, disrupting the dew or frost layer optical detection as the primary cause of chilled mirror malfunction. The deposition of pollutants eliminated by circulating the mirror temperature at some sufficient frequency at elevated temperatures. Aggregation of contaminants avoided by adjusting the mirror temperature to high temperatures at an acceptable level.
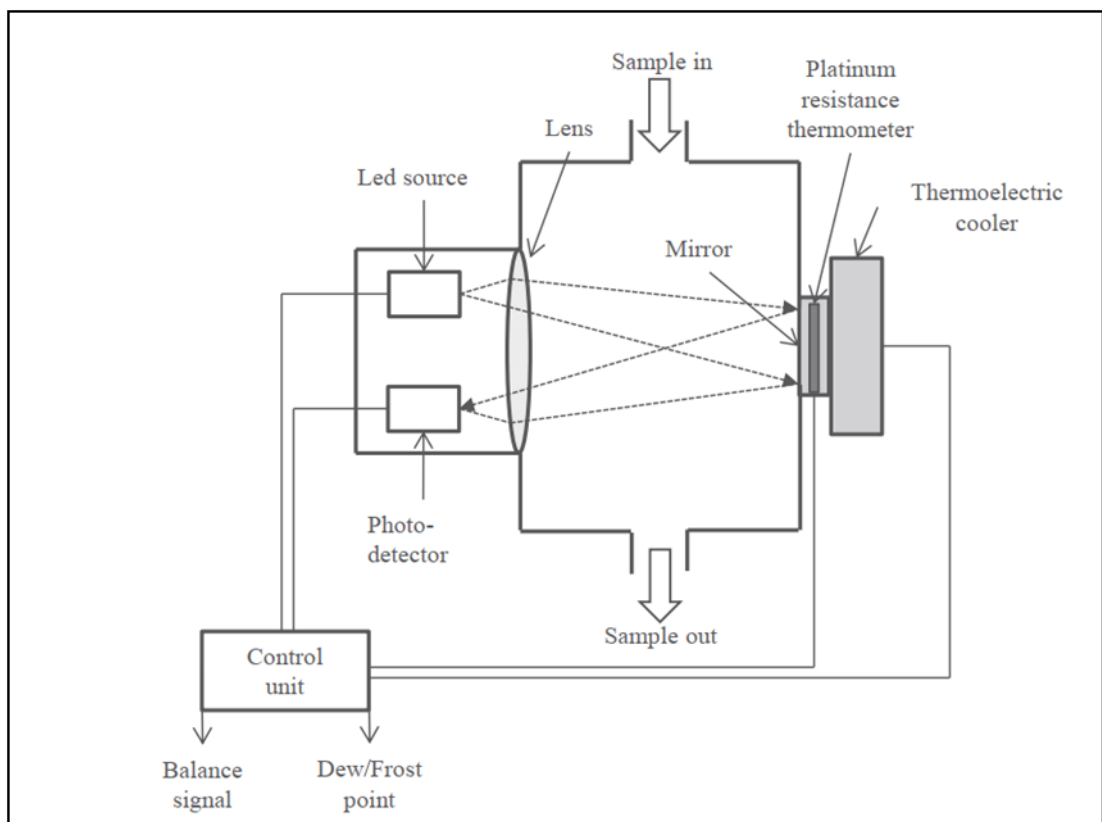
Figure 1-1. Schematic diagram of Chilled mirror hygrometer [12].

1.2. QCM based humidity Sensor:

Piezoelectric humidity sensors typically called oscillating quartz crystal microbalances (QCM sensors) frequently used in analytical chemistry. Many researchers examined the QCM sensor for humidity sensing applications. QCM sensors are bulk acoustic-wave resonators with extensive measuring range, low-cost, compact, robust, and highly sensitive to mass detection changes with low detection limits, making them an ideal choice for humidity sensing applications.

1.2.1. Working Principle:

The change in mass (Δm) on the QCM surface is related to resonance frequency shift (Δf) provided by the Sauerbrey equation (1).

$$\Delta f = - c_m \Delta m \qquad (1)$$

Whereas Δf is the shift in the crystal resonance frequency response to change in mass Δm per unit surface area and the constant c_m is a property of the crystal used:

The QCM sensor is subjected to wet and dry humid air at set continuous cycle intervals. Water molecules form on the surface of the QCM sensor. Water mass reduces the resonance frequency of the QCM sensor. The variation between wet and dry frequency is directly proportional to humidity. This constant switching between wet and dry moisture often ensures the sensor never reaches a complete moisture equilibrium. Therefore, the QCM sensor is known to be a fast-responding sensor. Depending on the level of contaminants, the sensor must also be substituted with a certain frequency. (e.g., seasonal or biannual). Figure 1-2 shows the schematic diagram of the QCM based sensor with the hygroscopic film deposited on the QCM surface. QCMs based moisture sensors have been extensively investigated by depositing them with water-absorbing

materials, such as polymers [13, 14], nanotubes [15, 16], nanocomposites [14, 17], graphene oxide [18, 19], and graphene quantum dots [20]. However, adequate quality assurance and regular maintenance procedures will be mandatory for QCM based humidity sensors.
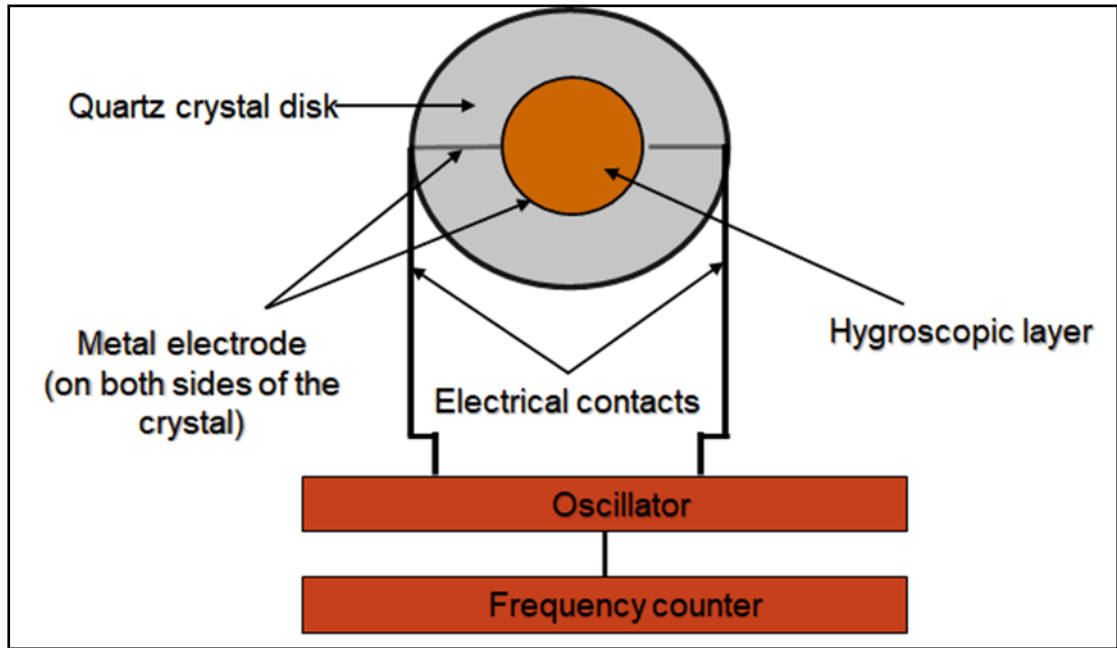
Figure 1-2. Schematic diagram of the QCM sensor.

1.3.   Fiber-optic humidity sensor:

The advancement in fiber optic technology has centered on extensive research on fiber optics moisture sensing methods. Small dimensions, immunity to electromagnetic interference, multiplexing, and remote sensing are appealing to fiber optic hygrometers. There are various sensing types, including active, evanescent, spectroscopic, and interferometric. Interferometric methods have been used for applications of natural gas for many years.

1.3.1. Working principle:

The development of optical fiber technology has led to extensive research on fiber-dependent moisture sensing techniques. Humidity-induced changes in the refractive index are usually ultra-small, leading to significant difficulties in directly measuring relative humidity (RH). Many kinds of materials combined with various fiber structures have been investigated and exploited to enhance the sensitivity to RH. Figure 1-3 shows the schematic diagram of the Fiber optic hygrometer used in the natural gas flow environment. This hygrometer consists of an optical filter based on the Fabry-Pérot interference process and a fiber optic sensor for signal transmission through fiber optic cables. The sensor is a film with thin dielectric layers as high and low refractive indexes alternately. The sensor produces an array of micropores. Increasing the water vapor pressure increases the volume of water molecules in the porous layer of the sensor. Adsorbed water molecules may shift the refraction indexes of various layers to migrate to broader wavelengths.
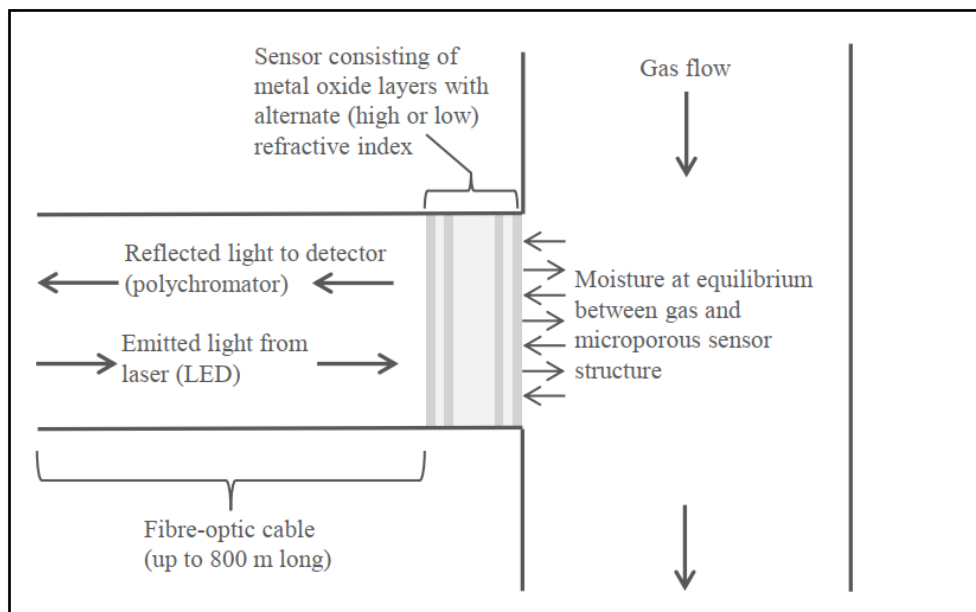
Figure 1-3. Schematic diagram of Fiber optic humidity sensor [12].

These technologies, which are used to sense moistures in different industries, have

specific limitations such as high labor cost, higher recalibration cost, external power unit, and regular maintenance. Therefore, we need to investigate the humidity sensors which are easy to fabricate, cost-effective, easy to deploy in industrial units, require no maintenance cost, and highly sensitive to humidity levels.

1.4. Capacitive Humidity sensor:

Capacitive humidity sensors are commonly used for humidity monitoring in the industrial process. They are easy to fabricate, flexible, and cost-effective. Capacitive humidity sensors respond to increased humidity, fast responsivity, and easy to operate at a wider humidity range. They are commonly used in industrial, commercial, and laboratory applications. Typically, capacitive humidity sensors are composed of two interdigitated electrodes (IDE) covered by a dielectric layer sensitive to humidity changes. The capacitive humidity sensors operating principle focused on the increase in the thin film's dielectric constant due to the accumulation of water molecules on the sensing film's surface. Different materials are used as moisture-sensitive dielectric layers; the most widely used ones are polymers, ceramics, and porous silicon. A capacitor is mainly a component in an electrical circuit that stores as an accumulation of electrical charge. The capacitive sensor comprises a pair of interdigitated electrodes on a substrate, deposited with humidity sensing thin film. The sensing mechanism of capacitive humidity sensors is based on the change in the sensing film's dielectric constant due to a water molecule's adsorption on the sensing film's surface. The difference in capacitance with respect to change in humidity level primarily depends on the hygroscopic nature of the sensing film and interdigitated electrode dimensions. Figure 1-4 shows the capacitive humidity sensor probed installed in the pipeline at the cooling circulation unit.
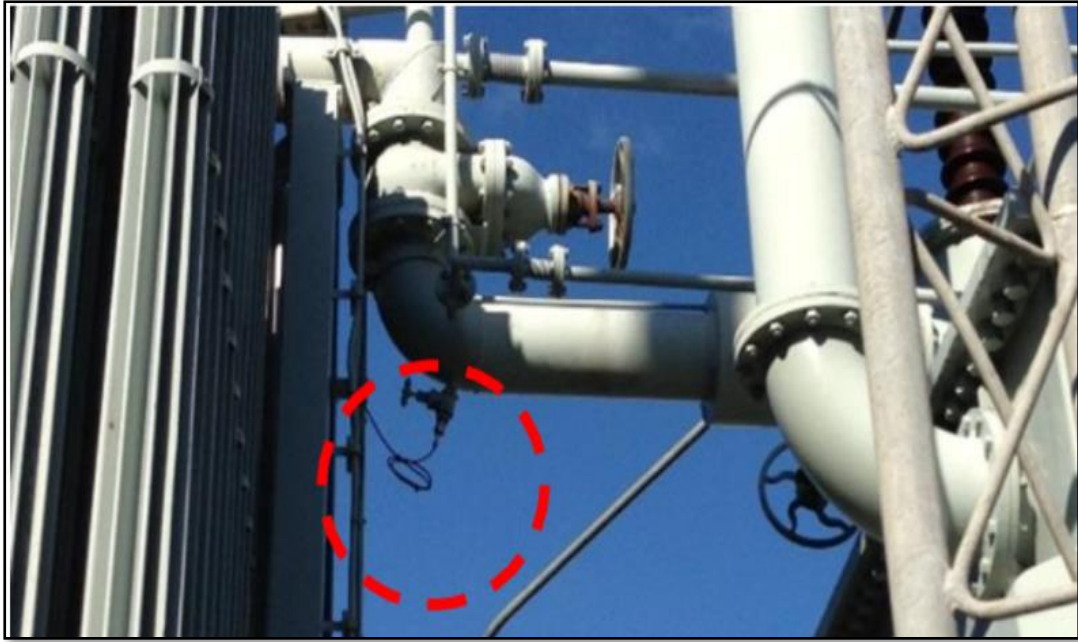
Figure 1-4. Humidity Sensor probed install in Oil cooling circulation [21].

1.4.1. *Working principle:*

Sensing materials are the most crucial component of capacitive humidity sensors. Typically, the capacitive polymeric humidity sensor configuration is designed to optimally utilize the sensing material's hygroscopic properties that usually more easily absorb water molecules. In the capacitance of two parallel plates structure, the Electrode area, electrode separation, and dielectric properties of sensing materials are the main elements that directly affect the development of the capacitive humidity sensor, as shown in equation 2.

$$C = \varepsilon_o \varepsilon_r \frac{A}{d} \qquad (2)$$

ε_o = dielectric constant

ε_r = relative dielectric constant

A= Area between electrodes

d= thickness of polymeric material

7

1.4.2. Sensing mechanism:

At low relative humidity level, the water molecules are firstly chemisorbed on dielectric sensing film. As the RH increases, water molecules' physisorption will occur on the chemisorbed layer [22]. When the film is exposed to a higher humidity level, multilayers of H_2O molecules are produced on the surface of sensing films during the physisorption process, with a steady increase in humidity levels and capacitance humidity sensor to increase exponentially. This physiosorbed multilayer shows bulk liquid-like behavior since many layers of water condense, and protons may have much more freedom to travel within the condensed water through the Grotthuss mechanism. The moisture sensing mechanism on the surface of the polymeric film is shown in Figure 1-5.
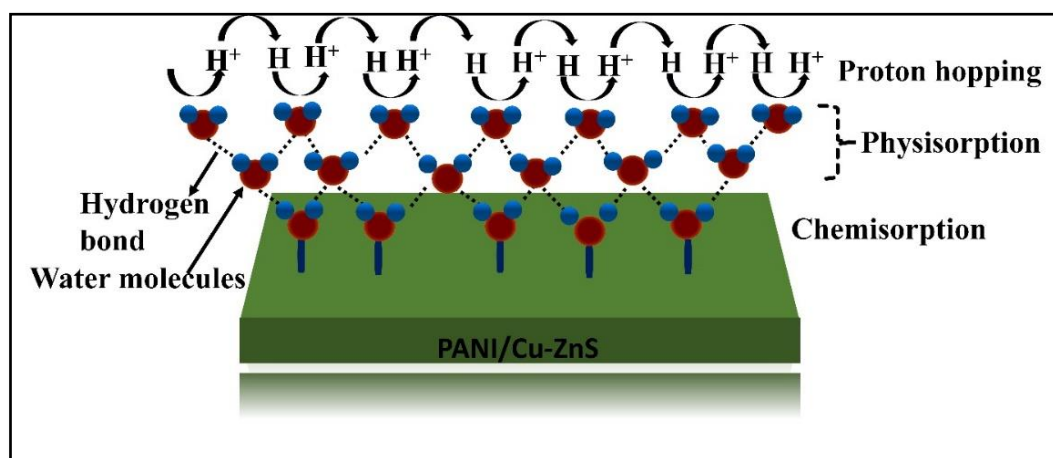
Figure 1-5. Schematic diagram of Humidity sensing mechanism on the surface of the film [23].

1.4.3. Sensor Design:

The capacitive humidity-sensor can be fabricated in two different configurations, including the parallel plate structure and planar structure. In a parallel plate structure, the dielectric layer is sandwiched between the top and bottom electrodes. In the planar

configuration, we have an interdigitated design. The parallel plate structure-based sensor shows better stability and reliability as the active layer is protected from contamination. The planar design, however, has the benefits of ease of processing and greater sensitivity at lower levels of humidity. The parallel plate structure is more complicated than the planar configuration. The capacitive humidity sensor with a parallel plate structure and interdigitated electrode are shown in Figure 1-6.
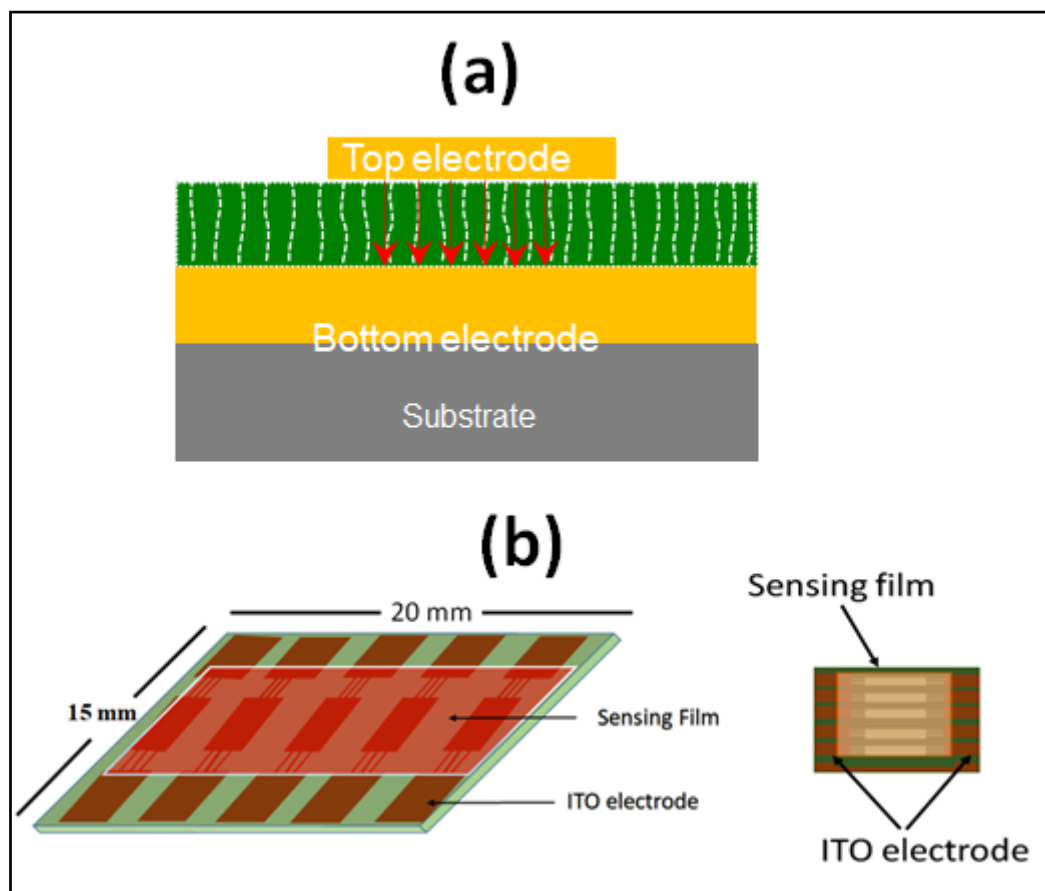
Figure 1-6. Schematic diagram of sensor design structure (a) Parallel plate structure, (b) Interdigitated electrode.

1.5.   Resistive humidity sensor:

The resistive humidity sensor detects water vapors that directly influence the electrical conductivity of the sensing film. Since moisture significantly changes the device's

electrical resistance or impedance, this concept was used to build resistive humidity sensors. Impedance varies when the water vapors strongly concentrate the surface of the sensing film at high humidity. The consequence is that the ionic hydroxyl groups of the water molecules dissociated. Both capacitive and resistive type sensors are easy to fabricate, and the characterization of these sensors can be done quickly. Figure 1-7 shows a resistive humidity sensor's schematic diagram using an interdigitated electrode comb structure with the sensitive film deposited on the top of the interdigitated electrode
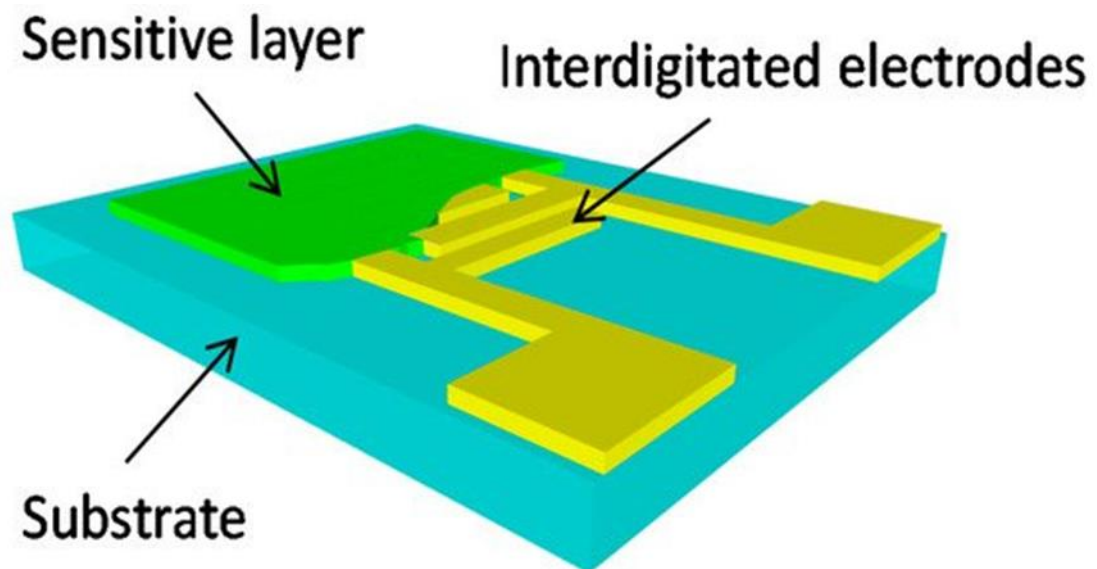
Figure 1-7. Schematic diagram of Resistive humidity sensor using an interdigitated electrode design structure [13].

1.6.   Motivation and Background:

Controlling humidity levels are highly significant in several industrial and manufacturing processes. An ideal humidity sensor can be selected based on some parameters such as the sensor's sensitivity, linear response of the sensor at a wider humidity range, shorter response and recovery time, good reproducibility, smaller

lesser hysteresis, chemical and thermally stable and ability to withstand contaminants. Many researchers focus on improving these parameters, which mainly depend on the active sensing material properties and sensing materials surface modification. Polymer-based nanocomposites and nanostructured have gained much attraction in moisture sensor applications due to its low cost, easy to fabricate, and flexibility. The motivation of this research work is to improve the surface morphology of the polymeric sensing film by embedding different nanoparticles within the polymeric matrix and develop a humidity sensor that shows the linear response with respect to change in humidity levels, high sensitivity, fast response, and recovery time and offers a stable and repeatable response.

1.7. Research Problem:

Despite the significant characteristics of organic polymer, the polymer-based capacitive and impedance humidity sensors have some significant limitations, including low sensitivity, higher response time, the nonlinear response of sensors at higher humidity levels, and high hysteresis loss. After a specific time, the polymeric film deforms, and the electrical response of the humidity sensors are not stable due to this deformation in sensing film. We need to develop a humidity sensor that shows higher thermal stability, linear response at higher humidity level, shorter response and recovery time, and low hysteresis loss. We will develop both capacitive and impedance-based humidity sensors and investigate different polymeric nanocomposites films to improve humidity sensors' characteristics.

1.8. Research Objectives:

This research focuses on designing a polymeric moisture sensor that can operate at a wider humidity level range, higher sensitivity, low hysteresis loss, and shorter response

and recovery time. Different methods employed, including copolymerization, the addition of nanoparticles within the polymer matrix, and blending techniques to improve the humidity sensor's characteristics. We investigate the sensing properties of thin-film polymer nanocomposites and their application in moisture sensing applications. Our first objective is to study the incorporation of different nanoparticles within the polymer matrix to improve the morphology and humidity sensing characteristic of capacitive humidity sensors. These nanoparticles include hydrophilic nanoparticles and piezoelectric nanoparticles, and metallic nanoparticles. The second objective is to study the resistive polymeric humidity sensor. For this purpose, we will use the blending techniques to blend polymers to improve the resistive humidity sensor's sensitivity. We will also investigate the effect of conducting polymer and inorganic nanoparticle hybridization for humidity sensing applications. In the last chapter, we will prepare the Graphene Quantum dots through Graphite waste and evaluate potential applications for resistive humidity sensors.

1.9. Main Contribution:

This research work has the following specific contribution to the body of knowledge:

- ➢ Embedded the hydrophilic TiO_2 nanoparticles within the biodegradable polymer and fabricated the humidity sensor and improved its sensitivity.
- ➢ Incorporate the hydrophilic nanoparticles (TiO_2) within the hydrophobic polymer (PVDF) to achieve a linear response at a wider humidity range.
- ➢ Studied the Piezoelectric nanoparticles ($BaTiO_3$) incorporation within PVDF polymer and studied the hysteresis response of humidity sensor while applying different concentrations of $BaTiO_3$.
- ➢ Blend PVDF with different concentrations of sulfonated polyether ether ketone (SPEEK) to develop resistive humidity sensors that can operate at lower

humidity levels.

➢ Prepare Halloysite-polypyrrole-silver nanocomposite (HNT-PPY-Ag) using the in-situ photopolymerization technique to develop the resistive humidity sensor.

➢ Demonstrate a cost-effective and facile way to prepare highly photoluminescent graphene quantum dots (GQDs) from Graphite waste. The resulting GQDs were evaluated for the potential application for resistive humidity sensors.

1.10. Thesis organization:

The dissertation has been organized into the following chapters:

➢ Chapter 1 Covers different Humidity techniques used in the Natural gas Industry. Give a brief description of the sensing mechanism of the Capacitive and impedance humidity sensor. The chapter also illustrates the research problem, outlines the research objectives, and presents the contribution of this dissertation.

➢ Chapter 2 Covers a literature review on sensing materials used in capacitive and impedance humidity sensors. Also discussed the various method to improve the sensitivity of the humidity sensors.

➢ Chapter 3 Covers the materials and characterization techniques used in this research work.

➢ Chapter 4 presents the biodegradable polymer nanocomposite-based humidity sensor.

➢ Chapter 5 Study the effect of nanoparticles on morphology and humidity sensing characteristics of the piezoelectric polymer.

➢ Chapter 6 Investigate the effect of $BaTiO_3$ nanoparticles on PVDF based humidity sensor and improve the hysteresis loss.

➢ Chapter 7 Study the blending of PVDF and SPEEK with different

concentrations of SPEEK applied to improve the humidity sensor's sensitivity at a lower humidity level.

➢ Chapter 8 Covers the In-situ photopolymerization process used to prepare Halloysite-polypyrrole-silver nanocomposite (HNT-PPY-Ag) for moisture sensing applications.

➢ Chapter 9 In this chapter, we aim to prepare graphene quantum dots (GQDs) from graphitic waste and study morphology and electrical response of Graphene Quantum Dots based impedance humidity sensor.

➢ Chapter 10 Summarized the research work presented in this thesis and provide the future aspect of this research work.

CHAPTER 2: LITERATURE REVIEW

In this section, we will study different sensing materials used for capacitive and resistive humidity sensor applications. We will also explore various techniques to improve the hydrophobicity and hydrophilicity of the polymer. We also explain different fabrication techniques used in the deposition of polymeric films.

2.1.   Materials for Humidity Sensing

Numerous materials have been studied as sensing materials for humidity sensing applications, including polymers, ceramics, piezoelectric materials, hydrophobic polymer, hydrophilic polymer, polymer composites, and Graphene Quantum dots.

2.2.   Ceramic:

Humidity sensors based on ceramic materials are widely used in humidity sensing applications due to their low cost, excellent thermal stability, high mechanical strength, and fast responsivity [24, 25]. Ceramic based humidity sensors have gained importance among other forms of humidity sensors are mainly attributed to the properties of its sensing component, i.e., its mechanical properties, thermal stability, tolerance to chemical attacks [2]. These properties make Ceramic a promising material used to develop humidity sensors. The excellent configuration of ceramic materials consisting of grain surfaces, grain boundaries, and strictly regulated porous microstructures allows them suitable for moisture sensors [26, 27]. Excellent water absorption and desorption properties of metal oxide ceramics such as Al_2O_3 [28], TiO_2 [29], ZnO [30] have been widely utilized in humidity sensing applications. Due to water molecule chemisorption properties over a wide humidity range, most ceramic-based humidity sensors have reduced sensitivity, lack of reproducibility, and response stability.

2.2.1. *Sensing mechanism:*

The sensing mechanism of ceramic humidity sensors based on ionic conduction of electronic conduction. In ionic conduction, as the relative humidity level increases, the conductivity of the sensing film decreases. As water molecules increase in the sensing film, the proton conduction is the leading carrier for the electrical conductivity. In the electronic conduction, the sensing film's conductivity changes linearly with respect to the change in water vapor concentration. Water molecules serve as an electron-donator, and, based on whether the substrate is an n or p-type semiconductor, their chemisorption increases or decreases electronic conductivity. However, aging process, and higher hysteresis loss have constrained their effectiveness as monitoring sensors that require long-term operation and higher precision.

2.3.   Polymers:

Polymeric humidity sensors have been extensively studied in research and implemented to industry for more than 20 years. The key advantages of polymers that have garnered this attraction are their lightweight, easy preparation, and low cost of both materials and fabrication process. Polymeric sensing film, when exposed to change in humidity level, the electrical conductance of the sensing film also varies. Polymer sensing film can be used for resistive and capacitive humidity sensors. Several kinds of polymer-based sensing materials have been considered for humidity sensing applications[31-34]. In a polymer-based moisture sensor, the hygroscopic polymer can accumulate water vapor from a sensor's surrounding environment. Consequently, with the change in the amount of water absorbed, the polymer changes' dielectric permittivity changes linearly. The organic polymers used as the capacitive humidity sensor sensing layer must be partially hygroscopic and hydrophobic. Sensing film absorbs water molecules fast and is stable for a longer period. Fratoddi et al. [35] studied different polymer-based nanostructured

humidity sensors. They developed other theoretical models based on dielectric permittivity and electrical conductivity parameters and showed that nanostructured polymer materials could be used to measure relative humidity (RH) level. Choi et al. [36] studied the PEDOT: PSS-PVA composite thin films based humidity sensors, which are deposited on a piezoelectric substrate (LiNbO$_3$). The sensor's response in terms of change in impedance and capacitance was observed with respect to changes in relative humidity level from 0 %RH to 80 %RH range. They observed that adding more PEDOT: PSS to a fixed amount of PVA decreases a sensor's sensitivity at the lower RH region.

2.3.1. Sensing mechanism:

Figure 2-1 depicts the adsorption of water molecules on the polymeric sensing film. Two simultaneous processes during the humidity sensing method, i.e., chemisorption and physisorption, explain water molecule adsorption on the sensor surface [37]. The sensing film is primarily exposed to water molecules, and after that, the water molecules are adsorbed on the sensing film's surface. At low humidity levels, water molecules are first chemisorbed on sensing film. When the relative humidity level increases, water molecules' physisorption happens on the chemisorbed surface [22]. This physisorbed multilayer exhibits bulk liquid behavior, H$_3$O+ can be easily dissociated into H$_2$O and H+ ions. This proton (H+) ions can move freely on the sensing film surface, enhancing the sensing film's ionic conductivity, which increases the sensing film's sensitivity at higher RH levels. This proton conductivity mechanism at the sensing film's surface can be described by the Grotthuss mechanism [38].
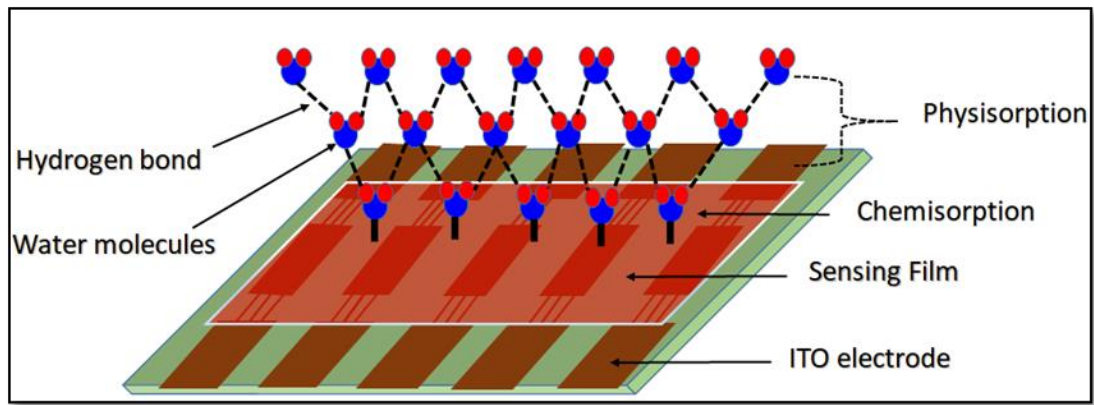
Figure 2-1. Schematic diagram of the humidity sensing mechanism for resistive sensing film.

Table 2-1. Shows the Polymer based Humidity sensors.

Materials	Sensor Type	Range (%RH)	Response time (s)	Recovery time(s)	Hysteresis	Year	Ref
Polyelectrolytes	Resistive	20-95	90	90	1.2%	2005	[39]
Co-Polyaniline	NA	20-95	8	1 min	8	2008	[40]
Polyimide	Capacitive	10-90	33	NA	2.05%	2010	[41]
PANI	Resistive	20-90	8	6	~1 %	2012	[42]
SPEEK	Resistive	11-97	100	105	<3%	2017	[43]

2.4. Conducting polymers:

Conducting polymers were investigated as sensing materials by various researchers. Conducting polymers such as polyaniline, polypyrrole, and polythiophene exhibits unique electrical, electrochemical, and optical properties [44-46]. The origin of sensing is a difference in the electrical resistance of conducting polymers when subjected to change in humidity level, UV irradiation, and changes in temperature. In a humid environment, the interaction between the conducting polymer and water molecules has been shown to result in a change in the sensing film's resistance. In the humid environment, the interaction between the conductive polymer and the water molecules has been shown to result in a difference (increase or decrease) in resistance. In polymer-

based resistive sensors difficult to detect low humidity levels owing to certain problems with high impedance measurements. As electronically conductive polymers were applied to the polymer matrix, the impedance of the sensor was reduced to readily detectable values. However, due to their weak mechanical properties and solubility in traditional organic solvents, they suffer from reduced processability. Various composites, mixtures, and copolymers of conjugated conductive polymers with other functional polymers and inorganic additives have been used to enhance conductive polymers' properties. The incorporation of metal nanoparticles in the conducting polymer has become a very effective way to obtain nanocomposites with improved physical and chemical properties [47]. L. Kabir et al. [48] investigate the properties of conducting PPY-Ag nanocomposite nanowires for humidity sensing. They adapted the metal-polymer interface and observed that corresponding interlayer water molecules play an essential role in establishing the electrical flow and hence the sensitivity of the nanocomposite's humidity sensor.

2.5. Hydrophobic Polymer-Based:

Several capacitive polymeric humidity sensors have been developed utilizing hydrophobic polymer. Such polymers are therefore meant to be nonionic while being highly polar macromolecules. Although they are more costly than resistive humidity sensors, capacitive polymeric humidity sensors typically exhibit impressive linearity and stability even at higher humidity levels [49, 50]. In the case of hydrophobic polymers, the absorbed water usually remains between the voids permeating the polymeric film molecules. The linear change can be seen in the dielectric properties of the polymeric film in response to the number of water molecules absorbed on the polymeric film. Also, it is observed that the hysteresis loss correlated with hydrophobic capacitive sensors. The formation of absorbed water clusters within the bulk Polymer

19

can be attributed to an increase in hysteresis. These undesirable hydroclusters will contribute to the structural degradation of sensing films; hence, the humidity sensors' lifespan further reduced. The different technique has been introduced to reduce the hysteresis loss within hydrophobic humidity sensor, which includes crosslinking of polymer, copolymerization, and formation of organic/inorganic hybrid structure. The crosslinking method was introduced mainly to reduce the hygroscopic characteristics of the sensor while improving its thermal stability and reducing hysteresis loss. The additions of hygroscopic crosslinking agents have also been shown to increase the sensitivity of the polymeric film. To date, Polyimides [51], Polyvinyl crotonate (PVC) [52], Polysulfone [53], and PETT [54] are the most commonly used the hydrophobic polymer used for humidity sensing application. Polymide base humidity sensor has a linear response, apart from having a decent sensitivity even at a lower humidity level [55, 56]. Lee et al. [57] modified the polyimide sensing film surface by chemical etching, which developed the nano-grass morphology over the polyimide film's surface, which enhancing the surface area of the sensing film, hence improving the humidity sensor's sensitivity and response time.

2.6.   Hydrophilic Polymer:

Hydrophilic polymers appear to be absorbed water vapors, and some hydrophilic polymers may be soluble in water. Hydrophilic polymers have higher water permeability due to ionic groups such as acid or in the form of a salt such as sulfonate ammonium and carboxylate, which enable them to dissolve water molecules [58].

2.6.1.   Classification of Hydrophilic Polymers:

The hydrophilic Polymers are classified into three categories 1) natural hydrophilic Polymer, 2) semi-natural hydrophilic polymer 3) synthetic hydrophilic polymer. The

natural hydrophilic Polymer is divided into two groups a) plant origin and b) animal origin. Plant origin hydrophilic polymers are starch, inulin, and dextrane. Hydrophilic Polymer of animal origin is serum albumen and chitosan. Natural hydrophilic polymers' properties are not reproducible for many applications—the semisynthetic hydrophilic Polymer obtained by chemical modification of natural Polymer. Natural hydrophilic polymers have not always been ideal because they did not always replicate their properties in many applications. Therefore, the development of polymeric materials for many applications has a great deal of interest. The synthetic hydrophilic Polymer has a variety of medicinal, biotechnological, and chemical applications. One of the severe deficiencies of hydrophilic polymers is that they are soluble in water. The polymeric film made of hydrophilic materials is soluble in water and cannot be used in high humidity regions or attract dew. In the case of hydrophilic Polymer-based humidity sensors, many improved methods have been used to design and manufacture water-resistant components to reduce water solubility and prevent water deformation through dissolution. Some of these approaches include the application of hydrophobic groups using Copolymerization [59], grafting of copolymer [60], crosslinking [61], interpenetrating network structures [62], and preparation of organic /inorganic nanocomposites [63].

2.7.   Copolymerization:

Copolymerization is the process of combining two monomers. Copolymerization permits the synthesis of an almost unlimited range of polymers and is often used, therefore, to obtain a better balance of properties for the commercial application of polymeric materials. Copolymerization enables the development of a potentially unlimited array of polymers that are often used to achieve a greater combination of properties for polymeric materials' industrial use. It allows a far broader

spectrum of configurations than may be done when a homopolymer is mixed. A variety of hydrophilic and hydrophobic copolymers were developed and used as sensing materials to improve the humidity characteristics and stability of polymer-based humidity sensors in a too humid environment [64]. Su et al. [65] studied the in situ copolymerizations of methyl methacrylate (MMA) and [3-(methacrylamino)propyl] trimethyl ammonium chloride (MAPTAC) copolymer. They observed that the copolymerized humidity sensor shows higher sensitivity, fast response time, small hysteresis loss, and longer stability as compared to the pure MMA based humidity sensor. Geng, Wangchang, et al. [66] synthesized PDEAEMA-b-PS block copolymer via the reversible polymerization chain transfer (RAFT) process. They showed that PDEAEMAb-PS copolymer exhibited higher sensitivity than pure PDEAEMA and pure PS. Figure 2-2 shows the schematic diagram of copolymerization method.
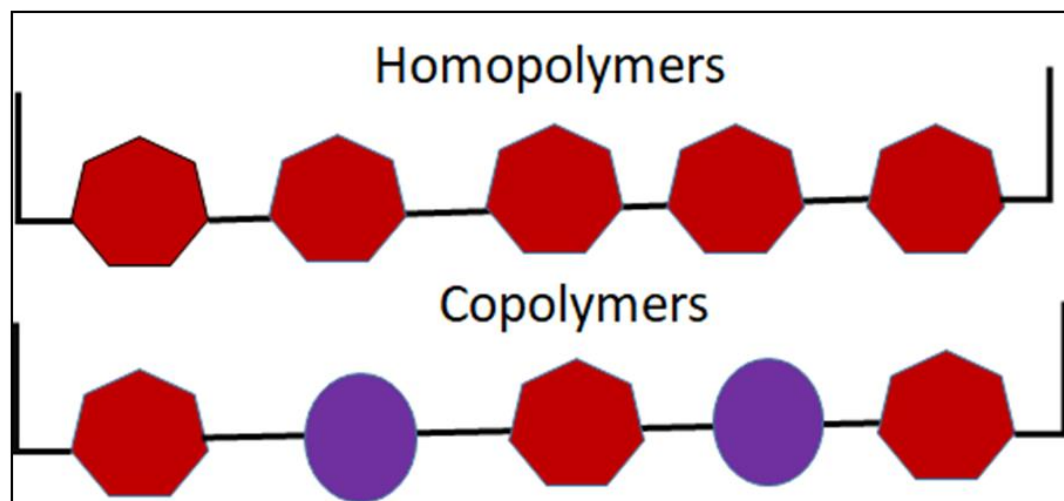
Figure 2-2. Schematic diagram of Copolymerization.

Table 2-2 shows that different researchers using copolymerization techniques to improve the humidity sensors characteristics.

Table 2-2. Copolymerization method.

Materials	Range (%RH)	Response time (s)	Recovery time (s)	Hysteresis	Year	Ref
MMA-MAPTAC	10-90	30	150	NA	2004	[67]
Poly-MMA-MAPTAC	20-90	15	20	2%	2013	[68]
P(Py-co-FPy)	11-97	5	NA	NA	2015	[69]
PDEAEMA-b-PS	22-95	60	206	8%	2016	[66]

2.8. Graft Polymerization:

Grafting is a useful method for adding a variety of specific groups to a polymer. Graft polymerization is a technique in which monomers are covalently attached as side chains to the primary polymer chain. Graft polymerization is an excellent way to prepare water-insoluble products for the use of humidity sensing applications. During grafting, gamma rays radiation chemically bounded the hydrophilic Polymer to a hydrophobic polymer film; these grafting polymer films are suitable for humidity sensor ideal properties for humidity sensors [70]. Y.Sakai et al. [71] grafted the sulfonated polystyrene branch on the surface of tetrafluoroethylene (PTFE) film by utilizing an ionizing radiation polymerization techniques. They also grafted the poly(vinylpyridine) on to the surface of a poly(tetrafluoroethylene)film. The grafted films became fully insoluble in water and absorbed a small amount of moisture, which lowered the surface electrical resistivity. K.S.Chen et al. [72] used grafting polymerization of P-styrenesulfonic acid sodium salt (Nass) through UV irradiation to form a homogeneous hydrophilic film. The drawback of these grafting films is that it takes a certain amount of time for the water vapor to penetrate into or out of the grafted layer, and, as a result, the response time for the detection of humidity change is long. Graft polymerization of

technique is depicted in the Figure 2-3.
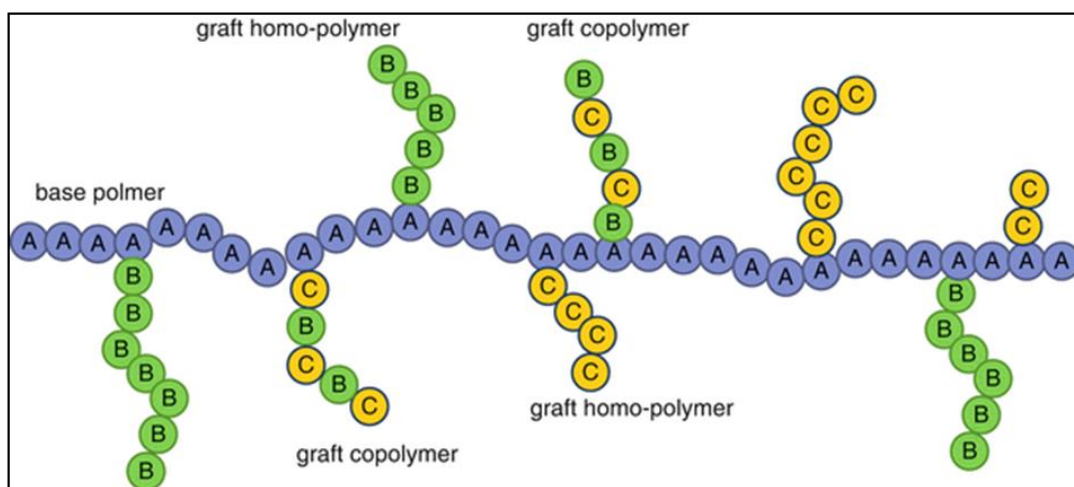
Figure 2-3. Schematic diagram of Graft Polymerization [51].

2.9. Crosslinked Polymer Film-Based Humidity Sensors:

When several linear polymer chains are interconnected at several points on the chains, they finally become a single macromolecule with a network structure. This kind of polymer is called a cross-linked polymer. Cross-links are categorized as covalently bonded chemical crosslinks or physical cross-links. Polymers which are cross-linked are insoluble in many solvents, though they can swell in suitable solvents for the corresponding linear polymers. The sensing properties is greatly influenced by the cross-linked configuration of the polymer. The sensitivity of the humidity was particularly influenced by the degree of cross-linking [73]. Sakai et al. [74] Proposed a possible configuration of crosslink the hydrophilic Polymer with a suitable reaction to make the polymer coating insoluble in water but prone to humidity sensing. Hydrophilic polymer solution and crosslinking reagent were dip-coated on the substrate surface to create a crosslinked polymer film. Gong et al. [75] synthesized cross-linked polyelectrolyte materials utilizing the ink-jet process. The impedance of the sensors after 30 minutes of immersion in the water shows a measurable improvement and the

findings suggested that the cross-linked polyelectrolyte increases the insolubility of the water. Figure 2-4 shows the schematic diagram of crosslinking polymerization technique.
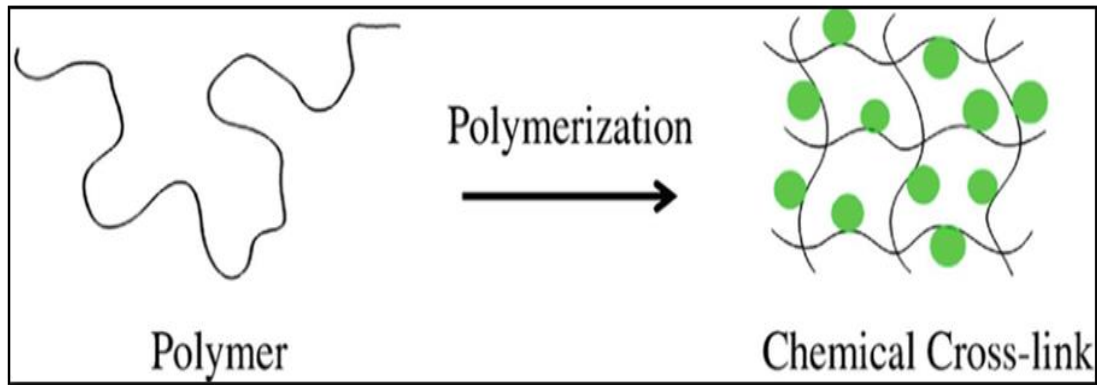
Figure 2-4. Schematic representation of Crosslinking Polymerization [55].

2.10. Polymer nanocomposite-based humidity sensor:

In the past 20 years, organic-inorganic nanocomposite materials have been considered a new type for many emerging electrical and optical sensing applications since polymer mechanical and electrical properties can be improved as compared to the base polymers. Polymer nanocomposite-based humidity sensors exhibits high sensitivity, small hysteresis, faster response and recovery times, and better stability than the only polymeric humidity sensors. Adding nanoparticles to the polymer matrix is widely used to enhance polymer film's electrical and mechanical properties [76-78]. Small size and large surface area f nanoparticles can enhance polymer film sensitivity [79]. Su PG et al. [80] studied the impact of TiO_2 nanoparticles on polypyrrole (Ppy); they reported that the humidity sensor fabricated using TiO_2 NPs/PPy composite thin films showed the highest sensitivity, smaller hysteresis, better linearity and short response and recovery time as compared to the Pure PPY based humidity sensor. Taccola et al. [81]

studied the morphology of the PEDOT: PSS/iron oxide nanoparticle composite film by using AFM and SEM analysis. They observed that the dispersion of iron oxide nanoparticles on the surface of PEDOT: PSS composite film improves the film's conductivity. Therefore, the humidity sensitivity of PEDOT: PSS/iron oxide nanoparticle composites got enhanced. Polymer nanocomposite-based humidity sensors are shown in Table 2-3.

Table 2-3. Comparison of different polymer nanocomposite based humidity sensors.

Materials	Sensor Type	Range (%RH)	Response time (s)	Recovery time(s)	Hysteresis	Year	Ref
TiO_2/PPy	Resistive		40	20	NA	2007	[82]
Au–PVA core–shell	Capacitive	11.3-93	145	94	NA	2010	[83]
PEDOT: PSS/Fe_2O_3	Resistive	30-70	1	NA	3%	2013	[84]
GO-PDDA	Capacitive	11-97			NA	2014	[85]

2.11.   The blending of hydrophobic and hydrophilic polymers:

The blending of polymers with their special characteristics is a well-established technique for improving the polymeric sensing film's mechanical and electrical properties [86]. A polymer blend is a combination of two or more polymers that can be miscible and form phase-related structures, either by a single-phase material or by immiscible material. Blending has traditionally been used as a process to improve the polymer 's bulk properties. Mixing may also be used to alter the surface properties of polymers. There generally are two ways of surface modulation through mixing: (1) hydrophilic or hydrophobic homopolymers or (2) incorporating amphiphilic

copolymers. Due to differences in chemical structure and surface energy, these blends tend to be immiscible, leading to high interfacial tension between polymers.

2.12. Biodegradable Polymer:

The development of polymer sensing film extracted from sustainable and renewable resources has been a hot topic of recent research and development [87]. The use of renewable resources means that such a sensor is sustainable and cost-effective. Polylactic acid (PLA) has attracted many researchers due to its advantages, including good biocompatibility and excellent mechanical properties, which makes it popular in biodegradable medical implants, in food packing, and in the biomaterials industry [88, 89]. PLA is a biodegradable polymer derived from lactic acid, which can be produced from renewable resources such as sugar cane, corn, wheat, and other starch products. The use of renewable resources means that such a sensor is sustainable and cost-effective.

2.13. Piezoelectric materials-based humidity sensor:

In sensing materials, piezoelectric materials are commonly used in sensor and actuator technologies due to their ability to couple electrical and mechanical displacements [90]. The most common piezoelectric materials include quartz, aluminum nitride (AlN), Lead Zirconate Titanate (PZT), and Barium Titanate ($BaTiO_3$). Low dielectric loss and high permittivity are essential parameters for piezoelectric materials to consider for humidity sensing applications. The water vapor adsorption on the piezoelectric sensing film causes changes in the dielectric constant of a sensing film, increasing the film's conductivity. He et al. [91] reported impedance-based humidity sensors using $BaTiO_3$ nanofibers as sensing film. $BaTiO_3$ based nanofibers obtained by electrospinning techniques. The moisture sensor response time was 5 sec, while the RH value changed

from 95 % to 11 %. Zhou et al. [92] reported that NaNbO3 piezoelectric nanofibers were synthesized on polymeric substrates (PDMS). The humidity sensors exhibited fast response time and high sensitivity with respect to the humidity level. Table 2-4 shows that the piezoelectric materials composite improve the humidity sensors characteristics.

Table 2-4. Comparison of different piezoelectric materials based humidity sensors

Materials	Sensor Type	Range (%RH)	Response time (s)	Recovery time(s)	Hysteresis	Year	Ref
RMX/BaTiO$_3$ composite	Resistive	33-98	15	120	3	2002	[93]
BaTiO$_3$/PSS composite	Resistive	33-98	50	120	8	2002	[94]
BaTiO$_3$-PMMA	Resistive	30-98	120	60	5%	2013	[95]
ZnO Nanosheets	Resistive	12-96	600	3		2014	[96]

2.14. Graphene Quantum dots-based humidity sensor:

Recently, carbon-based humidity sensors [97, 98] have captured substantial attention by their economical, easy-processing, and flexibility-accommodating attributes [99]. Among the different allotropes of carbon, graphene has attracted many researchers' attention in the emergent materials field, With the extraordinary chemical and physical properties such as remarkable electrical and thermal conductivity, excellent resistance to corrosion and stability, high strength, and graphene-based materials became the researcher's first choice for sensor fabrication [100]. Different dopants added to the graphene to support the alienation of adsorbed water into hydrogen and hydroxyl ions [101]. The bulk resistivity is decreased by the hydroxyl ions, which can later be

considered as an AC impedance. The water, which is captivated into the film due to diffusion through the capillary or bulk transport of water into the film's pores, variations in conductance or capacitance, can be calculated. Improvement in humidity response measurements of the sensors has been observed using the quantum dots (QDs), particularly in terms of the devices' sensitivity towards change in different relative humidity. Quantum dots constitute a new class of nanomaterials, between the molecular and bulk forms of material; because of their fluorescent properties, small size, and surface defect, quantum dots display outstanding optical and electrical properties, higher than those present in bulk material [102]. Quantum dots have been widely used in different domains; biomedical [103], agriculture [104], energy conversion[105], optoelectronics [106], and more recently in sensing applications [107, 108]. However, quantum dots materials were found to be very toxic [109, 110] and relatively expensive. Therefore, researchers are more interested nowadays in developing suitable low cost and non-toxic alternatives, namely carbon and graphene quantum dots (GQDs). The GQD's latter's attracted many researchers because of their unique and outstanding properties such as easy preparation [111], low cost, and toxicity[112, 113], photoluminescence, and bandgaps[114, 115]. GQDs have been prepared by a different route, mainly by chemical [116], ultrasonic assisted [117], microwave assisted [118], plasma-assisted, and laser-assisted methods [119]. These methods use expensive carbon sources such as carbon nanotubes [120] and carbon nanofiber [121], however more recently, the trends are using lost-cost carbon sources, especially carbon wastes materials, to prepare (GQDs) for added value applications [122].

2.15.   Humidity Sensor Characteristics:

2.15.1. Sensitivity:

Sensitivity is defined as the ratio between the variation in output capacitance and the variation in the dielectric constant of the test material that gives rise to it. Sensitivity formula is defined in equation 3.

$$S = \frac{C_{max} - C_{init}}{C_{init}} \times 100 \qquad (3)$$

where C_{max} is the capacitance recorded at maximum humidity level, and C_{init} is the capacitance measured at the initial humidity level.

2.15.2. Hysteresis Response:

Hysteresis is also a major characteristic of a humidity sensor in practical implementations. The Hysteresis effect can be defined as the maximum difference in capacitance value when the sensor is subjected to change in relative humidity level from lower to higher and higher to lower. The water molecules are absorbed in the sensing film's surface and form clusters that deform the sensing film. Due to this, the desorption process slows down, leading to the hysteresis phenomenon.

2.15.3. Response and Recovery time:

The response and recovery times are paramount in the practical implementation and performance of capacitive humidity sensors. The time taken by a sensor to achieve a 90 %RH level is referred to as the sensor's response time. On the other hand, the recovery time is the time that a sensor takes to drop from 90 %RH levels to 20 %RH (initial state).

2.15.4. Stability of Sensors:

Stability determines the sensor's ability to deliver the same performance over a given period and measure the same response. Sensitivity is the acceptable change in the sensor output to the physical parameter gradual shift established at the sensor's origin.

2.16.   Fabrication Techniques:

Numerous techniques have been adopted to deposition humidity sensing film on a substrate based on the application and materials. Some of these include spin coating, electrospinning, screen printing, drop-casting, and physical vapor deposition.

2.16.1. Spin Coating

Spin coating is often used in sensor fabrication. The spin coating process, when placed on smooth and flat substrates, provides a thin but reproducible material layer that can be used in a wide variety of applications. It is currently the leading technique for producing a uniform thin film of organic materials with a thickness of several micrometers and nanometers. Centrifugal force spreads the content radially from the center of the base to its edges. The viscosity and rotation speed of two independent parameters mainly affect film thickness and uniformity. The viscosity and rotation speed of two independent parameters primarily affect film thickness and uniformity. The spin coating can produce film thickness ranges from 1 μm to 200 μm. Figure 2-5 shows the schematic diagram of spin-coating techniques. Figure 2-5 shows the schematic diagram of spin-coating techniques.
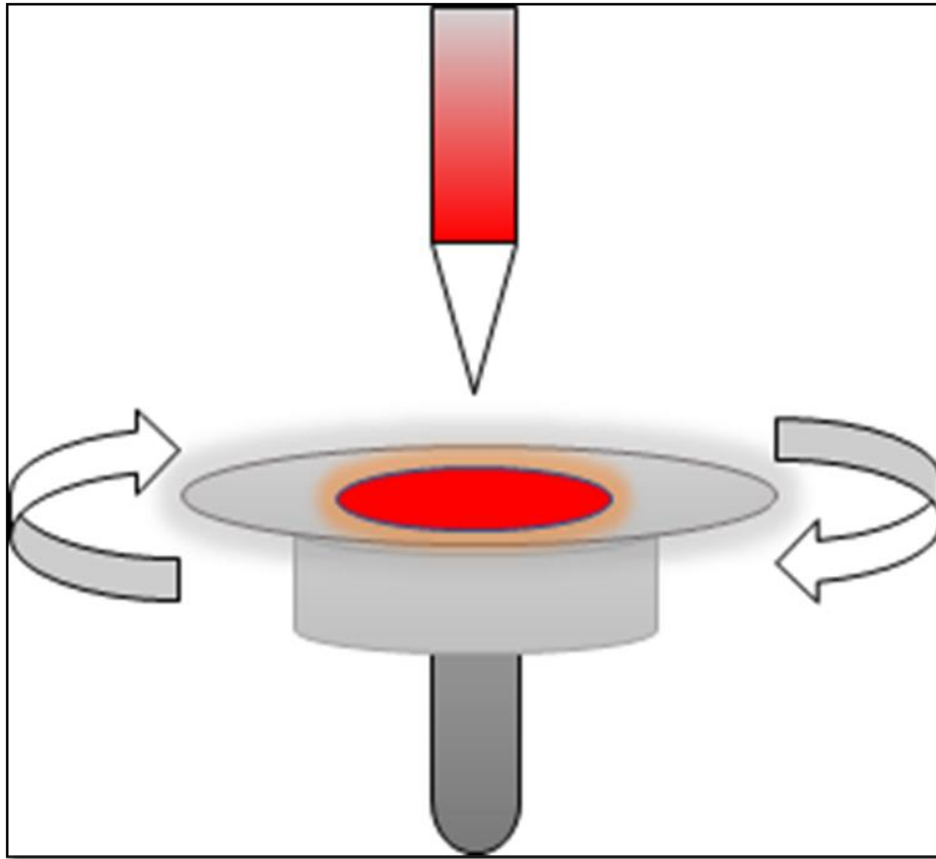
Figure 2-5. Schematic representation of Spin Coating Techniques.

2.16.2. Electrospinning

Electrospinning is effective technique for producing long, standardized nanofibers of organic, inorganic and organic / inorganic hybrid materials as an simple and flexible technique. [4,5]. Electrospinning is a simple and basic method for the deposition of ultrafine nanofibers from various materials, including polymer, composite materials, and ceramic materials. The electrospinning setup consists of three key elements: a high voltage power source, a metal needle syringe, and a conductive collector. There have been several reports of high-performance, one-dimensional nano-sized sensitive materials developed by electrospinning. However, it was observed that there are significant challenges when attempting to incorporate electrospun nanofibers into electrical/electronic systems [9]. Figure 2-6 shows the schematic diagram of the electrospinning technique used to deposit nanofibers on the substrate.
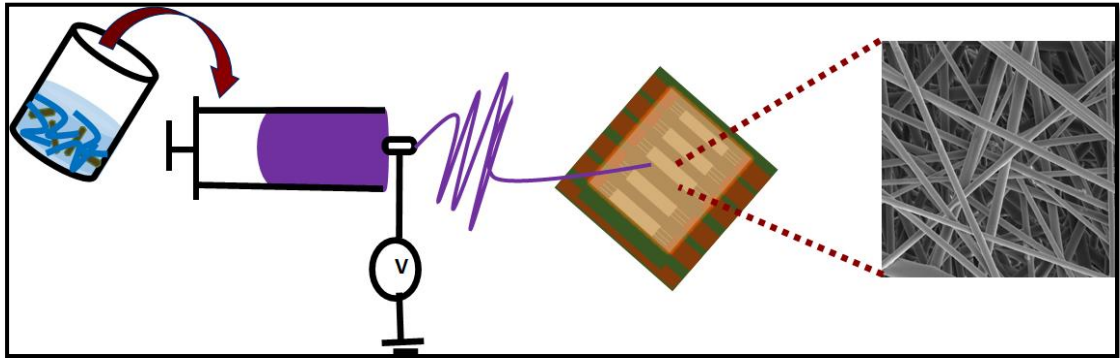
Figure 2-6. shows the schematic diagram of electrospinning techniques used to deposit the nanofiber of the Interdigitated electrode surface.

2.16.3. Drop casting:

Drop-cast is the formation of a thin film by lowering a solution to a smooth surface followed by evaporation. This technique is fast and simple, but the film thickness is not uniform. Drop casting is a cost-effective technique. This technique is similar to spin coating, but the primary difference is that substrate rotation is not required. Film thickness and characteristics also depend on solution spreading and concentration. Less wastage of the material is one of the advantages of the drop-casting technique. On the other hand, this method has various disadvantages, including difficulties in controlling film thickness and non-uniform film formation on the substrate's surface. Figure 2-7 shows the schematic representation of the drop-casting process.
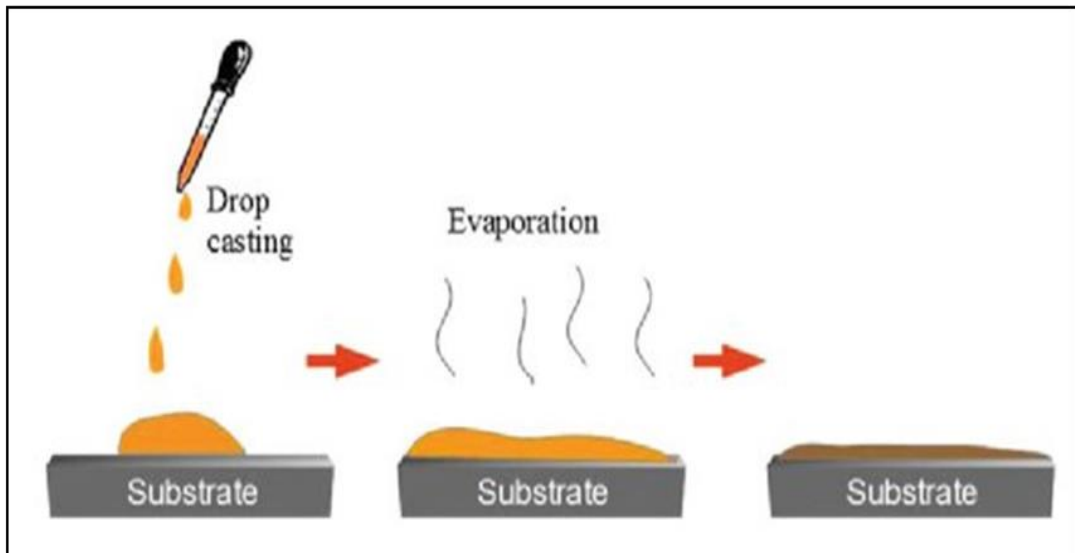
Figure 2-7. Schematic representation of drop-casting techniques [107].

2.16.4. Screen-Printing:

A screen-printing technique is a cost-effective, rapid, flexible design and large-scale production fabrication process used to deposit and print the substrate's sensing materials. The screen-printing method consists of layer-by-layer depositions of ink upon a substrate, using a screen or mesh, defining the sensor's geometry [123]. Figure 2-9 shows the schematic diagram of the screen-Printing process used in the fabrication of a humidity sensor.
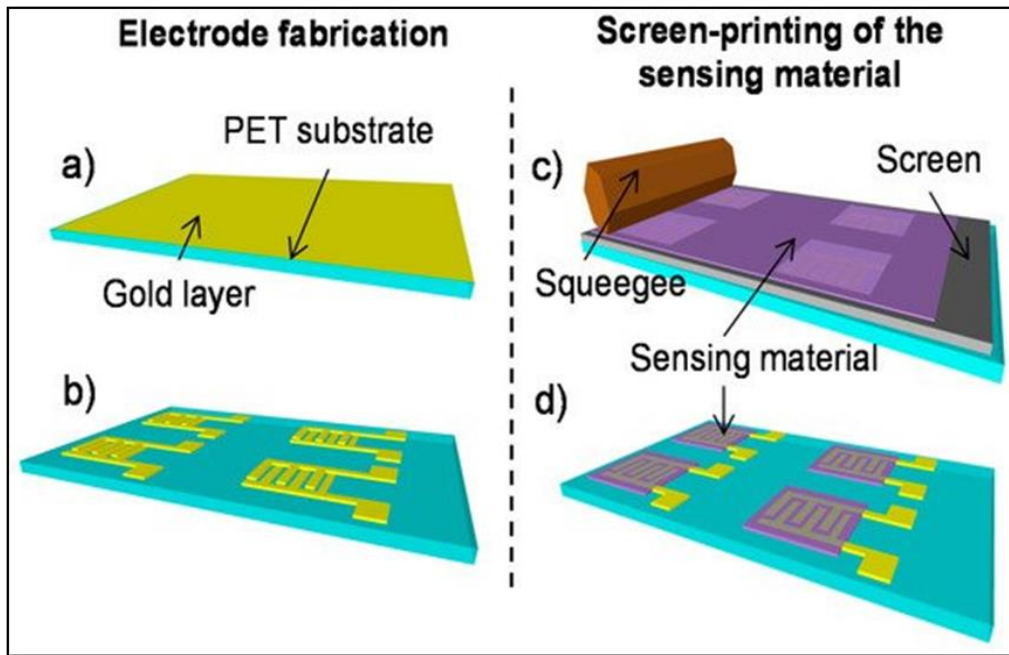
Figure 2-8. Schematic representation of Screen-Printing techniques [15].

CHAPTER 3: MATERIALS AND CHARACTERIZATION TOOLS

3.1.   Introduction:

The first chapter explained different humidity sensing techniques employed in the Natural gas environment and the working principle of capacitive and impedance humidity sensors. The second chapter gives a literature review of different materials used for capacitive and impedance humidity sensing applications and explains the various methods to improve the polymeric sensing film's hydrophilicity. The current chapter summarizes all the materials used in this thesis work, the fabrication techniques used, and characterization techniques used to study the sensor's morphology, stability, and electrical response of the humidity sensors.

3.2.   Materials:

PLA (Poly Lactic acid) is a biodegradable polymer derived from lactic acid, produced from renewable resources such as sugar cane, corn, wheat, and other starch products. The use of renewable resources means that such a sensor is sustainable and cost-effective. Polylactic acid (PLA) were obtained from Sigma Aldrich and used without any further purification. Figure 3-1 shows the molecular structure of the PLA.
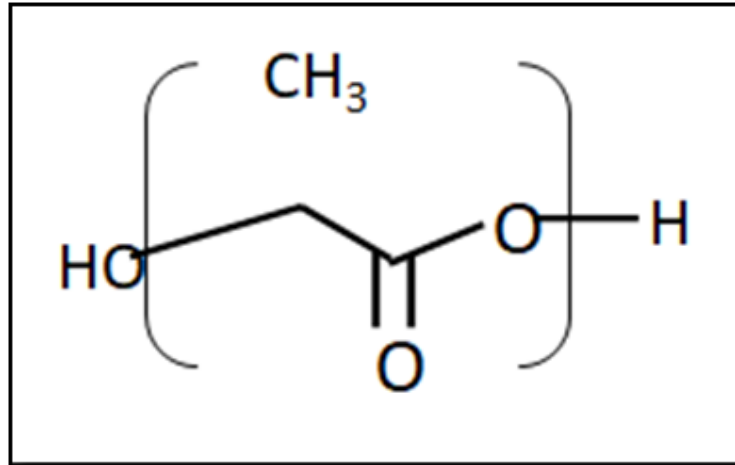
Figure 3-1. Molecular Structure of PLA.

3.2.1. TiO₂:

TiO$_2$ is an n-type semiconductor having a wide bandgap (3.2 eV for anatase and 3.0 eV for rutile). Titanium dioxide powder with 90 nm particle size was obtained from Sigma Aldrich and used without further purification. The TiO$_2$ nanomaterials are biocompatible and environmentally safe. Figure 3-2 shows the molecular structure of TiO$_2$.
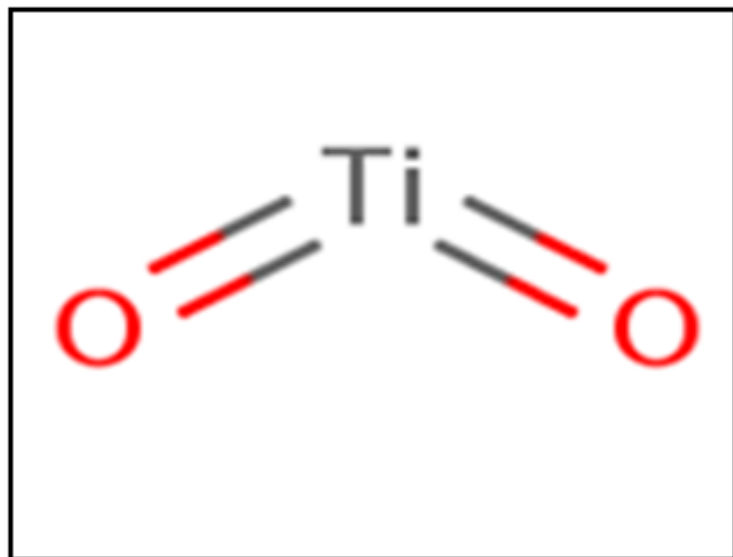
Figure 3-2. Molecular Structure of TiO$_2$.

3.2.2. PVDF:

PVDF (Polyvinylidene fluoride) is a semi-crystalline, high purity thermoplastic fluoropolymer. PVDF shows a good combination of properties such as UV and Chemical resistance, thermally stable, strong mechanical efficiency, piezoelectric, and pyroelectric properties. PVDF operate at a wide range of temperature from -20 °C to 150 °C. PVDF powder, having an average Molecular weight (Mw-534, 0000), was obtained from Sigma Aldrich and used without further purification. Figure 3-3 shows the molecular structure of PVDF.
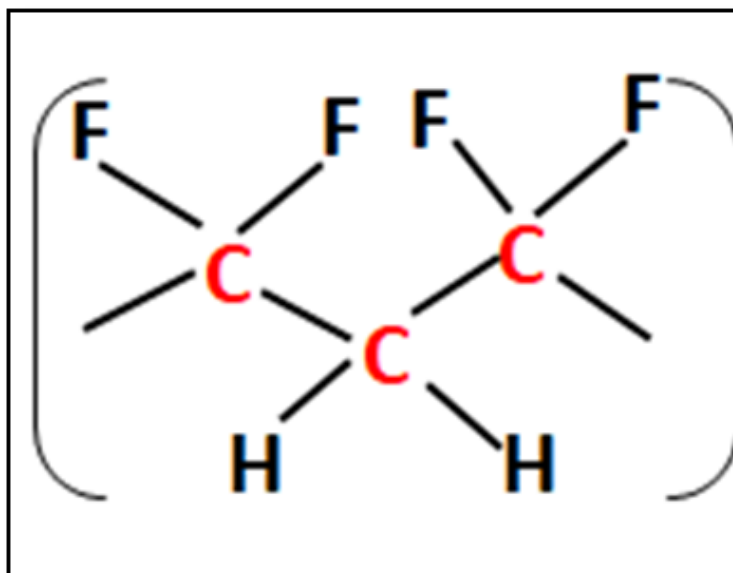
Figure 3-3. Molecular Structure of PVDF.

3.2.3. BaTiO₃:

Barium Titanate is a piezoelectric material; it was largely replaced by lead zirconate titanate but has been widely used in microphones and other transducers. $BaTiO_3$ has a dielectric constant between 1000-5000 and a wide bandgap around 3.2 eV. $BaTiO_3$ with microparticle sizes of ≤ 100 nm and PVDF powder with an average molecular weight, Mw, of 534,0000 were purchased from Sigma-Aldrich (St. Louis, Missouri, United

States) and used without further treatment. Figure 3-4 shows the molecular structure of BaTiO$_3$ material. Figure 3-4 shows the molecular structure of BaTiO$_3$.
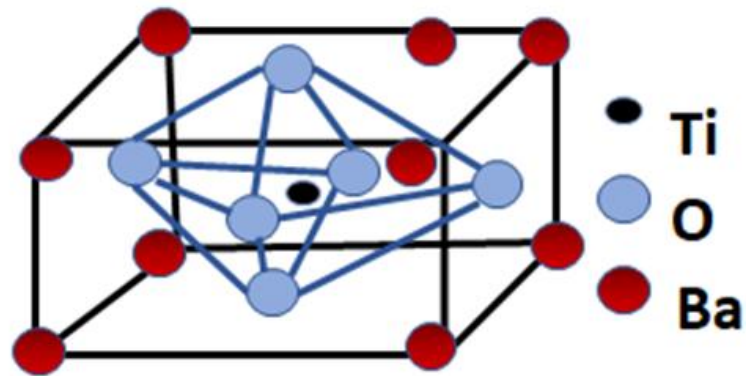
Figure 3-4. Molecular Structure of BaTiO$_3$.

3.2.4. *SPEEK:*

The sulfonation of poly ether ether ketone (PEEK) is a well-established method to improve the sensing film's hydrophilicity and proton conductivity [124]. The sulfonation occurs by introducing the hydrophilic sulfonic groups (SO$_3$H) within the PEEK. The sulfonation of polymer significantly improves the absorptions of water molecules and proton conductivity, increasing the sensitivity of the humidity sensors [125]. Sulfonated polyether ether ketone (fumion® E-590) with ion-exchange capacity (IEC) of 1.7 meq/g, was obtained from FuMA-Tech GmbH, Bietigheim-Bissingen, Germany. Figure 3-5 shows the sulfonated poly ether ether ketone structure.
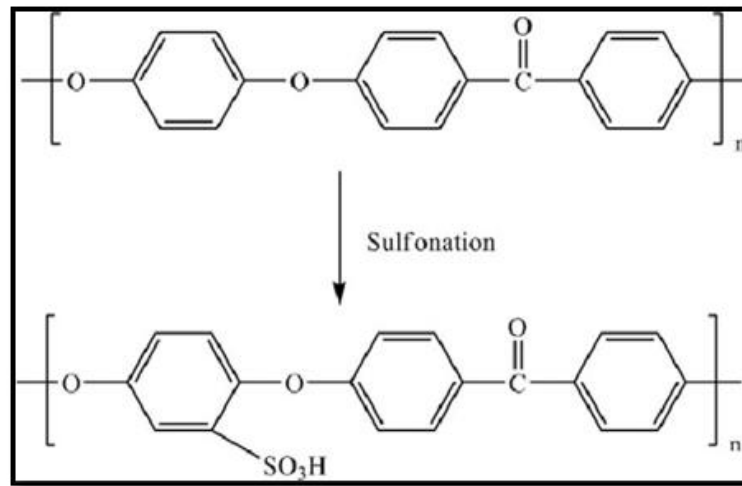
Figure 3-5. The Sulfonation of Poly (ether ether Ketone) [108].

3.2.5. ITO electrode:

Interdigitated ITO/glass substrate Purchased from Ossila and the substrate dimensions

are shown in Table 3-1.

Table 3-1. ITO/glass substrate and dimensions

Parameter	Value
Substrate dimensions	20 mm x 15 mm
Thickness of ITO electrodes on glass substrates	100 nm
Number of electrodes	5 (each consist of three interdigitated legs)

Figure 3-6 shows the graphical representation of the interdigitated ITO glass electrode.
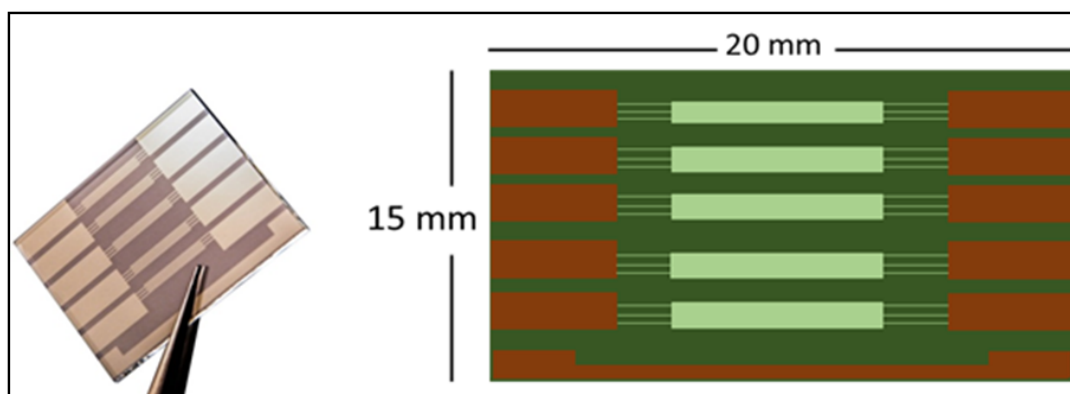
Figure 3-6. The dimensions and graphical illustration of the ITO electrodes used in the investigated sensors.

3.2.6. Substrate cleaning:

The ITO glass electrode was cleaned in a sequential step. Firstly the ITO electrode was sonicated in an ultrasonic bath in soap water for 30 min. Secondly, the ITO electrode was rinsed in DI water after that sonicated in acetone for 15 min. Thirdly ITO electrode was again rinsed in deionized water for 30 min, and the ITO electrode was dried using blow-drier. The ITO electrode was stored under a vacuum to maintain the surface of the ITO electrode clean. Figure 3-7 shows the image of the cleaning of ITO electrodes. Figure 3-7 shows the ITO electrode cleaning process.
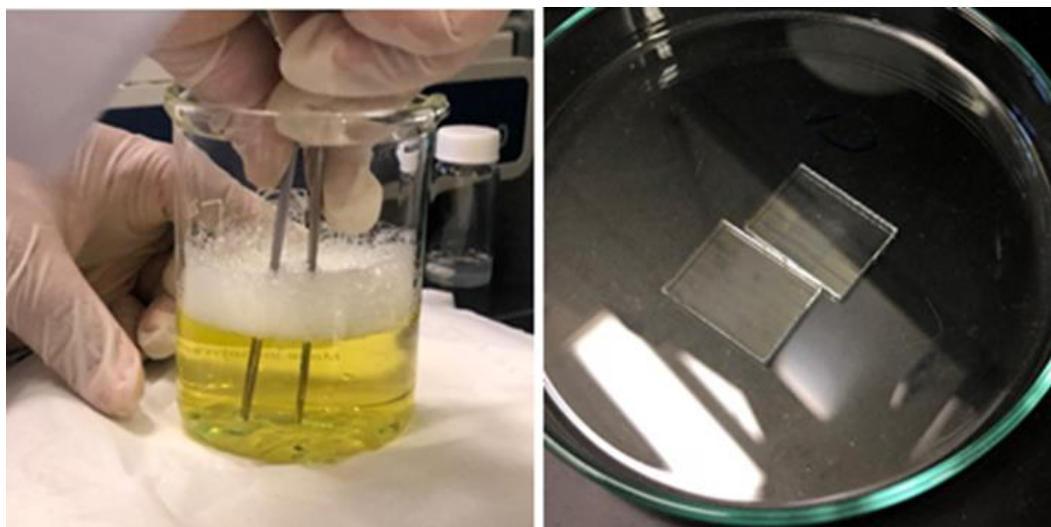
Figure 3-7. Image of cleaning of ITO electrodes using soap water.

3.3. Nanocomposite Preparation:

The polymeric nanocomposites solution is prepared by mixing polymer and nanoparticles following specific procedures.

3.3.1. PLA-TiO$_2$ nanocomposite:

The PLA: TiO$_2$ composites synthesized in a two-step process. The 2 wt% solution of PLA and ceramic TiO$_2$ nanoparticles were prepared in chloroform separately. Firstly PLA-chloroform solution was placed for 24 hours so that PLA dissolved in chloroform. In the second step, 2 wt% of ceramic TiO$_2$ nanoparticle was dissolved in chloroform with constant magnetic stirring for 30 min at 550 rpm. In the next step, prepared solutions of the PLA and TiO$_2$ were mixed with a proportion of (1:2). The composite solution was then magnetically stirred for 2 hr to form a uniform solution. To further study the impact of PLA solution on humidity sensing, we have prepared viscous and diluted PLA solution separately and mixed this solution with TiO$_2$ with the same ratio (1:2).

3.3.2. *PVDF-TiO$_2$ nanocomposites solution:*

The PVDF solution was magnetically stirred for 6 hours at room temperature to dissolve the PVDF in DMF solvent uniformly, and TiO$_2$ nanoparticles (0.5 wt%) were separately prepared in DMF solvent. Finally, PVDF and TiO$_2$ solutions were mixed with (1:2) proportion and stirred for 2 hours. We studied the impact of different concentrations of PVDF on PVDF-TiO$_2$ composite morphological and electrical response while kept the TiO$_2$ nanoparticles concentration constant. After optimizing the PVDF concentration in the first step, we prepared the PVDF-TiO$_2$ composite films with different TiO$_2$ concentrations (0.5 wt%, 1 wt%, and 2 wt%) and compared the humidity characteristics of the PVDF-TiO$_2$ nanocomposite humidity Sensor.

3.3.3. *PVDF-BaTiO$_3$ nanocomposites solution:*

The PVDF concentration is optimized (2.5 wt%, as shown in PVDF-TiO2 nanocomposites). We dissolve the PVDF in the DMF solvent. Different BaTiO$_3$ nanoparticles' concentrations were prepared in DMF solvent using magnetic stirring at

500 rpm for 60 minutes. The two individual solutions were homogeneously mixed and set for magnetic stirring at 500 rpm for 2 hours so that PVDF and $BaTiO_3$ completely blend. We studied the effect of different $BaTiO_3$ nanoparticles' concentration on the electrical characteristics, thermal stability, and PVDF-$BaTiO_3$ nanocomposites' morphology. Figure 3-8 shows the stirring process of PVDF-$BaTiO_3$ nanocomposite solutions.

Figure 3-8. Image of magnetic stirring of polymer and nanoparticles on a hot plate.

3.4.   Fabrication of the Humidity sensor:

The Spin coating technique is used to deposit a sensing film on the cleaned ITO electrode. An optimization process for the rotation speed and the rotation time to form an even equilateral spread of the solution were done. The rotation speed and rotation time were optimized to 6000 rpm and 50 seconds. Figure 3-9 shows the deposition of polymeric film using spin-coating techniques.

Figure 3-9. Image of Spin coating of polymeric film on the ITO electrode.

3.5.   Characterization Techniques:

3.5.1. *Electrical characterization:*

The humidity sensing response of sensors carried out in a controlled humidity chamber. The humidifier (model HM3000) is used to increase the humidity level inside the sealed humidity chamber. The Drierite based desiccant was connected to the humidity chamber through an inlet valve to decrease the chamber's humidity level. The RS-6109 humidity meter was used as a reference humidity sensor placed inside the humidity chamber to observe its humidity. The capacitive and impedance response of the polymer nanocomposite-based humidity sensor was measured by MS5308 LCR meter. Figure 1 demonstrates the humidity sensing measurement setup used in this study. It is important to note that We performed our experiment within the sealed chamber, where ambient air was used to increase and decrease the relative humidity levels. A humidifier has been connected to the sealed chamber by an inlet valve, which flows humid air into the sealed chamber to raise the moisture levels. Drierite based desiccant was to circulate the moist air to reduce the humidity level within the sealed chamber. Figure 3-10 shows the humidity sensor experiment setup employed in this research work.

44
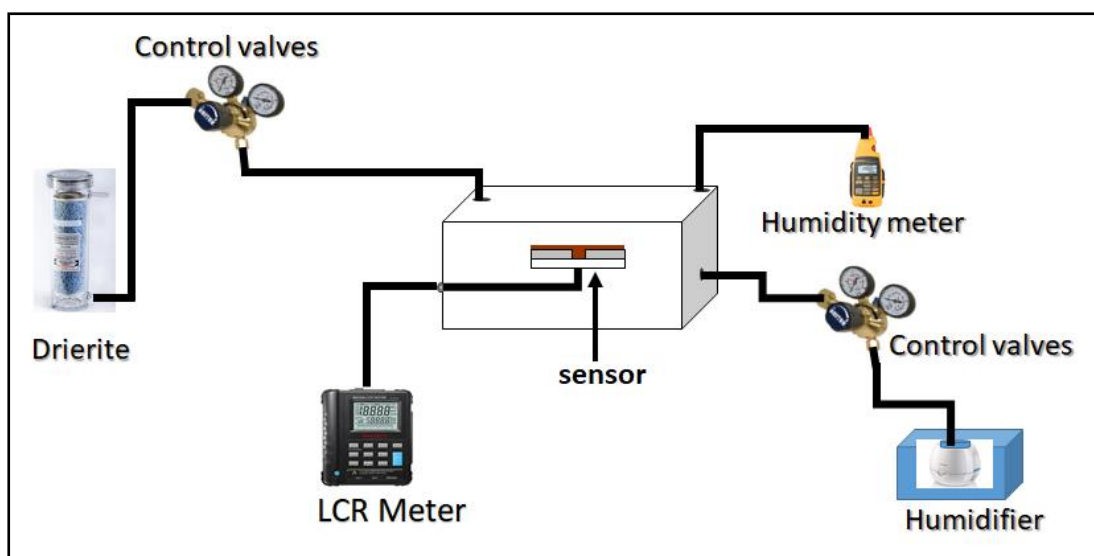
Figure 3-10. Graphical presentation of the humidity sensor experimental setup used in this project work.

3.5.2. *Electrochemical Impedance Spectroscopy (EIS):*

Electrochemical impedance spectroscopy (EIS) is a basic technique used to describe the electrical properties of materials, particularly regarding ion conductivity within the sensor. The EIS technique provides useful information on the nature of electrical conductivity associated with humidity changes. The EIS of humidity sensor were performed over the wide frequency range of 10 mHz–1 MHz using Gamry 3000 (Gamry Instrument). Figure 3-11 shows the Gamry 3000 setup used for EIS analysis of the humidity sensor.

Figure 3-11. Gamry 3000 use for Impedance response:

3.6.   Morphological Analysis:

The morphology of the polymeric sensing film played a vital role in determining a humidity sensor's character.

3.6.1. Scanning electron Microscopy Analysis:

Scanning electron microscopy (SEM) study the samples' surface morphology using Nova Nano Scanning Electron Microscopy. SEM is used to analyze the microstructure of the surface of biological and material samples. By concentrating a high-energy electron beam on the surface of materials, SEM generates images and provides high-resolution images that help understand the surface's morphology. SEM is used with various specimens to study surface morphology for application in biomedical devices

and sensing materials characterization for sensors and actuators. SEM usually has the potential to magnify up to 200,000 times. Figure 3-12 shows the SEM analysis setup installed at CLU.
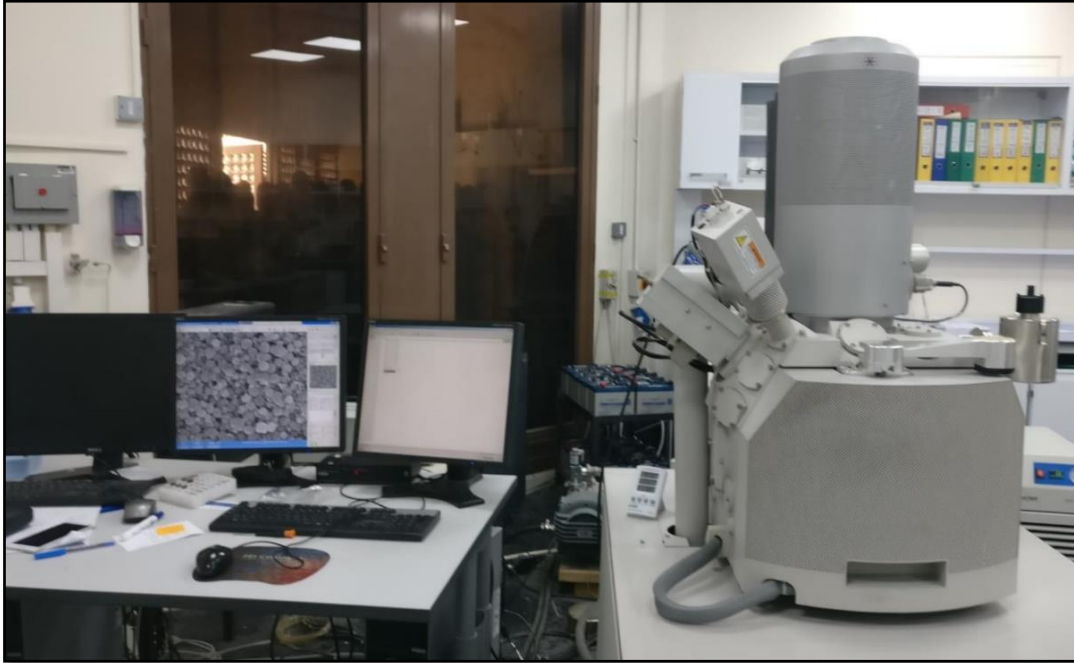
Figure 3-12. Scanning electron microscopy analysis.

3.6.2. *Transmission electron microscopy (TEM):*

Transmission Electron Microscope (TEM) model TECNAI G2 TEM, TF20 by Field Electron and Ion Company (FEI) has been used for material analysis. TEM is an essential technique in characterizing nanoparticles in electron microscopy. TEM provides nanoparticles' images at a spatial resolution equal to the atomic level. When the high electron beam interacts with the specimen, the electron beam from which the incident light is emitted into a thin foil electrode is converted into elastically or inelastically distributed electrons. The ratio of the distance between the objective lens, the specimen, and the image plane is considered as magnified by the lens. High TEM resolution is needed to determine nanomaterials' crystal structure, the shape of

nanomaterials, and the size of nanomaterials. Figure 3-13 shows the TEM experimental setup placed in CLU.

Figure 3-13. Transmission electron microscopy (TEM).

3.6.3. AFM analysis:

Atomic force microscopy is used to analyze the surface topography and provide an image with near-atomic resolution. In our research work, we have used Asylum Research's AFM measurement unit is a distinctive heavy-duty tribometer used to calculate 3D sample images. The AFM system consists of a cantilever with a small probe that interacts with the sample surface through a raster scanning motion. The AFM tip's up-to-down and side-to-side motion as it scans along the surface is scanned by a laser beam reflected off the cantilever. AFM can measure samples' surface roughness down to the angstrom-scale. It also provides the broad study of a thin film mechanical

48

property of surface at the nanoscale level. Figure 3-14 shows the AFM setup deployed at the Center for Advanced Materials.
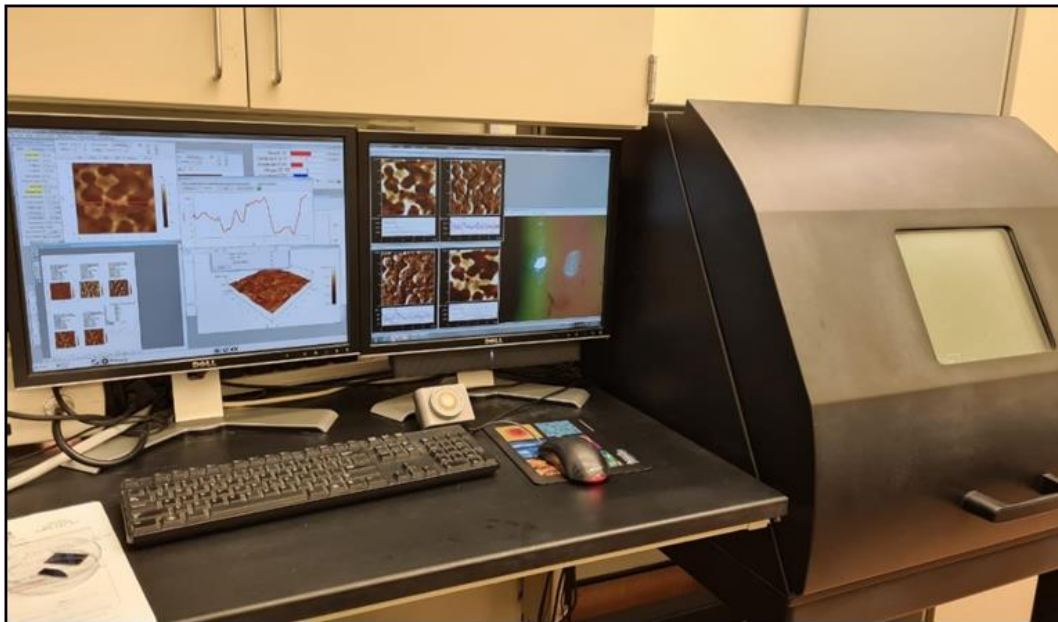
Figure 3-14 Atomic Force microscopy setup.

3.7.　Contact angle analysis:

The optical angle measurement device OCA 25 is used for contact angle analysis manufactured by Data Physics instruments. A highly magnified camera captured the contact angle measurement of the water droplets on the composite film's surface with six-fold zoom lenses, which can record 2450 frames/sec. SCA software is used to measure the angle of the captured images. The sessile drop method is used to measure the contact angle of the nanocomposite film. Figure 3-15 shows the OCA 25 contact angle set up at the Center for Advanced Materials.
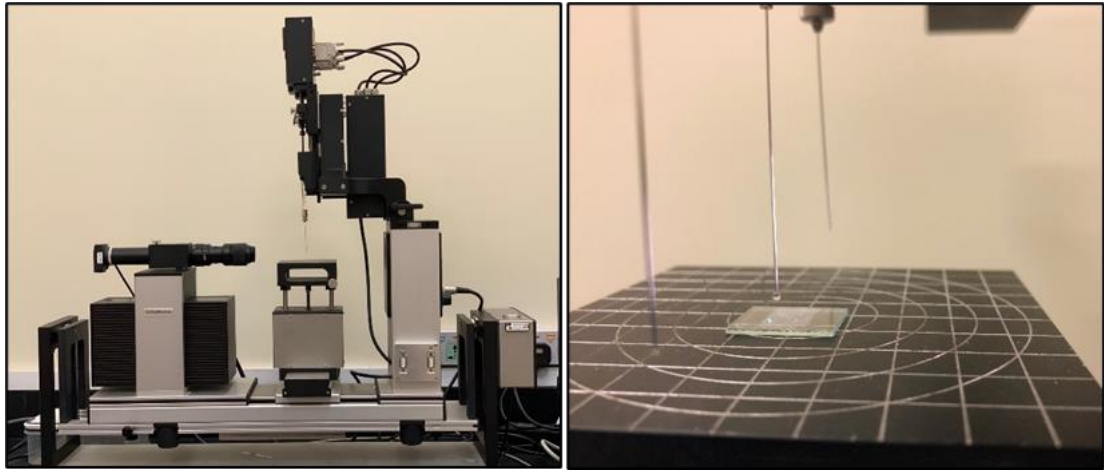
Figure 3-15. Contact angle measurements setup.

3.8.   Structural Analysis of Sensing film:

3.8.1. XRD Analysis:

X-ray diffraction analysis is the characterization technique used for analyzing the various physical and chemical properties of materials, compounds, and composites. It is used for determining the crystallography of a material, which includes crystal orientation, crystal structure, and indicate the different phases in the crystalline structure. X-ray diffraction analysis also shows the effect of different content in the composition of polycrystalline materials on grain size and grain boundaries. X-ray diffractions analysis techniques build based on Bragg's law.

$$\lambda = 2d_{hkl}\sin\theta$$

X-rays incident on the crystal structure of objects due to the shorter wave lights of x-rays they penetrate within the crystal structure's atomic plane. As the atomic plane reflected these x-rays and it forms constructive interference, it satisfied Bragg's law. The diffraction peaks position is determined by the distance d_{hkl} between parallel planes of atoms [2]. X-ray diffraction (XRD) patterns were recorded with EMPYREAN Advanced diffractometer, which generates x-rays by establishing the high potential

between filament and anode. In our case, we have used at 45 kV potential and 40 mA with K-Alpha1 wavelength radiation 69 1.540598Å and K-Alpha2 wavelength radiation 1.544426 Å with 1 s / phase scan speed and 0.013 ° 2 stage scale. Figure 3-16 shows the X-ray diffraction analysis setup used in this project.

Figure 3-16. X-ray powder diffraction analysis.

3.9. Thermal Characterization:

Thermal analysis is the analytical, experimental technique to analyze the various properties as a function of temperatures such as enthalpy, heat coefficient, and phase transition [4]. In this thesis work, the differential scanning calorimetry method (DSC) and thermogravimetric analysis (TGA) were used to investigate polymer

nanocomposite's thermal stability at different temperature ranges.

3.9.1. DSC Analysis:

Differential scanning calorimetry measurement was conducted on a Perkin- Elmer DSC (8500) instrument under a nitrogen environment. DSC (8500) consists of two crucibles, the sample material placed in one crucible, and this crucible is placed in a temperature-controlled furnace. The second crucible i used for the reference material, which is empty; both crucibles are made of aluminum. The samples are analyzed over a wide temperature range (30°C to 700°C). The sample is heated under the fixed heating rate of 10°C /min with nitrogen gas in the furnace, which removes air from the furnace. While increasing the temperature melting point of the lower density polymer observed. After reaching the melting point, the temperature is decreased from 700 °C to 30 °C to observe both crystallization processes. The information provided by DSC analysis is used to understand the thermal degradation of materials and the thermal stability of the nanocomposite's materials at a higher temperature range. Figure 3-17 shows the DSC setup used to analyze the thermal stability of the nanocomposite's materials.
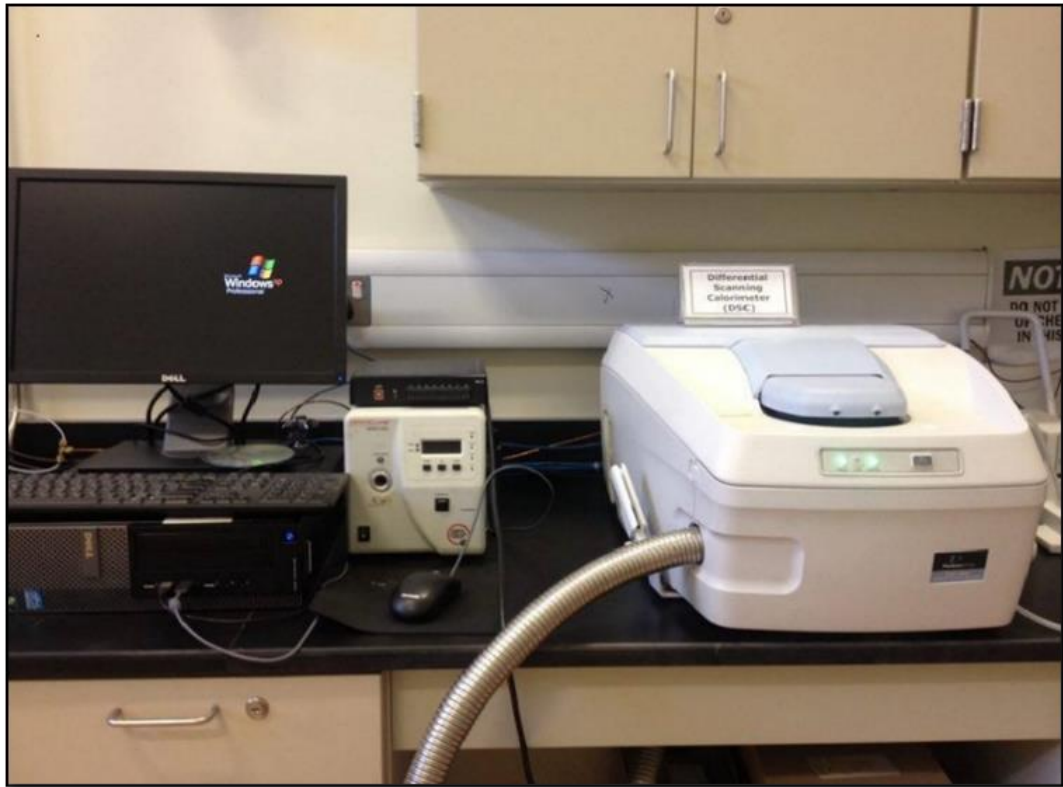
Figure 3-17. Differential scanning calorimetry (8500) setup at CAM.

3.9.2. TGA Analysis:

TGA analysis is conducted on a Perkin- Elmer TGA (4000). TGA is used for the mass loss of the sample material. A sample of the polymer having a weight of 10 mg is inserted in the aluminum oxide pan (crucible). TGA has only one furnace, and there is no need for reference material. The sample has no cover so that gases can escape to the environment, and the gases are sucked by a sucker system so that gases will not directly release to the environment. The room temperature (30 °C) of the sample material is increased from room temperature to 600 °C at a heating rate of 20 °C /min. Nitrogen gas is inserted at a flow rate of 19 ml/min. Figure 3-18 shows the TGA analysis setup used in this research work.

Figure 3-18. Thermogravimetric analysis setup at CAM.

3.10.   Spectroscopic Analysis:

3.10.1. FTIR Analysis:

Fourier transform infrared spectroscopy (Spectrum 2000, Perkin Elmer), spectra were collected with a resolution of 2 cm^{-1} over the wavenumber range 4000~400 cm^{-1}. FTIR detects chemical bonds in a molecule by producing an infrared absorption spectrum. FTIR may examine samples as solid, liquid, or gaseous. For organic and inorganic materials, FTIR provides quantitative and qualitative research. FTIR is an efficient technique for detecting functional units, characterizing covalent bonding features. Figure 3-19 shows the FTIR analysis setup used to measure the structural analysis of nanocomposite.
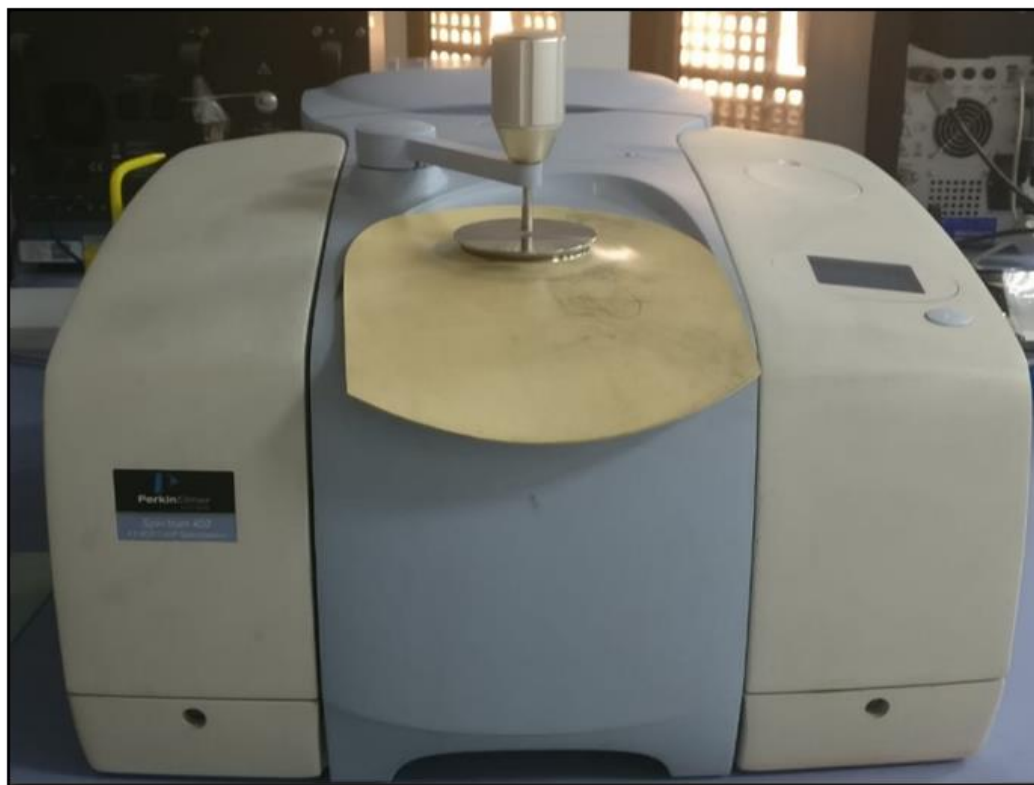
Figure 3-19. Fourier Transform Infrared Spectroscopy Analysis (FTIR).

3.10.2. Raman spectroscopy:

The Raman spectra were recorded by a Raman spectroscopy, Jobin-Yvon HR800 UVVis-NIR Raman spectrometer fitted with an Olympus BX 40 attachment. Raman spectroscopy provides information on molecular motions that can be used for sample detection and quantitation. In Raman spectroscopy, a monochromatic light source applied on a sample as light interacts with materials due to molecular vibration light scattered, and these scattered lights recorded. The Raman spectra were collected using backscattering geometry with an acquisition time of 50 seconds. Figure 3-20 shows the Raman spectroscopy setup used in this work.

Figure 3-20. shows the Raman spectrometer.

3.10.3. Dielectric spectroscopy:

The dielectric properties were measured by using the Novocontrol technology Broadband dielectric spectrometer. The experiment can conduct at room temperature with a frequency range is from mHz to GHz. The dielectric spectrometer is fitted with a sample cell having a diameter of 20 to 40 mm. Figure 3-21 shows the Broadband dielectric spectrometer setup used to measure the dielectric properties of nanocomposite materials.

Figure 3-21. Broadband Dielectric spectrometer.

CHAPTER 4: TO INVESTIGATE THE BIODEGRADABLE POLYMER FOR
HUMIDITY SENSING APPLICATIONS.

4.1. Introduction:

The first objective is to investigate sustainable and renewable resources for humidity sensing applications. Polylactic acid (PLA) is a biodegradable polymer derived from lactic acid, which can be produced from renewable resources such as sugar cane, corn, wheat, and other starch products. The use of renewable resources means that such a sensor is sustainable and cost-effective. PLA has attracted the attention of many researchers due to its salient advantages, including good biocompatibility and excellent mechanical properties, which makes it popular in medical implants, in food packing, and in the biomaterials industry [88, 89]. Zhang et al. [126] studied the thermal properties of PLA-fumed silica nanocomposites and reported that the addition of fumed silica nanoparticles into PLA polymeric matrix increases the glass transition temperature (Tg), which may improve the thermal stability of PLA. Among various inorganic nanoparticles choices, TiO_2 nanoparticles have a special peculiarity because of its good stability, UV resistance, high refractive index, and excellent photostability [127, 128]. Luo et al. [129] synthesized the PLA-TiO_2 nanocomposites film applying a grafting method and investigated the mechanical and physical properties of the PLA-TiO_2 nanocomposites. Zhang et al. [130] prepared the PLA-TiO_2 nanocomposites by van extruder technique and investigated the scattering mechanism under elongation. Marra, Antonella, et al. [131] studied the impact of functionalized TiO_2 nanoparticle on the structure, morphological, mechanical, and thermal properties of PLA. The functionalization of TiO_2 nanoparticles with fluorocarbon enhanced nanoparticle dispersion, which improved PLA's mechanical properties. Despite such investigations, to the best of our knowledge, there is not enough literature available on the TiO_2

dispersion mechanism and its impact on the electrical behavior of PLA-TiO$_2$ nanocomposites for humidity sensing applications. Our objective is to study the effect of TiO$_2$ nanoparticles on the structural, thermal, morphological, and electrical properties of the PLA for their potential applications in humidity sensing applications. The PLA-TiO$_2$ nanocomposite films were prepared through the spin coating process.

4.2.   Experimental Details:

The PLA: TiO$_2$ nanocomposites films were prepared, as depicted in Figure 4-1(a). First, 2.0 wt% solution of PLA and ceramic TiO$_2$ nanoparticles were prepared in chloroform separately. Then, prepared solutions of the PLA and TiO$_2$ were mixed in the proportion of (1:2). The composite solution was then magnetically stirred for 2 hrs to ensure uniform composition. The composite solution was then deposited on the ITO/glass substrate using the spin coating technique. The optimized rotation speed and rotation time were 5000 rpm and 60 sec, respectively. After deposition of the nanocomposite film on the ITO/glass substrate, wet etching of the sensing film was performed by placing ITO/glass substrate in acetone for 10 sec. After etching in acetone, the morphological and structural study of the developed surface morphology was performed by field emission scanning electron microscopy (FE-SEM) and atomic force microscopy (AFM). The humidity sensors' electrical characterization was carried out in a humidity-controlled sealed chamber (dimensions 60 cm x 80 cm). The inlet and outlet valves connections were provided in the closed chamber to humid and dry air flows inside the chamber. To increase the relative humidity level (RH) inside the chamber, the chamber was connected with a commercially available Philips Respironics humidifier. The reduction in RH level inside the chamber was maintained by flowing nitrogen gas. The MS5308 LCR meter measured the capacitance and resistance of the fabricated sensors at different RH levels. The RS-6109 humidity meter was used as a

reference humidity sensor and placed within the closed chamber to monitor the RH and temperature levels. Figure 4-1(b) shows the schematic diagram of the characterization setup employed in this work.
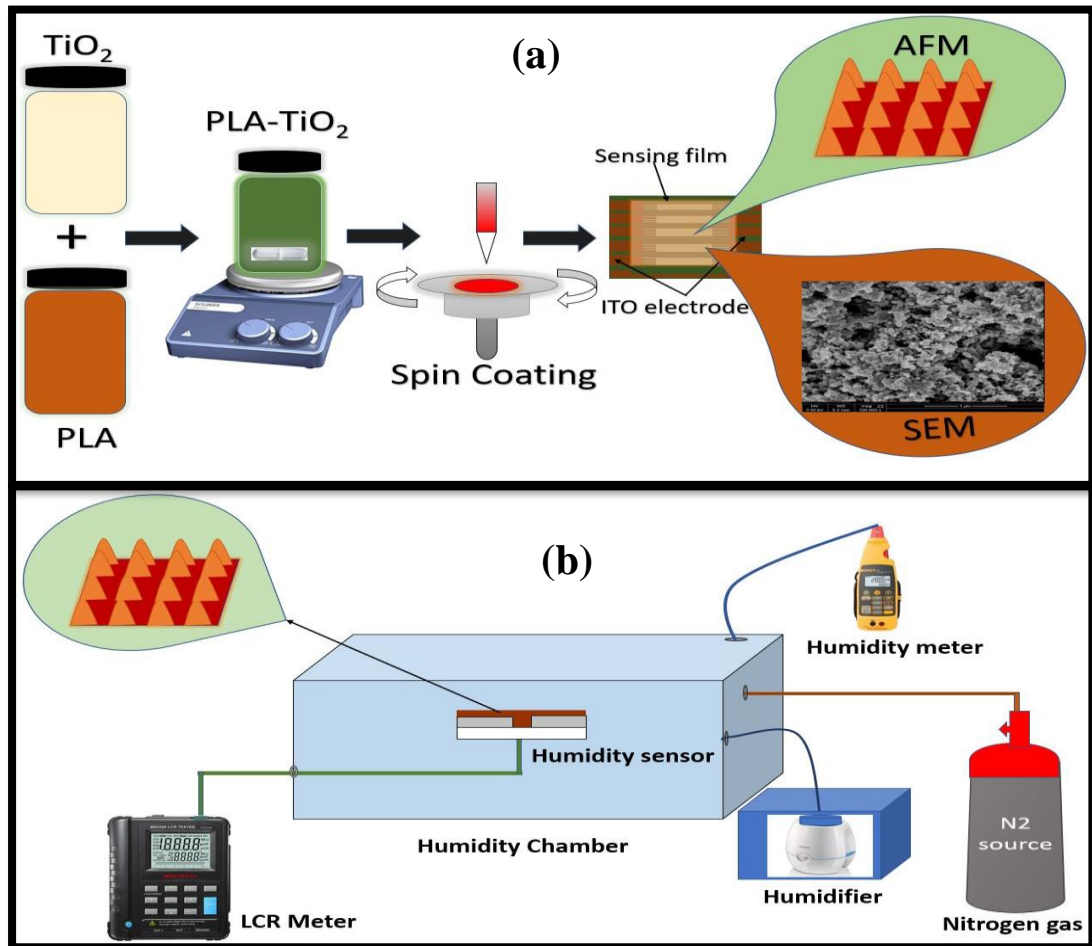
Figure 4-1. (a) Schematic diagram of the spin coating procedure for the fabrication of humidity sensors. (b) Schematic diagram of electrical characterization setup for the humidity sensors.

4.3. Thermal analysis:

The polymer nanocomposite material's thermal stability plays a key role in determining the conditions required for the device fabrication process and the applications in which the device can be employed. Differential Scanning Calorimetry (DSC) and Thermogravimetric analysis (TGA) were used to investigate the thermal stability and

thermal weight loss of materials. The Tm of pure PLA and PLA-TiO$_2$ nanocomposite

is presented in Figure 4-2(a). The Tm for PLA in TiO$_2$ composites and PLA alone was

144.34 °C and 149.60 °C, respectively. This decrease in the melting temperature of the

PLA nanocomposite is because TiO$_2$ nanoparticles disrupt the PLA chain structures'

regularity and increase the spacing between the chains. The exothermic peaks of the

PLA crystallization temperature Tc and glass Transition temperature Tg were 108.5 °C

and 50.9 °C, respectively. However, these peaks were not apparent for the PLA-TiO$_2$

nanocomposite. This may be due to the fact that the TiO$_2$ nanoparticles disrupt the PLA

chain structure and increase the spacing between the PLA molecular chain hence the

Tg and Tc for PLA disappear in the composite film [132]. In Figure 4-2(b), the TGA

curve shows the thermal weight loss of PLA-TiO$_2$ nanocomposite and pure PLA. It can

be observed that the initial onset decomposition temperature of pure PLA and PLA-

TiO$_2$ nanocomposite are ~200 °C and ~160 °C, respectively. The first step of weight

loss that started below 50 °C might be related to the vaporization of the solvent or

moisture, which remains even after drying the samples at room temperature. Figure 4-

2b shows that the final weight loss of the polymer nanocomposite remained well below

as compared to the PLA alone; this is because of the remaining of the TiO$_2$ particles.
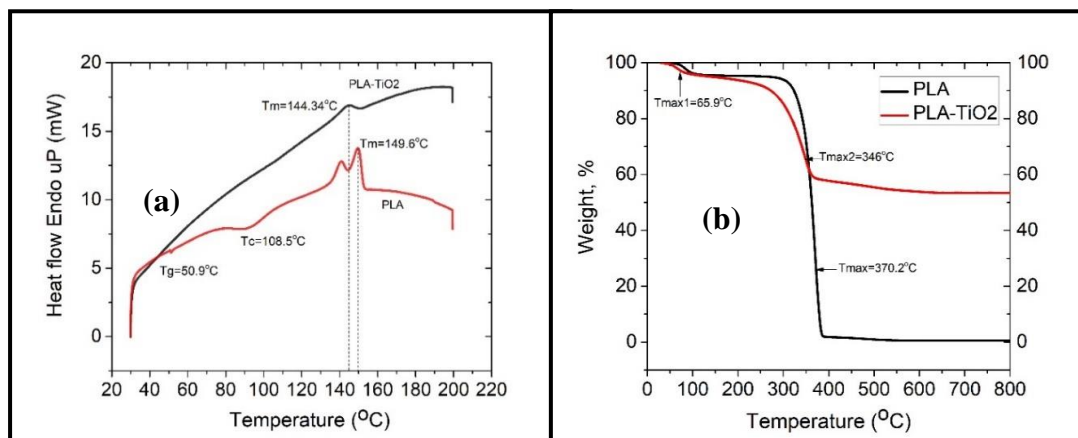
Figure 4-2. (a) DSC curve of pure PLA and PLA-TiO2 nanocomposite (b) TGA thermogram

of PLA and PLA-TiO2 nanocomposite.

4.4. Structural analysis:

Figure 4-3(a) shows the Raman spectra of the TiO_2, PLA, and PLA-TiO_2 nanocomposite films, respectively. In TiO_2, Raman analysis showed the Ti-O and the Ti-O-Ti absorption band appears between 200 cm^{-1} and 1000 cm^{-1}. PLA showed a strong C=O stretching band at 1784 cm^{-1} and a C-O stretching band at 1059 cm^{-1} and 113 cm^{-1} [133]. The symmetric and asymmetric stretching bands of C-H from CH3 group were observed at 2949 cm^{-1} and 2887 cm^{-1}, whereas their bending vibration was observed at 1462 cm^{-1}. No clear effect of TiO_2 nanoparticles on the Raman mode of PLA-TiO_2 composite has been observed. The only difference in the Raman analysis can be noticed in terms of Raman intensities. LA composite The X-ray diffraction patterns of PLA, TiO_2, and PLA-TiO_2 nanocomposite thin film in the range of $10°<2\theta<90°$ are described in Figure 4-3(b) respectively. X-ray diffraction patterns (XRD, Panalytical Empyrean model) employed $CuK\alpha$ radiation with a wavelength of 1.54056Å and an acceleration voltage of 45 kV with a step size 0.01313° and the time per step is 43.095 s. The TiO_2 nanoparticles showed peaks at 25.4°, 27.5°, 38°, 48.1°, 54.05°, 55.21°, 62.9°, 68.9°, 70.4°, 75.1°, and 82.9°, which correspond to the anatase phase of TiO_2 nanoparticles [134]. The XRD pattern of the PLA matrix showed a hump below 2θ ~20°, indicating the amorphous nature of PLA polymer film.
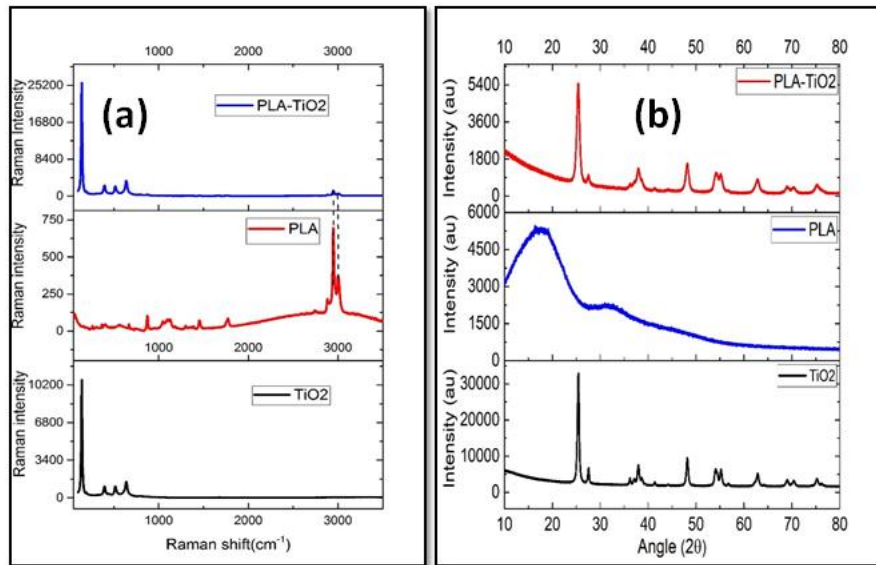
Figure 4-3. (a) Raman spectra of TiO_2, PLA and PLA-TiO_2 nanocomposite (b) XRD spectrum of TiO2, PLA and PLA-TiO_2 composite.

4.5. Morphological analysis of nanocomposite sensing film:

The morphological properties of a sensing film play a vital role in determining the sensitivity of a sensor. For instance, in humidity sensing, the adsorption of water vapor within the polymer matrix increases as the polymer film's porosity increases. The water entrapment is directly proportional to porosity. The AFM is used to study the sensing film's surface topography, whereas the FESEM is used to investigate TiO_2 nanoparticles' dispersion within the PLA matrix. The FESEM images in Figures 4-4(a) and 4-4(b) show the dispersion of TiO_2 nanoparticles on the surface of the PLA-TiO_2 nanocomposite film before and after acetone etching. After etching, TiO_2 nanoparticles agglomeration is reduced, and the nanoparticles become more uniformly dispersed. Figure 4-4(c) represents the AFM image of the PLA-TiO_2 nanocomposite before acetone etching. It is observed that the composite film's surface is not uniform (due to the aggregation of nanoparticles in PLA matrix), and rms roughness of the film was found to be 112.55 nm. However, Figure 4-4(d) shows that after etching with acetone,

TiO$_2$ nanoparticles seem to be well scattered (due to the etching of the PLA) and form a more porous surface. The rms surface roughness of the etched composite film was found to decrease significantly to 64.483nm. Even though the roughness seems to be reduced (due to the removal of extra PLA highland like shapes), the distribution of the nanoparticles (over the surface) in the composite increased as shown in FESEM. The even distribution of the nanoparticles increases the sensing film's surface area, which favors the adsorption and trapping of water vapors [135]. The above results indicate that PLA-TiO$_2$ nanocomposites film's surface after etching becomes more appropriate for moisture sensing applications. Nevertheless, it is essential to highlight that adjusting several parameters such as etching time can control the surface roughness. It is well established that nanocomposite films favor adsorption of water molecules and enhance a humidity sensor's sensitivity. This is because rough or uneven structures are developed on the composite films due to the nanoparticles' exitance. This rough and uneven surface is also consolidated by the AFM results obtained in Figure 4-4(d). The porosity of the composite has motivated us to investigate the sensing properties of the PLA and its composite with the TiO$_2$ nanoparticles.
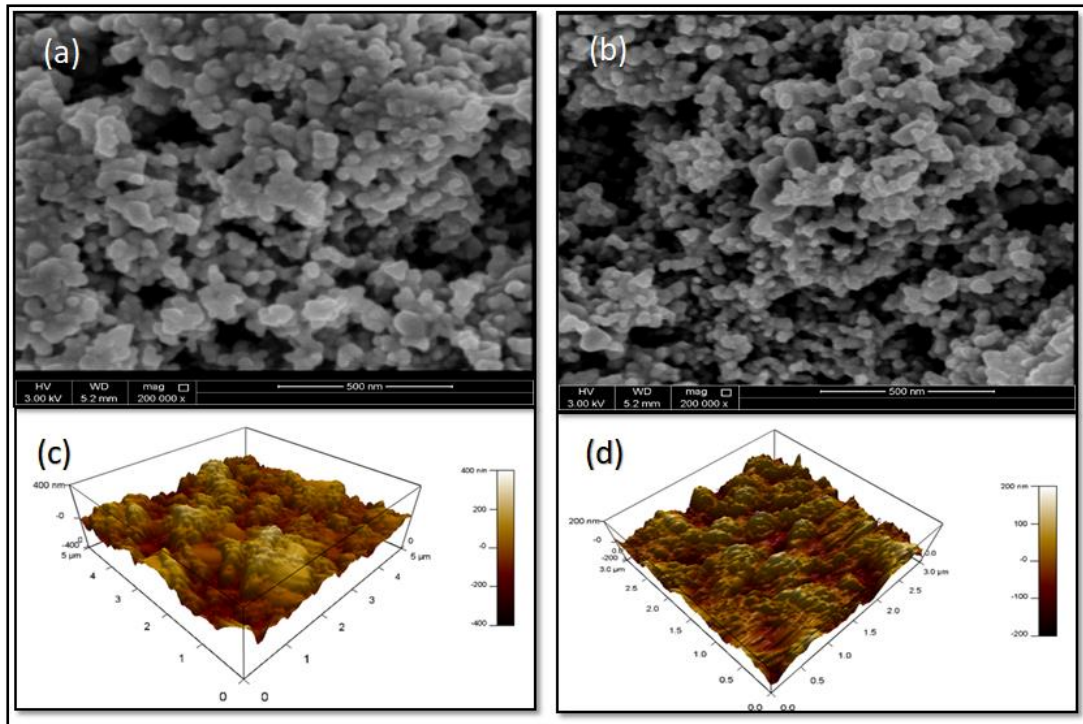
Figure 4-4. FESEM micro image of (a) un-etched surface of PLA-TiO2 nanocomposites film and (b) etched surface of PLA-TiO$_2$ nanocomposite film. AFM image of (c) un-etched surface of PLA-TiO$_2$ nanocomposites film and (d) etched surface of the PLA-TiO$_2$ nanocomposite film.

4.6.   Electrical Characterization:

The capacitance C of the proposed humidity sensors is directly proportional to dielectric permittivity ε, as shown in equation1. The permittivity of organic composites is approximately ~5, while the dielectric permittivity of water is approximately 80. As the moisture level increases, more water vapors are absorbed on the sensing film's surface, which increases the dielectric permittivity of the sensing film (PLA: TiO$_2$ nanocomposites); hence, it increases the sensitivity of the capacitive humidity sensor. In figure 4-5(a), the red line indicates no change in capacitance with respect to humidity levels in the case of unetched, while the black curve (etched sample) shows that as humidity increases, the capacitance also increases. This can be explained by the results obtained above where the PLA alone does not contain adsorption sites; it can be considered a binder or matrix to hold the nanoparticles. However, the porous surface

65

developed due to the nanoparticles in the composite is responsible for the humidity sensing of the composite system. The inset in Figure 4-5(a) shows the hysteresis of the PLA:TiO$_2$ capacitive humidity sensor. The maximum hysteresis of the proposed capacitive humidity sensor is around 12%. The response and recovery time are very important parameters to analyze the performance and practical implementation of humidity sensors. Figure 4-5(b) shows the response and recovery curve for the PLA: TiO$_2$ nanocomposite based capacitive humidity sensors. The average response and recovery times of the sensor found to be 40 sec and 20 sec, respectively. Figure 4-5(c) shows the comparison between the impedance spectra of the PLA: TiO$_2$ sensing film-based moisture sensors at 70 %RH and 90 %RH. As humidity level increases from 70 % RH to 90 %RH, the PLA's impedance: TiO$_2$ sensing film decrease hence increase in humidity level change the electrical response of the moisture sensor. To model the experimental results of the EIS analysis of the PLA: TiO$_2$ based moisture sensor, REAP2CPE equivalent circuit model applied shown in the inset of Figure 4-5(c). EIS results showed that the PLA-TiO$_2$ nanocomposite sensing films could also work as an impedance-based humidity sensor.
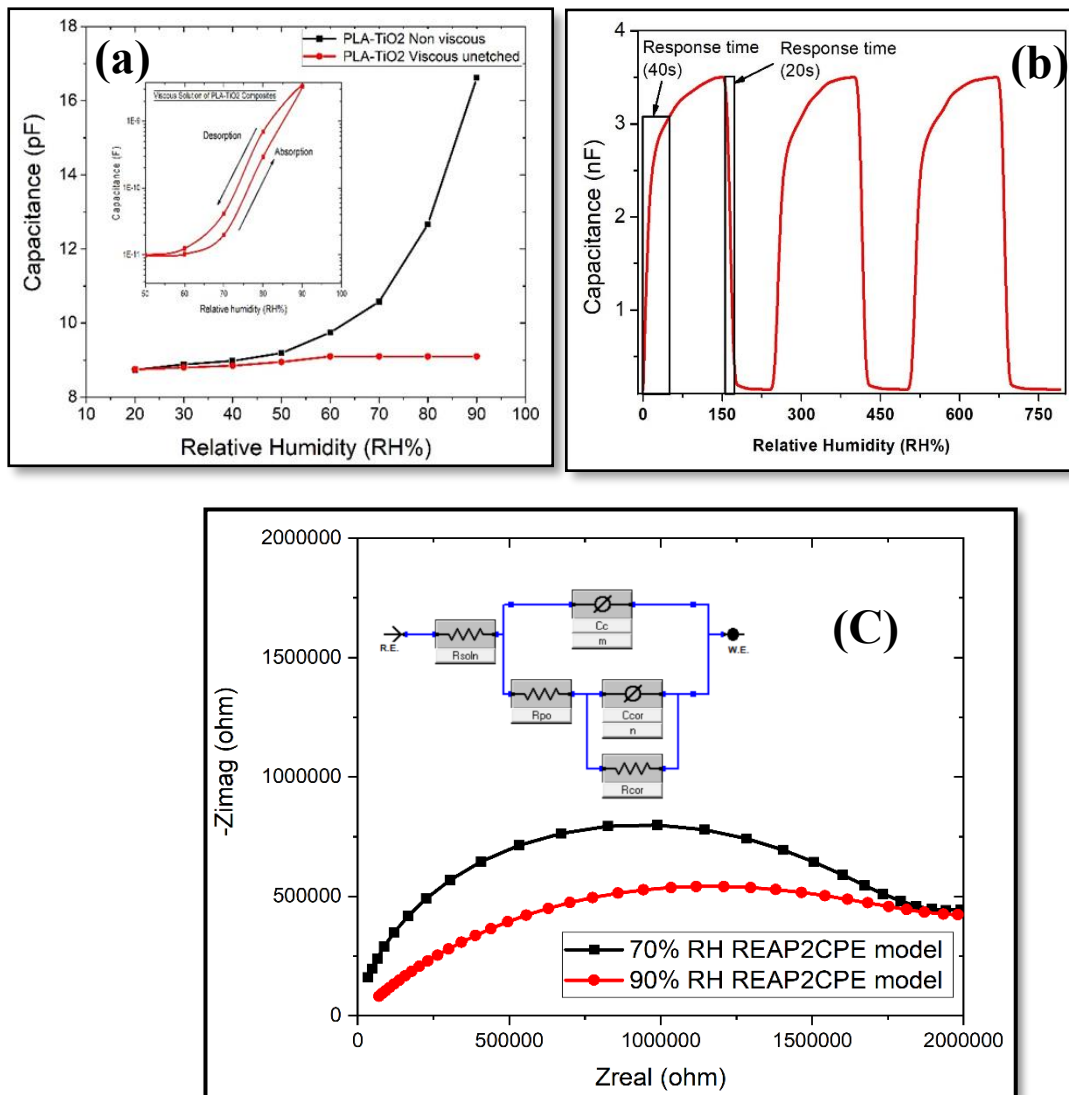
Figure 4-5. (a) Plots the capacitance vs. relative humidity levels for pristine and etched samples. (b) shows the response-recovery cycles (c) shows the Nyquist plot of the effect of relative humidity level using the REAP2CPE model and the REAP2CPE equivalent circuit model.

4.7. Conclusion and Summary:

We have studied the effects of TiO_2 nanoparticles on the structural, thermal, morphological, and electrical properties of PLA-TiO_2 composite film. The XRD pattern of PLA-TiO_2 composite film showed that the coexistence of PLA and TiO_2. The thermal analysis of PLA-TiO_2 composites showed TiO_2 nanoparticles slowing down the mobility of PLA molecular chains. The FESEM and AFM image of etched PLA: TiO_2 composites showed uniform dispersion of TiO_2 nanoparticles in the PLA matrix,

67

creating a porous structure on the surface composite film surfaces. Due to the porous structure developed at the PLA-TiO$_2$ sensing films, the response time of capacitive sensors is fast as compared to the recovery time of the sensors. Our study confirms that, with a modified surface, the PLA-TiO$_2$ nanocomposite sensing films showed superior morphological and electrical efficiency characteristics compared to PLA-TiO$_2$ pristine samples. It is observed from the electrical response that at a higher humidity level (above 70 %RH) sensor responds to nonlinear behavior. Also, the maximum hysteresis loss of the sensor is around 12%. Therefore, we need to improve the capacitive humidity sensor linearity at a higher humidity level and reduce the sensor's hysteresis loss.

CHAPTER 5: TO STUDY HYDROPHOBIC POLYMER FOR HUMIDITY SENSING APPLICATIONS

5.1. Introduction:

Our objective is to improve the capacitive humidity sensor's linearity at a higher humidity level and reduce the capacitive humidity sensor's hysteresis loss. For this purpose, we aim to study the hydrophobic polymers for humidity sensing applications in this research work. In the hydrophobic polymer, Polyvinylidene fluoride (PVDF) polymer has a high dielectric constant, thermally stable, and chemically resistive. To enhance the PVDF sensing characteristics, we need to improve the surface roughness and porosity of a PVDF film. Different methods are employed to enhance the surface morphology, which includes copolymerization, synthesis of composites, and blending techniques. However, nanoparticles' addition to the polymer matrix is widely used to improve nanocomposites' optical, electrical, and mechanical properties [4]. Shuai et al. [5] blended the Zno nanoparticles within the PVDF polymer and studied the PVDF membrane's hydrophilic and antifouling properties. This research work modified the hydrophobic PVDF film to a highly hydrophilic film surface prepared by incorporating TiO_2 nanoparticles with PVDF polymer. Sensing composite film hydrophilicity characterized by contact angle measurement method, the morphology of the composite film was studied by the SEM and AFM analysis, the thermal stability of sensing film was determined by the DSC and TGA analysis.

5.2. Synthesis of PVDF: TiO_2 nanocomposite:

The PVDF: TiO_2 composites synthesized in a two-step process. The 2.5 wt% solution of PVDF and 0.5 wt% TiO_2 were prepared in N, N-dimethylformamide (DMF) solvent, which can dissolve PVDF at room temperature [7]. Firstly, we placed the PVDF

polymer on the DMF solution which was placed for magnetic stirring for 6 hours so that PVDF dissolved in DMF. Secondly, we made the 0.5wt% of TiO_2 nanoparticle and dissolved in DMF solvent with constant magnetic stirring for 1hour at 500 rpm. After homogeneously mixing both PVDF and TiO_2 in DMF solvent separately, we mixed the prepared PVDF and TiO_2 solutions with (1:2) proportion by using glass syringes. After mixing the solutions, we placed the PVDF-TiO_2 composite solutions for magnetically stirring for 2 hours so that it will be mixed completely and form the uniform solution. To study the effect of different concentrations of PVDF on PVDF-TiO_2 composite surface roughness and humidity sensing characteristics, we prepared 2.5wt% PVDF and 5wt% PVDF solutions separately. We employed a spin coating technique to deposit the prepared PVDF-TiO_2 composite solution on the ITO/glass substrate. We have optimized both the rotation speed and rotation time. The rotation speed was set to 6000 rpm, and the optimized rotation time was (50sec). After depositing the nanocomposite sensing film on the interdigitated ITO/glass electrode, we placed the sensors on acetone for 20 sec so that we etched the surface of the sensing film. After the wet etching, the sensing film's hydrophilicity was analyzed by the contact angle measurement method, and the morphology of the developed rough sensing film was observed by atomic force microscopy and scanning electron microscopy. Figure 5-1 shows the schematic diagram of the humidity sensors fabrication process and the interdigitated ITO electrode structure.
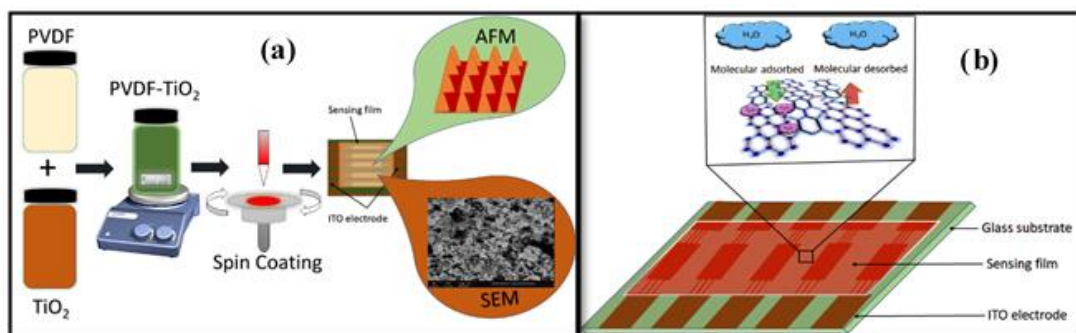
Figure 5-1. (a) Schematic diagram of the spin-coated PVDF-TiO2 moisture sensors and (b) ITO electrode active layer.

5.3. Thermal stability of nanocomposite film:

The thermal analysis test was carried out using DSC analysis to study the effect of the thermal stability of TiO_2 nanoparticles on PVDF-TiO_2 nanocomposite. The melting temperature (Tm) of PVDF powder and PVDF-TiO_2 nanocomposite is shown in Figure 5-2. The thermal behavior of PVDF and PVDF-TiO_2 composite showed a similar profile; however, it was observed that a small shift occurred in the melting temperature of PVDF and PVDF-TiO_2 composite. The Tm of PVDF powder was 161.68 °C and the Tm of PVDF-TiO_2 composite was 162.76 °C. The thermal transmission properties of TiO_2 nanoparticles hindered the decomposition of PVDF content and enhanced the stiffness of the PVDF polymer chain, and hence increased a little the melting temperature of the PVDF-TiO_2 composite [136]. Figure 5-2 (inset) represents the X-ray diffraction analysis of the nanocomposite film in the range of 10°<2θ<90°. The PVDF polymer powder form showed the reflection peaks occurring at 18.37°, 20.0°, 26.6°, and 38.6° that represent the (100), (020), (110), and (021) conventional peaks of the monoclinic α-phase crystal of the PVDF polymer [137, 138]. The XRD analysis of the PVDF-TiO_2 composite matrix showed that the X-ray diffraction peak intensity was reduced as TiO_2 nanoparticles incorporate within the PVDF matrix. The XRD spectrum

of the PVDF-TiO₂ composite with different TiO₂ concentrations showed that as the concentration of TiO₂ increased, the XRD peaks appear at 48.1°, 54.05°, 62.5°, which represent the anatase phase of TiO₂ nanoparticles [139].
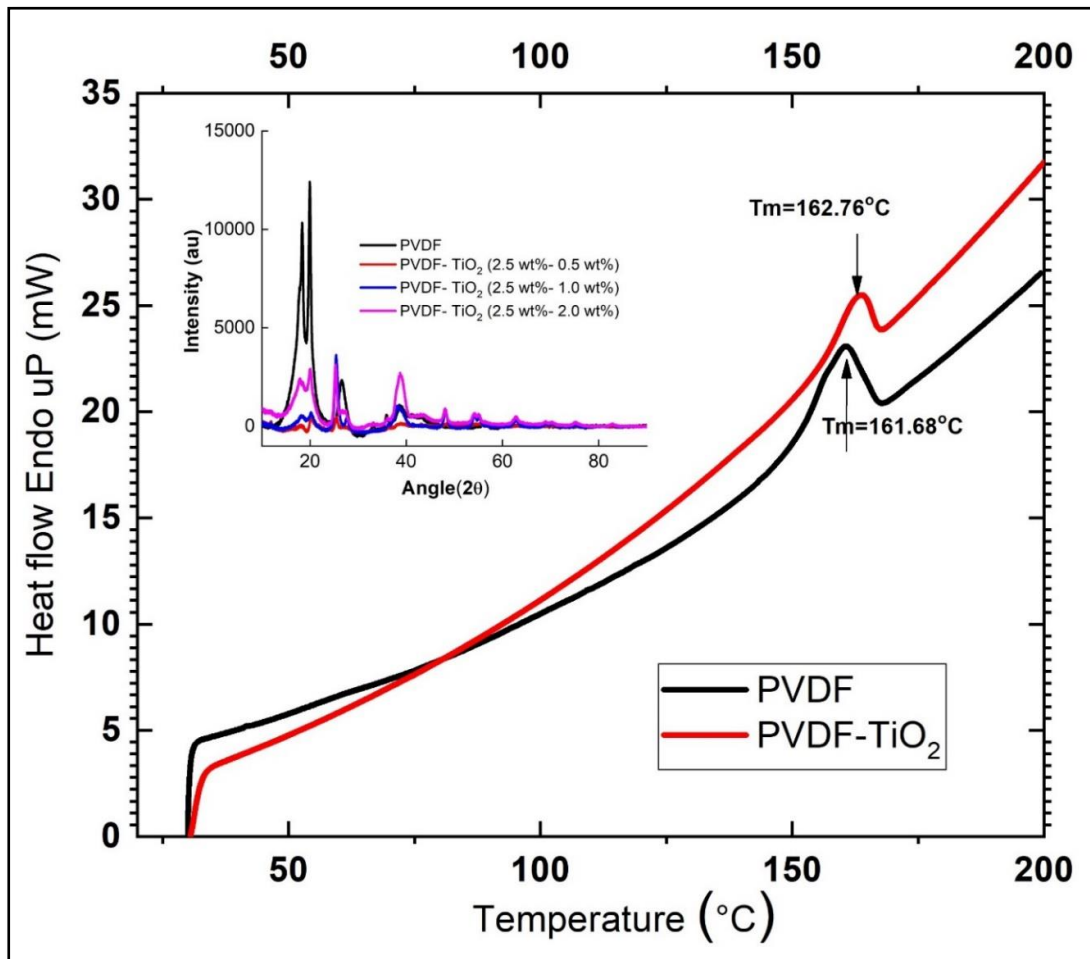
Figure 5-2. DSC curve of pure PVDF powder and PVDF-TiO2 nanocomposite. Inset show the XRD spectrum of 2.5 wt% PVDF, PVDF- TiO₂ (2.5 wt%- 0.5 wt%), PVDF- TiO2 (2.5 wt%- 1 wt%) and PVDF- TiO2 (2.5 wt%- 2 wt%).

The AFM and FESEM analysis were performed to study the polymer films' surface topography and examine nanofillers' effect on nanocomposite sensing films' surface. To study the effect of different concentrations of TiO₂ nanoparticles on the nanocomposite film roughness, we kept the concentration of PVDF fixed to 2.5 wt% in the nanocomposite and varied the concentration of TiO₂ nanoparticles. Figure 5-3 (a &

b) shows the AFM micrographs of the unetched and etched PVDF-TiO$_2$ (2.5 wt%- 0.5 wt%) nanocomposite films, respectively. The AFM image of 2.5 wt% of the PVDF-TiO$_2$ composite film after acetone etching (Figure 5-3b) shows rough surface morphology compared to the unetched and higher concentration of PVDF-TiO$_2$ composite film. Figure 5-3 (c & d) shows the AFM image of PVDF-TiO$_2$ composite films with different TiO$_2$ concentrations (1 wt% and 2 wt%) after etching in acetone. It was observed that as we increased the concentration of TiO$_2$ (0.5 wt% to 2 wt%) in PVDF-TiO$_2$ composites, the root means square (rms) roughness value increased from 24nm to 49.24nm. However, uniform distribution of the roughness was found in the samples with a TiO$_2$ concentration of 0.5 wt%. Therefore, for further investigation, the PVDF-TiO$_2$ (2.5 wt%- 0.5 wt%) nanocomposite was selected. The FESEM analysis was used to study the distribution of TiO$_2$ nanoparticles (at nanoscale) within the PVDF polymer matrix. Figure 5-3(e) shows the FESEM micrograph of the unetched PVDF-TiO$_2$ (2.5 wt% - 0.5 wt%), the accumulations of TiO$_2$ nanoparticles can be observed on the PVDF-TiO$_2$ nanocomposite sensing film. Figure 5-3(f) demonstrated the FESEM image of the PVDF-TiO$_2$ (2.5 wt% - 0.5 wt%) sensing film after treatment with acetone. It can be observed that after the etching of the nanocomposite, the TiO$_2$ nanoparticles seem to be well separated and exhibit more adsorption sites for water molecules.
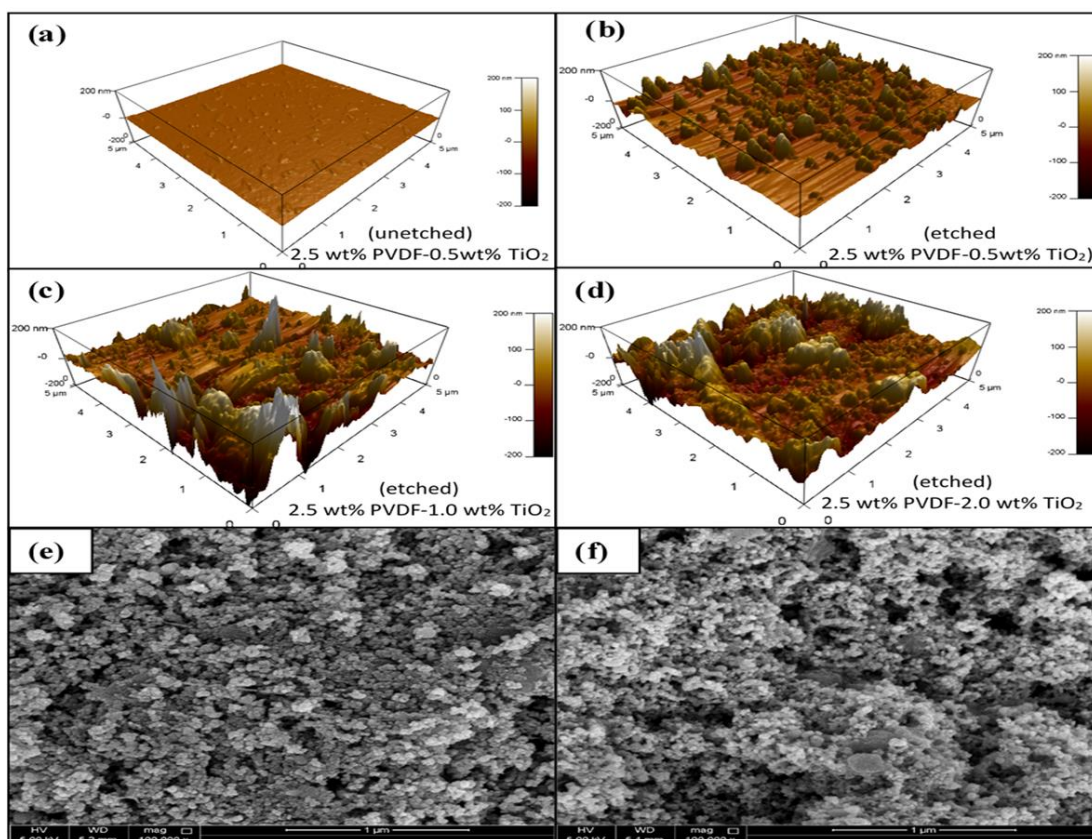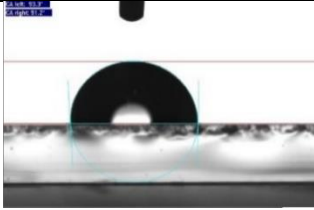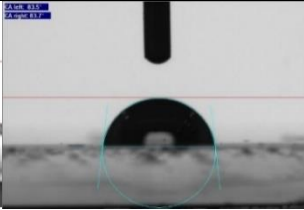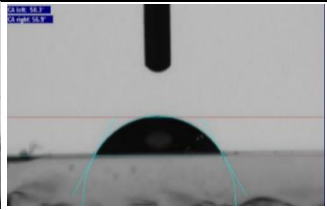
Figure 5-3. AFM and FESEM analysis of acetone etched and unetched PVDF-TiO$_2$ composite film with the different ration of the TiO$_2$ in the nanocomposite. (a) PVDF- TiO2 unetched (2.5 wt%‐ 0.5 wt%) (b) PVDF- TiO$_2$ etched (2.5 wt%‐ 0.5 wt%) (c) PVDF- TiO2 etched (2.5 wt%‐ 1 wt%) & (d) PVDF- TiO$_2$ etched (2.5 wt%‐ 2 wt%). FESEM micrograph of (e) PVDF- TiO$_2$ (2.5 wt%‐ 0.5 wt%) unetched surface of sensing film and (f) PVDF- TiO$_2$ (2.5 wt%‐ 0.5 wt%) etched nanocomposite films.

5.4.   Contact Angle Analysis:

The film's hydrophilicity indicates that the sensing film absorbed water drops on the polymeric film's surface. The contact angle of water drops on the sensing film's surface measured by the sessile drop method. Table 5-1 shows the contact angle measurements of the PVDF and PVDF-TiO$_2$ (2.5 wt%‐ 0.5 wt%) composite films. The contact angle of PVDF is 92.25°, which shows its hydrophobic nature. The PVDF-TiO$_2$ composite contact angle was 83.6°, which indicates that the addition of TiO$_2$ nanoparticles in the PVDF polymer enhanced the composite film's surface wettability and hence increased

its hydrophilicity. Acetone etching further decreased the contact angle to 57.6°. Increased hydrophilicity improved the water vapor absorption and settling at the surface of the nanocomposite film. An increase in the physisorption process at the sensing film's surface enhances capacitive humidity sensors' sensitivity.

Table 5-1. Contact angle measurement of PVDF film, PVDF-TiO$_2$ film, and acetone etched PVDF-TiO$_2$ film.

Sample Type	PVDF film	PVDF-TiO$_2$ composite film	Acetone etched PVDF-TiO$_2$
Image			
Contact Angle	92.25°	83.6°	57.6°

5.5. Humidity sensing Response:

The humidity sensing response of the PVDF-TiO$_2$ nanocomposite capacitive humidity sensor based is systematically investigated. Figure 5-4 shows the fabricated humidity sensors' capacitive response when the relative humidity (RH) level inside the humidity chamber was increased from 30 %RH to 80 %RH. In the nanocomposite, the concentration of TiO$_2$ is 0.5 wt% and PVDF concentration varied from 2.5 wt% (Figure 5-4(a)) and 5 wt% (Figure 5-4(b)), respectively. The change in electrical capacitance as a function of relative humidity shows that the 2.5 wt% PVDF-TiO$_2$ based capacitive humidity sensors are more linear and more sensitive compared to the 5 wt% PVDF-TiO$_2$ sensors. Figure 5-4(c) represents the response and recovery times of the fabricated PVDF-TiO$_2$ capacitive humidity sensors. These values were calculated to be 45 sec and 11 sec, respectively. The sensing film's hydrophilicity enhanced the absorption

mechanism on its surface, causing a reduction in its response and recovery times. The curve also shows that these results are repeatable and stable. The maximum hysteresis of the proposed humidity sensor was calculated to be 6%.
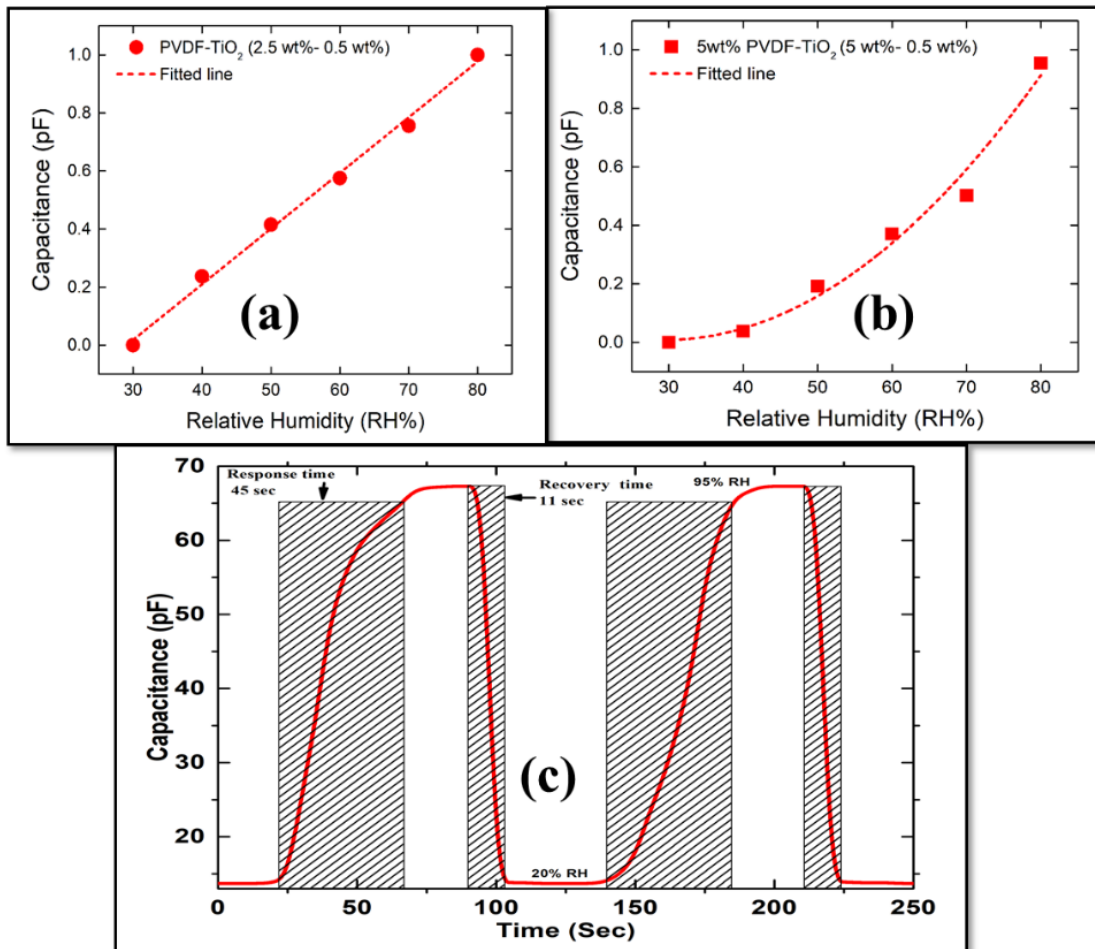
Figure 5-4. Capacitance vs Relative Humidity level for fabricated nanocomposite humidity sensors operate at 25 °C: (a) PVDF-TiO$_2$ (2.5 wt%- 0.5 wt%) (b) PVDF-TiO2 (5 wt%- 0.5 wt%) and (c) Response and Recovery time of the PVDF-TiO$_2$ (2.5 wt%- 0.5 wt%) nanocomposites-

5.6.   Conclusion and summary:

The effect of hydrophilic TiO$_2$ nanoparticles on the morphology and humidity sensing properties of the polyvinylidene fluoride titanium dioxide (PVDF-TiO$_2$) nanocomposites were investigated under a 30-80 % relative humidity (RH)

environment. The morphological study was performed by FESEM and AFM analysis, which confirmed that acetone etching developed surface roughness of the composite films. Optimization of PVDF concentration was achieved by using different concentrations of PVDF while maintaining the TiO_2 concentration. Results showed that the PVDF-TiO_2 (2.5 wt%- 0.5 wt%) based capacitive humidity sensors demonstrated linear response and increased sensitivity as compared to the PVDF-TiO_2 (5 wt%- 0.5 wt%) sensors over the whole investigated RH range. The response and recovery times of the optimized sensors were 45 sec and 11 sec, respectively. The optimized sensors showed a ~6% average hysteresis loss. The capacitive humidity sensor showed a linear response with respect to change in humidity level, as shown in the electrical characterization of the PVDF-TiO_2 humidity sensor. However, the hysteresis loss is still relatively high, which needs to reduce. Therefore, further investigation of PVDF polymer is required to improve the capacitive hysteresis of the humidity sensor.

CHAPTER 6: TO STUDY THE IMPACT OF PIEZOELECTRIC

NANOPARTICLES WITHIN HYDROPHOBIC POLYMER

6.1. Introduction:

In chapter 5, we have investigated the PVDF-TiO$_2$ nanocomposite for humidity sensing applications. We have achieved a linear response at a wider humidity range. However, they exhibit higher hysteresis loss. In this phase, our objective is to reduce the hysteresis loss of the PVDF based capacitive sensor. For this purpose, we will investigate the effect of piezoelectric nanoparticles within the PVDF polymer matrix on dielectric properties, thermal stability, and humidity sensing properties. Among the piezoelectric materials, BaTiO$_3$ is an excellent candidate for capacitive sensors because of its high dielectric constant, good ferroelectric properties, high hydrophilicity, and good thermal stability. Zhou et al. [140] studied the dielectric properties of the PVDF-surface-hydroxylated BaTiO$_3$. They reported a high dielectric constant and lower dielectric loss for the PVDF-BaTiO$_3$ nanocomposite film. Chanmal et al. [141] prepared the PVDF-BaTiO$_3$ nanocomposite by melt compounding method and observed that by increasing the concentration of BaTiO$_3$, the dielectric property of the nanocomposite film could be improved. A systematic study is conducted herein to enhance the hydrophilicity and surface morphology of the PVDF-BaTiO$_3$ nanocomposite film-based capacitive humidity sensors while retaining the thermal stability and dielectric properties.

6.2. Experimental Details:

The PVDF-BaTiO$_3$ nanocomposites solution was prepared in a two-step. First, the PVDF with a concentration of 2.5 wt% was placed in N, N-dimethylformamide (DMF) solvent. After 6 hours of continuous magnetic stirring at 500 rpm PVDF dissolves in DMF solvent. After that, 0.5 wt% of BaTiO$_3$ were prepared in the DMF solvent

separately. The respective BaTiO$_3$-DMF solutions were also left for magnetic stirring at 500 rpm for 60 minutes. The two individual solutions were homogeneously dissolved after that 2.5 wt% PVDF, and 0.5 wt% of the BaTiO$_3$ were mixed to 1:2 ratio via glass syringes manufactured by Osilla. The mixed PVDF- BaTiO$_3$ solutions were set for magnetic stirring at 500 rpm for 2 hours so that PVDF and BaTiO$_3$ thoroughly blend. For the deposition of the PVDF-BaTiO$_3$ composite solution on the ITO/glass electrode (from Osilla), the spin coating technique was employed. An optimization process for the rotation speed and the rotation time to form an even equilateral spread of the solution were done. The rotation speed and rotation time were optimized to 6000 rpm and 50 seconds. The electrodes with the deposited composites were then etched in acetone for 20 seconds. Acetone has low solubility to PVDF [142]; therefore, it modifies the sensing film's surface and develops a rough and uneven structure on the sensing film's surface. To analyze the effect of different concentrations of BaTiO$_3$ on PVDF-BaTiO$_3$ nanocomposite hydrophilicity, surface roughness, dielectric properties, and humidity sensing characteristics, we prepared 0.5 wt %, 1wt%, and 2 wt% of BaTiO$_3$ separately and kept the PVDF concentration constant at 2.5 wt%. Figure 6-1 shows the schematic diagram of the humidity sensors fabrication process.
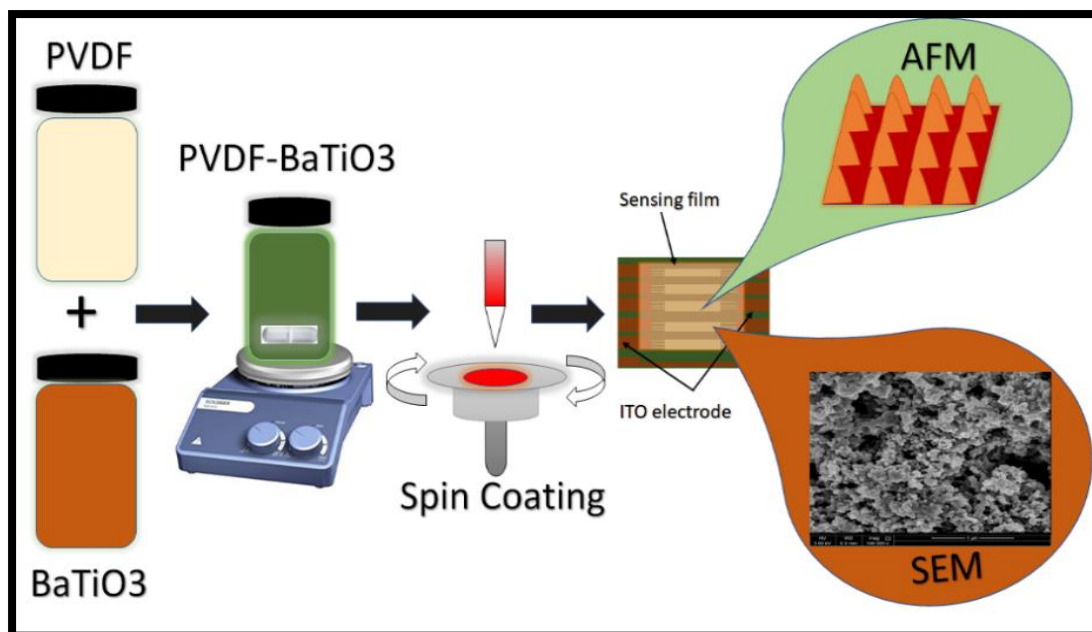
Figure 6-1. Schematic diagram of the spin-coated PVDF-BaTiO$_3$ humidity sensors.

FESEM analysis of the composite sensing films was performed to investigate the sensing film morphology, an important characteristic of the humidity sensor. The water vapor absorption is directly related to the sensing film's surface roughness, porosity, and hydrophilicity. FESEM images of the PVDF-BaTiO$_3$ composite films with three different concentrations (0.5, 1, and 2 wt%) of the PVDF-BaTiO$_3$ composite are shown in Figure 6-2. The PVDF concentration is maintained constant at 2.5 wt% in the composite film, but the BaTiO$_3$ concentration is varied (0.5, 1, and 2 wt%). Figure 6-2(a) shows that the BaTiO$_3$ particles are almost entirely buried in the PVDF matrix, while in Figure 6-2(b), the BaTiO$_3$ particles are well-spread, and a regular rough surface is observed. However, the BaTiO$_3$ microparticles agglomerate at the surface of the composite film (Figure 6-2(c)). Therefore, the PVDF-BaTiO$_3$ composite with 1 wt% BaTiO$_3$ (Figure 6-2(b)) concentration is selected for further investigation. The uniform distribution of the BaTiO$_3$ microparticles in the sensing film can facilitate water molecules' entrapment over the sensing film's surface and enhance the humidity sensors'

sensitivity.
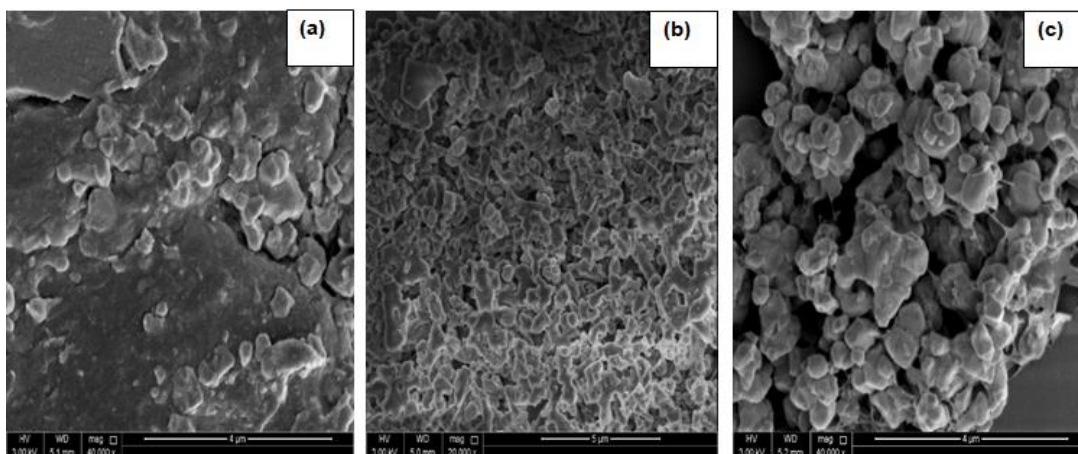
Figure 6-2. FESEM images of the PVDF-BaTiO₃ composite films with different concentrations of BaTiO₃: (a) 0.5 wt%, (b) 1 wt%, and (c) 2 wt%.

6.3. Structural and thermal stability of composite film:

Figure 6-3 shows the XRD data of the composite films in the $15° < 2\theta < 90°$ range. XRD analysis of the nanocomposite films reveals that the reflection peaks are observed at 22.30°, 31.51°, 39.38°, 45.86°, 51.16°, 66.19°, 70.47°, 75.24°, 79.51°, and 83.62°, corresponding to the typical (100), (101), (111), (200), (201), (211), (202), (103), (230), (311), and (222) peaks of the barium titanate, respectively [143]. The peak at $2\theta = 20.3$ corresponds to PVDF [144]. To determine the effect of $BaTiO_3$ on the thermal stability of the PVDF-BaTiO₃ composite, thermogravimetric analysis (TGA) was performed. The inset in Figure 6-3 shows the weight losses in the PVDF powder and PVDF-BaTiO₃ composite. Both thermograms exhibit almost similar behaviors; the weight loss of the PVDF-BaTiO₃ composite is less than 30% (~ 500 °C), whereas, for the PVDF powder, the weight loss is almost 60% at the same temperature. The final weight loss in the composite remains lower than the weight loss observed in the case of the only PVDF.

At 800 °C, the total thermal weight loss of PVDF is 78% in comparison to 34% for PVDF-BaTiO$_3$ composite. This is because of the remaining BaTiO$_3$ particles, which have high thermal stability compared to PVDF. The 1st step of weight loss in the PVDF-BaTiO$_3$ composite film starts at ~100 °C can be due to the evaporation of moisture or solvent that remains even after drying the samples at room temperature.
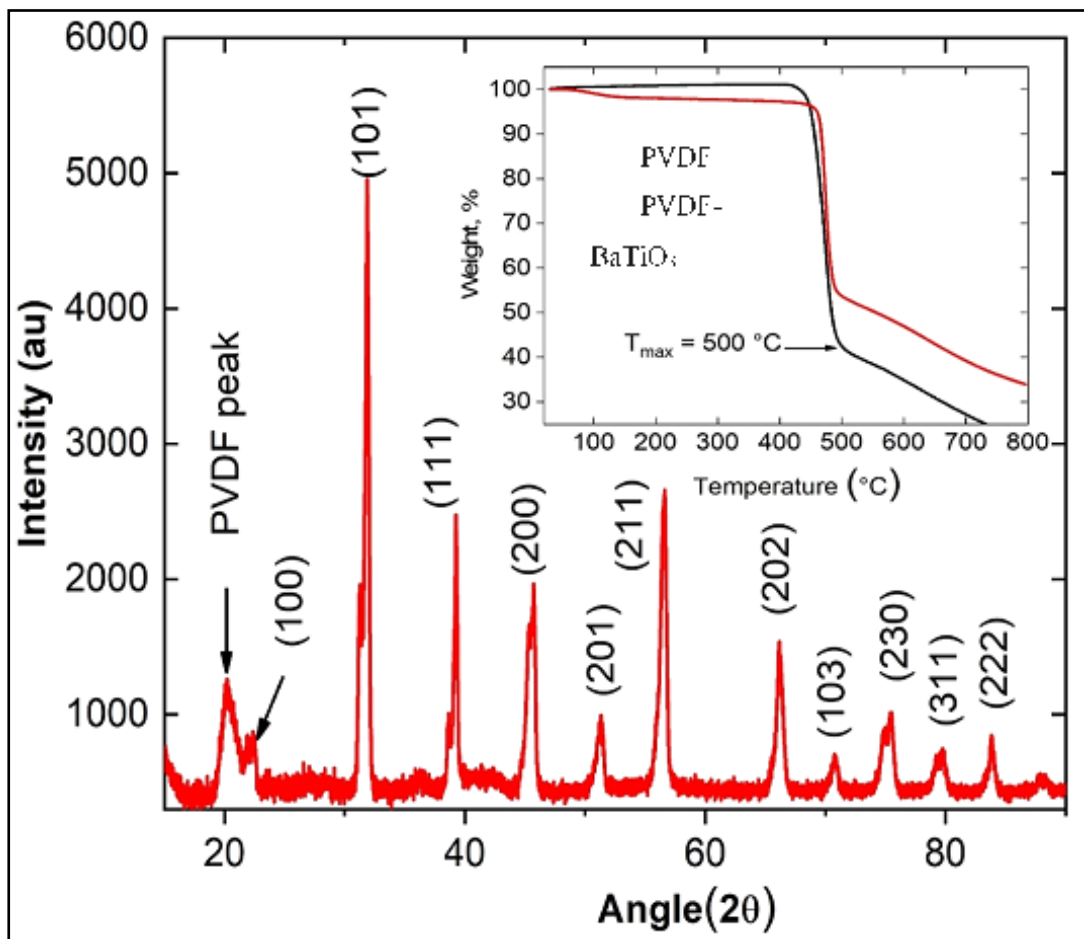
Figure 6-3. XRD pattern of the PVDF-BaTiO$_3$ composite films at room temperature (25 ± 1 °C). The inset shows the TGA thermograms of PVDF and PVDF-BaTiO$_3$ composite.

Dielectric Study of Composite film:

The dielectric properties were measured by using the Novocontrol technology Broadband dielectric spectrometer. The experiments were conducted at room

temperature over a broad frequency range (101 Hz to 106 Hz). Figure 6-4 shows the variation in dielectric properties of the PVDF polymer and PVDF-BaTiO$_3$ nanocomposite film as a function of frequency. The dielectric properties of PVDF-BaTiO$_3$ composite film demonstrate a similar behavior as compare to the PVDF polymer film. Figure 6-4(a) shows the dielectric constants (ε') of PVDF and PVDF-BaTiO$_3$ composite. As expected, the introduction of BaTiO$_3$ particles increases the dielectric constant of the PVDF-BaTiO$_3$ nanocomposite film. The dielectric constant is slightly high in the low-frequency region and decreases with an increase in frequency from 101 to 106 Hz; this may be due to the polarization relaxation effects. As the electric field is applied at low frequencies, the accumulation of charges increases the interfacial polarization. However, in the high-frequency region, the interfacial polarization decreases as the charge carrier do not align with the applied electric field, and the dielectric constant decreases. At 10 kHz, the dielectric constant of the PVDF film is 2.07. The addition of BaTiO$_3$ microparticles (1 wt%) within the PVDF matrix increases the composite film's dielectric constant to 2.46. This increase in dielectric constant improves the capacitance of the film. The dielectric loss (ε'') describe as the energy dissipation in a dielectric material through conduction loss, dipolar loss, and interfacial polarization [145]. Figure 6-4(b) shows the dielectric loss (ε'') of PVDF and PVDF-BaTiO$_3$ composite as a function of frequency. At lower frequency regions, dielectric loss is due to the interfacial polarization and conductivity; however, the dielectric loss at a higher frequency is associated with dipolar relaxation[146]. At 10 kHz, the dielectric loss of PVDF film measure to be 0.01; however, the introduction of BaTiO$_3$ microparticles (1wt%) within the PVDF film increases the dielectric loss of the nanocomposite film to 0.019.
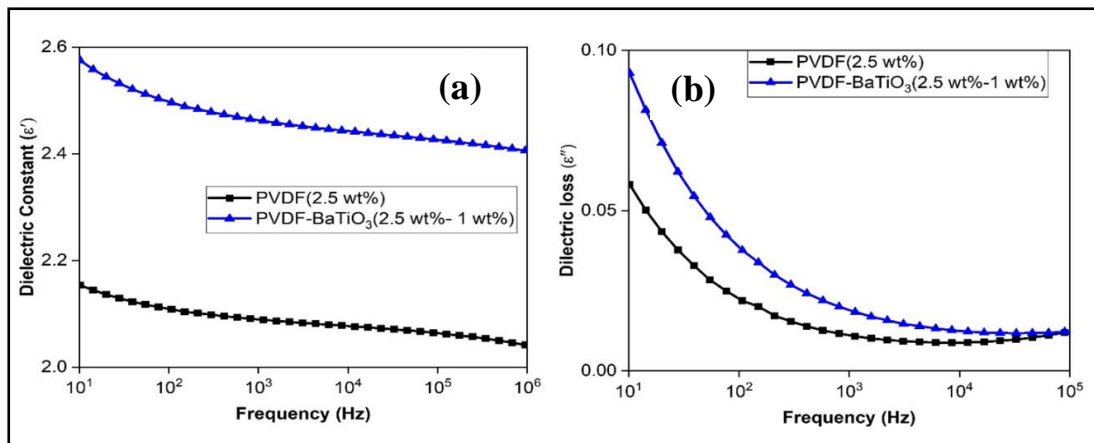
Figure 6-4. Variation in (a) dielectric constants (ε') and (b) dielectric losses (ε'') of PVDF and PVDF-BaTiO$_3$ composite films with frequency. Both measurements were recorded at 25 °C.

6.4.   Electrical Response:

The increase in humidity level allows more water absorbed on the sensing film's surface, which increases the capacitance of the sensors that can be observed in figure 6-5. The capacitive response of PVDF-BaTiO$_3$ nanocomposite sensors with different concentrations of BaTiO$_3$ shown in figure 6-5(a). Nanocomposites with 2 wt% BaTiO$_3$ concentration show a sharp increase in capacitance response above 80 %RH, indicating a nonlinear response at higher humidity level. The nanocomposite film with 0.5 wt% BaTiO$_3$ concentration shows low sensitivity to change in humidity level. The 2.5 wt% PVDF- 1 wt% BaTiO$_3$ nanocomposite based capacitive sensors shows a stable and linear capacitive response (figure 6-5b). Figure 6-5(b) shows the adsorption and desorption characteristics of the 2.5 wt% PVDF- 1 wt% BaTiO$_3$ nanocomposite based capacitive sensors. The adsorption and desorption curves represent the hysteresis response of the sensor. The maximum hysteresis of the capacitive PVDF-BaTiO$_3$ (2.5 wt%- 1 wt%) humidity sensor is ~2.5% at 60 %RH. The inset in figure 6-5(b) shows the response and recovery times of the fabricated PVDF-BaTiO$_3$ capacitive humidity

sensor, which is calculated as 40 s and 25 s, respectively.
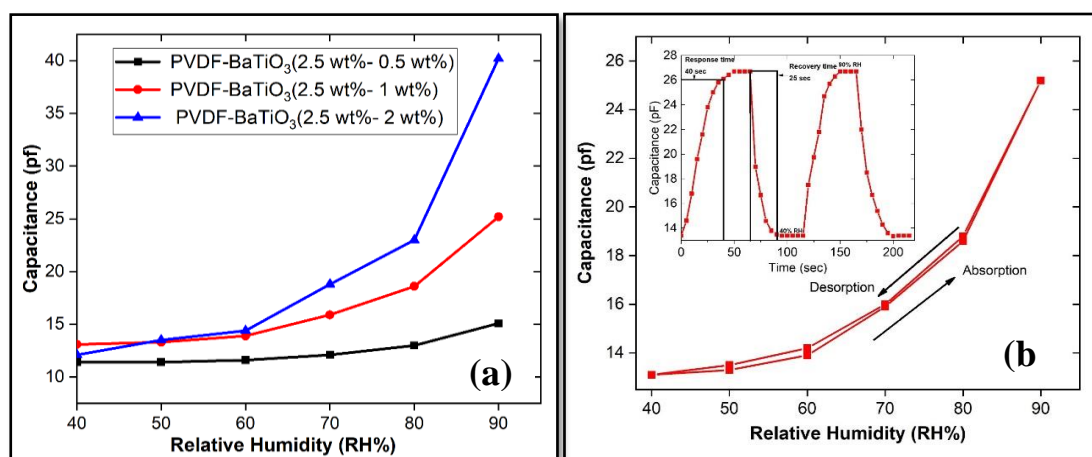
Figure 6-5. Capacitance vs. relative humidity levels for PVDF-BaTiO$_3$ composite sensors with different concentrations of BaTiO$_3$ (0.5, 1, and 2 wt%) (b) Hysteresis response PVDF-BaTiO$_3$ (2.5 wt%-1 wt%) with inset shows the response and recovery time of the composite.

6.5.   Conclusion and Summary:

BaTiO$_3$ microparticles' effect on the thermal stability, morphology, hydrophilicity, and humidity sensing response of the PVDF-BaTiO$_3$-based humidity sensor is investigated at 40–90% relative humidity level. PVDF-BaTiO$_3$ (2.5 wt%-1 wt%) composite films exhibit regular and even distribution of BaTiO$_3$ in the composite films in comparison to the composite films with other ratios of PVDF and BaTiO$_3$. The composite films' wettability analyses show that acetone treatment reduces the contact angle and enhances the films' hydrophilicity. The dielectric study of the composite film demonstrates that the addition of BaTiO$_3$ increases the dielectric constant and decreases the dielectric loss. PVDF-BaTiO$_3$ (2.5 wt%-1 wt%) composite-based humidity sensors exhibit a stable and more linear capacitive response with reduced hysteresis over the 40–90 % RH range in comparison to the sensors with 0.5 and 2 wt% of BaTiO$_3$. The optimized capacitive sensor shows 2.5% maximum hysteresis.

CHAPTER 7: TO BLEND THE POLYMERS AND STUDY THE ELECTRICAL RESPONSE OF THE HUMIDITY SENSOR.

7.1.   Introduction:

Our objective is to investigate how to enhance the resistive humidity sensor sensitivity at lower humidity levels in this phase. The sensing film's essential property is its electrical conductivity and hydrophilicity. Different methods are used to enhance the hydrophilicity and electrical conductivity of polymeric films. The blending of polymers, which have unique characteristics, is a well-known method to improve the sensing film's mechanical and electrical properties [86]. Poly ether ether ketone (PEEK) is a high-performance polymer that has excellent mechanical properties, thermally stability, and chemical resistance [147, 148]. The sulfonation of PEEK is a well-established method to improve the sensing film's hydrophilicity and proton conductivity [124, 149]. The sulfonation occurs by introducing the hydrophilic sulfonic groups (SO3H) within the PEEK. The sulfonation of polymer significantly improves the adsorption of water molecules and proton conductivity, increasing the sensitivity of the humidity sensors [125]. Carretta et al. [150] prepared the sulfonated poly (styrene) (SPS); they observed that the casting of the sulfonic group improves the proton conductivity of the membrane. Rubinger et al. [151] fabricated resistive humidity sensors by depositing sulfonated poly (styrene) (SPS) on a ceramic substrate using the dip-coating method, and they reported a higher desorption time (around 5 min) as a result of sulfonation. Zhuang et al. [43] investigated the sulfonated poly (ether ether ketone) (SPEEK) based resistive humidity sensors, and they observed that the sulfonation degree plays a crucial role in improving the humidity sensitivity of the PEEK. Resistive humidity sensors based on hydrophilic polymers are easily dissolved in water, as the sensors are exposed to high humidity levels. Resistive sensor's accuracy

and stability degrade with time, and sensors don't exhibit repeatable and stable response [152, 153]. Therefore, to improve the stability and durability of resistive humidity sensors, we need to blend SPEEK with a polymer that is mechanically and thermally stable and improves the sensitivity of the humidity sensor. In this study, PVDF is blended with different concentrations of SPEEK to enhance the sensitivity of the resistive humidity sensor.

7.2. Preparation of PVDF-SPEEK blend solution:

The PVDF-SPEEK blended solution was prepared in a two-step process. First, the PVDF with a concentration of 2.5 wt% placed in the DMAC solvent. PVDF dissolves in DMAC solvent after 5 hours of continuous magnetic stirring at 500 rpm. Different concentrations of SPEEK (1 wt%, 3 wt%, 5 wt%, 7.5 wt%, 10 wt%, and 15 wt%) were prepared separately in the DMAC solvent. To dissolve SPEEK completely in DMAC, it needs stirring at 500 rpm for 6 hours. PVDF and SPEEK solutions in DMAC are then mixed in a 1:2 volumetric proportion. Again, the mixed solution was stirred magnetically for 3 hours to ensure thorough blending of the PVDF and SPEEK solutions. The fabrication processes involved in this study are schematically represented in Figure 7-1.
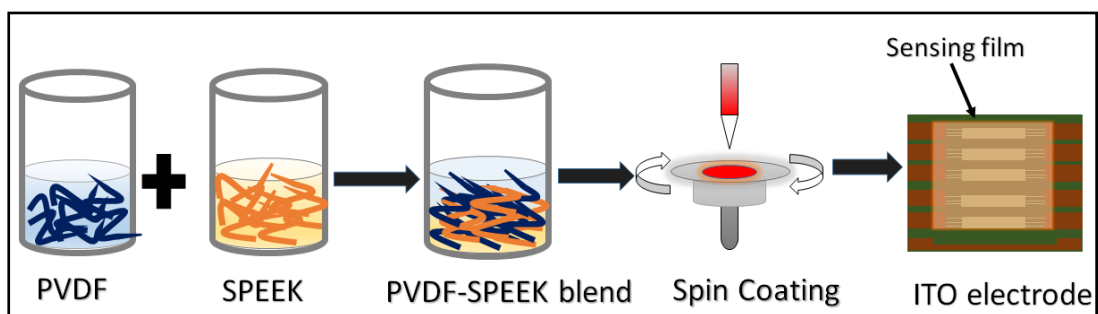
Figure 7-1. Graphical representation of the blending of PVDF and SPEEK and deposition of the sensing film using a spin coating technique.

7.3.   Morphological Analysis:

Morphology of the PVDF-SPEEK blend film determines the distribution of SPEEK within the blend film matrix, the morphological study of the PVDF-SPEEK blend film performed by FESEM analysis. Figure 7-2 determine the SEM analysis of PVDF-SPEEK blend with different concentration of SPEEK. Figures 7-2(a) and 7-2(b) shows the FESEM analysis of PVDF-SPEEK blend film with a concentration of SPEEK is 5wt% and 7.5 wt%. The FESEM analysis reveals that PVDF-SPEEK (5 wt% and 7.5 wt%) blend film has a uniform distribution of SPEEK with film surface is defect free. Figures 7-2(c) and 7-2(d) determine the FESEM analysis of PVDF-SPEEK blend film with a concentration of SPEEK is 10 wt% and 15 wt%. The FESEM analysis shows that as the concentration of SPEEK increases within the blend membrane, the spherical structures appear on the film's surface. Due to the higher concentration of SPEEK higher amount of sulfonic group (SO_3H) presents on the blend membrane, which may form the spherical formation [154].
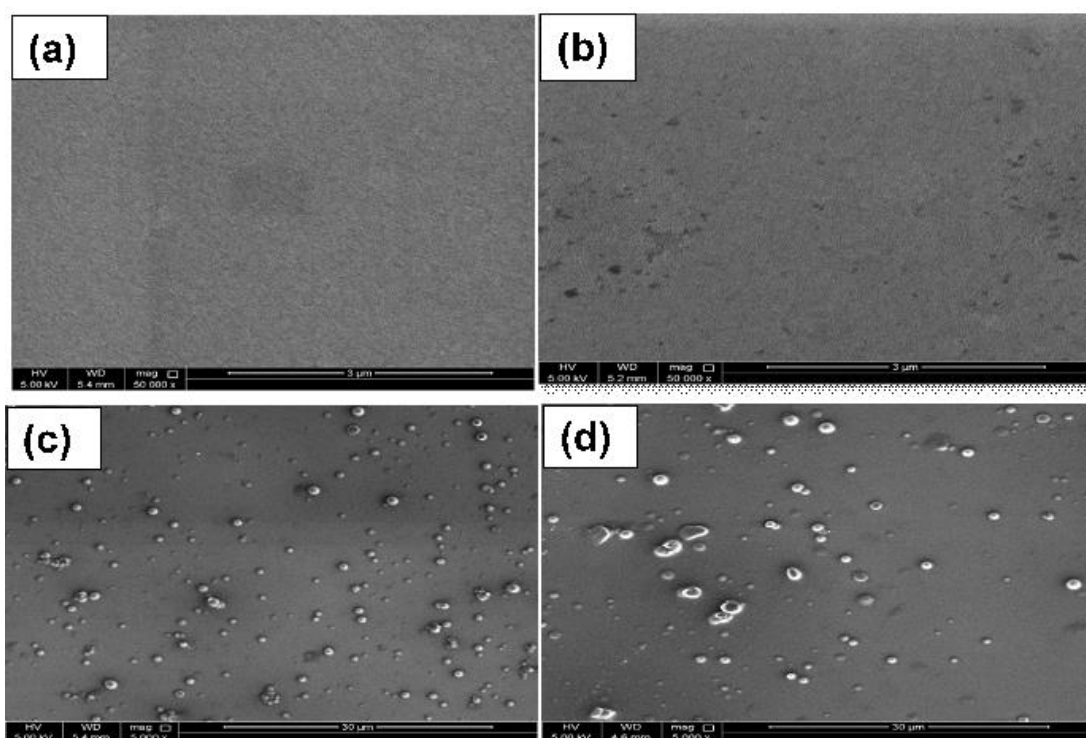
Figure 7-2. FESEM micrographs of PVDF- SPEEK blend films with SPEEK concentrations of (a) 5 wt%, (b) 7.5 wt%, (c) 10 wt%, and (d) 15 wt%.

AFM analysis was conducted further to examine the surface roughness and topography of PVDF- SPEEK blend with different concentrations of SPEEK (5, 7.5, 10, and 15 wt%). Figure 7-3(a) represents the AFM image of the PVDF-SPEEK blend (2.5 wt%-5 wt%). It is observed that the surface of the blend film is uniform and homogenous. The root means square (rms) roughness value of PVDF-SPEEK (2.5 wt%- 5 wt%) was found to be 9.54 nm. As the concentration of SPEEK increases to 7.5 wt% (7-3(b)), 10 wt% (7-3(c)), and 15 wt% (7-3(d)), the rms roughness value of the sensing film increases to 14.974 nm, 35.267 nm, and 39.74 nm, respectively. However, at higher concentrations of SPEEK, due to the poor dispersion of PVDF and SPEEK blends, the blend membrane's surface becomes non-homogeneous and irregular. Therefore, based on FESEM and AFM analysis, PVDF-SPEEK (2.5 wt%- 5 wt%) blend films are selected for further investigations.
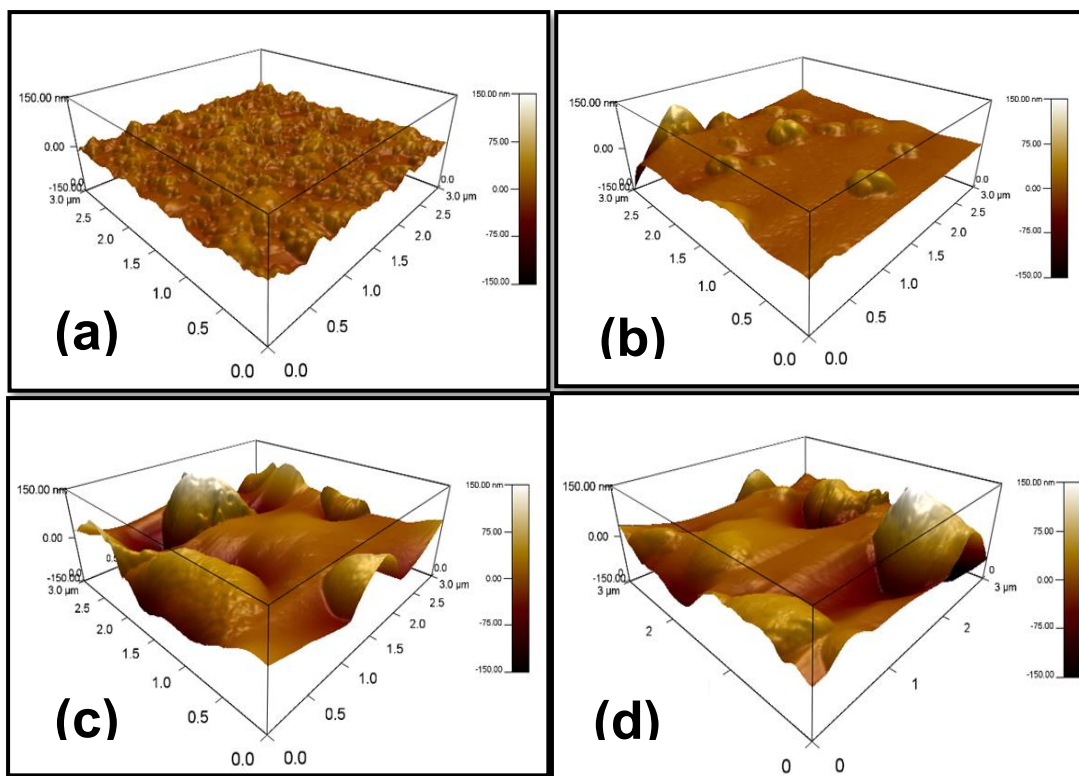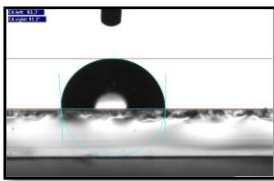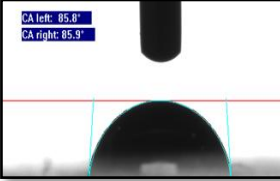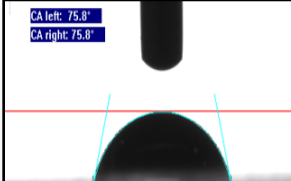
Figure 7-3. Shows the AFM image of the PVDF- SPEEK blend films with SPEEK concentrations of (a) 5 wt%, (b) 7.5 wt%, (c) 10 wt%, and (d) 15 wt%.

7.4.   Contact Angle Measurement:

The film's hydrophilicity indicates that the sensing film adsorbs water drops on the polymeric film's surface. The contact angle of water drops on the sensing film's surface measured by the sessile drop method. Table 7-1 shows the contact angle measurements of the PVDF, PVDF-SPEEK blend films with SPEEK concentrations of 1 wt% and 5 wt%. The contact angle of pure PVDF is 92.25° shows its hydrophobic nature. As the SPEEKblended with PVDF, the hydrophilicity of the PVDF-SPEEK blend film increases. The contact angle of PVDF-SPEEK (2.5 wt%, 1 wt%) blend film decrease to 85°. As the concentration of SPEEK increases further to 5 wt%, its contact angle decreases to 75.8°. This decrease in the PVDF-SPEEK blend film's contact angle is

mainly associated with the increase in the sulfonic group in the PVDF-SPEEK blend. The sulfonic group is hydrophilic; hence, the addition of SPEEK increases the water adsorption affinity on the PVDF-SPEEK blended film's surface, which is in agreement with the TGA results.

Table 7-1. Contact angle measurements of PVDF film and PVDF-SPEEK blend films with SPEEK concentrations of 1 wt% and 5 wt%.

Sample	PVDF Film	PVDF-SPEEK blend film (1wt%)	PVDF-SPEEK blend film (5 wt%)
Contact angle image			
Contact angle	92.25°	85°	75.8°

7.5. Electrical Response:

The humidity sensitivity of the PVDF-SPEEK blend film based resistive sensors was investigated. Figure 7-4(a) shows the resistive response of PVDF-SPEEK blend humidity sensors with different concentrations of SPEEK. The sensors' resistance decreases as the relative humidity level increases (10 %RH to 90 %RH) inside the humidity chamber. Its also been observed that as the concentration of SPEEK increases from 1 wt% to 7.5 wt%, the sensitivity of the resistive humidity sensors increases as well. The PVDF-SPEEK blend (5 wt% and 7.5 wt%) based resistive sensors are more sensitive to lower humidity levels as compared to the lower concentration of SPEEK (1 wt% and 3 wt%). The increase in the concentration of SPEEK within the blend

membrane increases the concentration of hydrophilic sulfonation group (SO3), which enhances the absorption of water vapors on the sensing film's surface; hence the sensitivity of the humidity sensor increases. Hysteresis is an essential parameter to evaluate the humidity sensor's performance. Figures 7-4(b), 7-4(c), and 7-4(d) show the hysteresis response of the PVDF-SPEEK blend (5 wt%, 7.5 wt%, and 10 wt%) on resistive humidity sensors. It has been observed that PVDF-SPEEK based resistive humidity sensors with a higher concentration of SPEEK demonstrate higher hysteresis loss. The higher hysteresis loss is observed as the concentration of SPEEK increases within the blend membrane. More water molecules absorbed on the sensing film's surface will aggregate more water molecules and form clusters on the sensing film's surface to increase the desorption process.
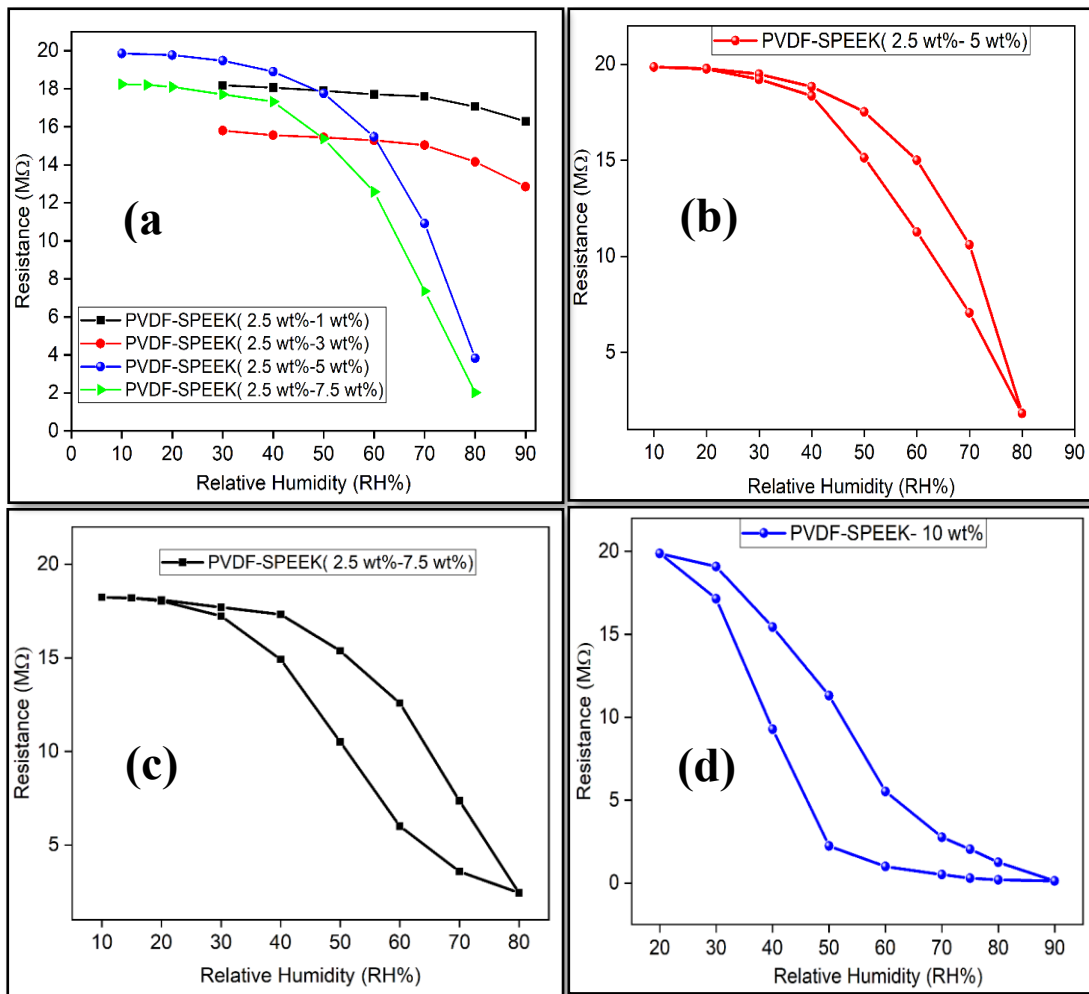
Figure 7-4. (a) Resistance vs Relative Humidity level of PVDF-SPEEK (1 wt%, 3 wt%, 5 wt% and 7.5 wt%) sensor. Hysteresis response of PVDF-SPEEK (5 wt%) (c) PVDF-SPEEK (7.5 wt%) (d) PVDF-SPEEK (10 wt%).

The response and recovery time of the PVDF-SPEEK (5 wt%) blend resistive sensors computed to be 25 s and 40 s respectively at room temperature 25 °C. The response and recovery curve also demonstrate that the results are stable and repeatable. Figure 7-5 shows the response and recovery curve of the PVDF-SPEEK based humidity sensor.
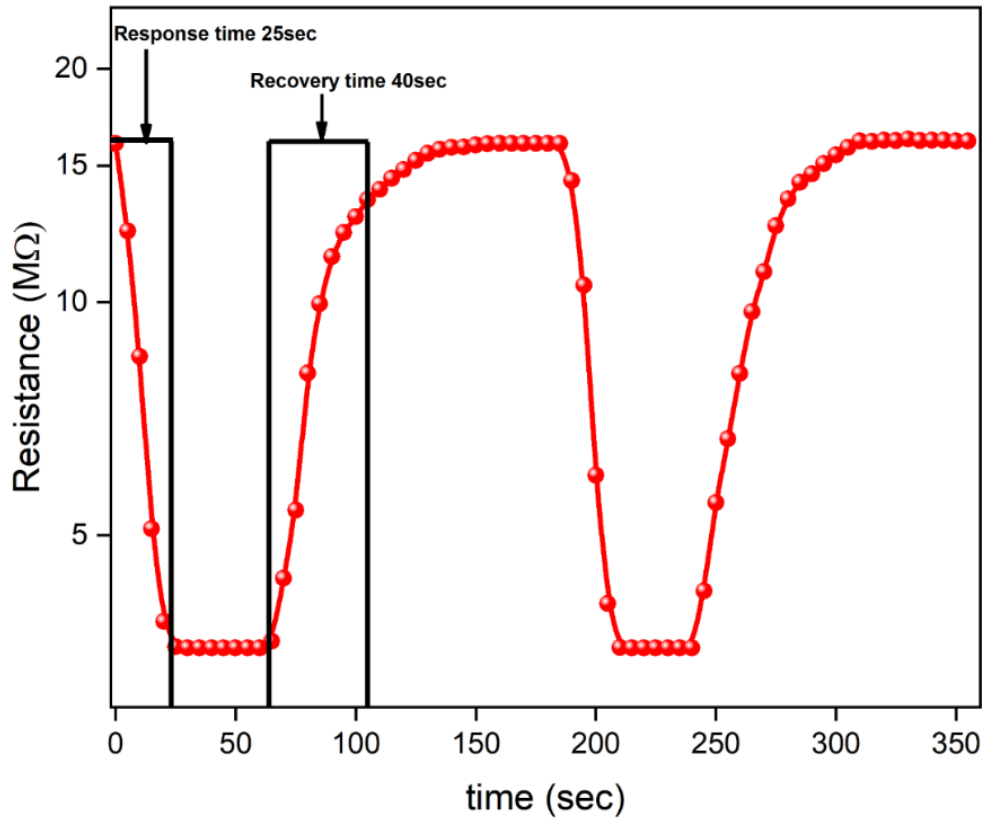
Figure 7-5. The response and recovery cycle (40- 95%RH) of PVDF-SPEEK blend (5 wt%) based resistive humidity sensors.

Table 7-2 summarizes the response and recovery times of different SPEEK blend resistive humidity sensors compared to data obtained in this work.

Table 7-2. Response and recovery time of PVDF-SPEEK blend resistive humidity sensors.

Material	Fabrication Method	Response time (sec)	Recovery time (sec)
SPEEK[43]	Spin coating	100	105
Sulfonated polystyrene polymer[151]	Dip coating	30	300
Sulfonated polymer aromatic electrolytes (PAEK-SO3Na-x)[155]	Dip coating	90	100
PVDF-SPEEK (Present work)	Spin coating	25	40

7.6. Conclusion and Summary:

The spin coating technique fabricated PVDF-SPEEK blend based resistive humidity sensors. The morphology of the PVDF-SPEEK blended film was investigated by FESEM and AFM analyses. The results showed that at higher concentrations of SPEEK (10 wt% and 15 wt%), the distribution of SPEEK is not homogenous due to a higher amount of SO3H group present within the PVDF-SPEEK blend. Also, when the concentration of SPEEK within the blend film increased, the sensing film's hydrophilicity also increased, which improved the sensitivity of sensors at lower humidity levels. The PVDF-SPEEK (5 wt%) blend resistive sensors showed higher sensitivity; also, the response and recovery times of the PVDF-SPEEK (5 wt%) blend resistive humidity sensor estimated to be 25 s and 65 s, respectively. These results indicate that the blending of SPEEK within the PVDF significantly improves the humidity sensors' performance, but an optimum SPEEK concentration of 5 wt% recommended.

CHAPTER 8: TO STUDY THE HALLOYSITE-POLYPYRROLE@SILVER NANOCOMPOSITES FOR HUMIDITY SENSING APPLICATIONS

8.1. Introduction:

This research aims to prepare hybrid material using a polymer with inorganic materials to improve the resistive humidity sensor sensing characteristics. Among the polymeric materials, polypyrrole (PPy) has been broadly investigated for many applications due to its easy preparation, mechanical stability, and interesting electrical properties [156, 157]. The electrical properties of PPy are very sensitive to the change in the relative humidity levels, which make it a very promising candidate for potential application in humidity sensors [158]. In the current study, ppy polymer has been hybridized with the inorganic materials halloysite (HNT). HNT is a kaolinite based naturally abundant clay mineral and possesses good chemical stability, high porosity, large surface area [159, 160]. The unique tubular structure and high surface area of HNT improve the physicochemical properties of the HNT based nanocomposites [161]. To enhance the water vapors adsorption in HNT, the incorporation of hydrophilic materials in HNT is a well-known approach [162-164]. Here, halloysite was selected as an inorganic template; this latter was modified using hydrogen donor silane: N,N-dimethylaminopropyltrimethoxysilane (DMA), to design a hybrid macro photoinitiator for pyrrole grafting, through radical in situ photopolymerizations. This study aimed to develop a fast, reliable, and efficient humidity sensor using the novel hydrophilic organic-inorganic hybrid materials.

8.2. Preparation of silanized halloysite/polypyrrole-silver hybrid materials:

The silanized halloysite/polypyrrole-silver hybrid materials were tailored through the

in situ photochemical -polymerization technique. 1g of HNT-DMA dissolved in 100 ml of deionized water followed by the addition of the AgNO3 aqueous solution (0.84 g in 50ml) and pyrrole (1.2 g in 40 ml corresponding to 0.5 mol/L) under stirring. Afterward, the mixture was transferred to a glass vessel and placed 15 cm below the six lamps of the UV-reactor (Spectrolinker 1500) and irradiated at the wavelength of 365 nm for 20 min. The resulting material was centrifuged then washed several times with deionized water and ethanol to remove unreacted monomers. Then dried in vacuum at 40 °C for 48 h to obtain silanized halloysite/polypyrrole-silver hybrid materials, hereafter called HNT-DMA-PPy@Ag nanocomposite.

8.3.   Preparation of humidity sensor based HNT-DMA-PPy@Ag:

The spin coating technique has been used to deposit the HNT-DMA-PPy@Ag nanocomposite solution on the ITO/glass electrode. The interdigitated ITO electrodes (S161) were purchased from Ossila UK. First, the ITO electrode cleaning process has been performed by sonicating the substrate in soap water for 10 min and placed the electrode in distilled water. After that, the ITO electrodes were sonicated in acetone and distilled water for 10 min each, and then dry the substrate by dry nitrogen gas.

8.4.   Preparation and visual inspection of HNT-DMA-PPy@Ag:

Figure 8-1 shows the consecutive steps for the HNT-DMA-PPy@Ag hybrid material preparation. After the acid activation, the HNT was first silanized using the DMA coupling agent. Subsequently, it was used as a macro-initiator for the pyrrole photopolymerization in the presence of AgNO$_3$ as a photosensitizer [165]. Figure 8-1 shows that the digital photograph (1) shows that the pristine HNT is like a white dry powder. After grafting the DMA layer on the surface of HNT clay, it shows a sticky texture (photograph 2), demonstrating the sequential modification steps of the HNT

surface. Digital photo (3) displays black colored HNT after the in-situ preparation of PPy@Ag.
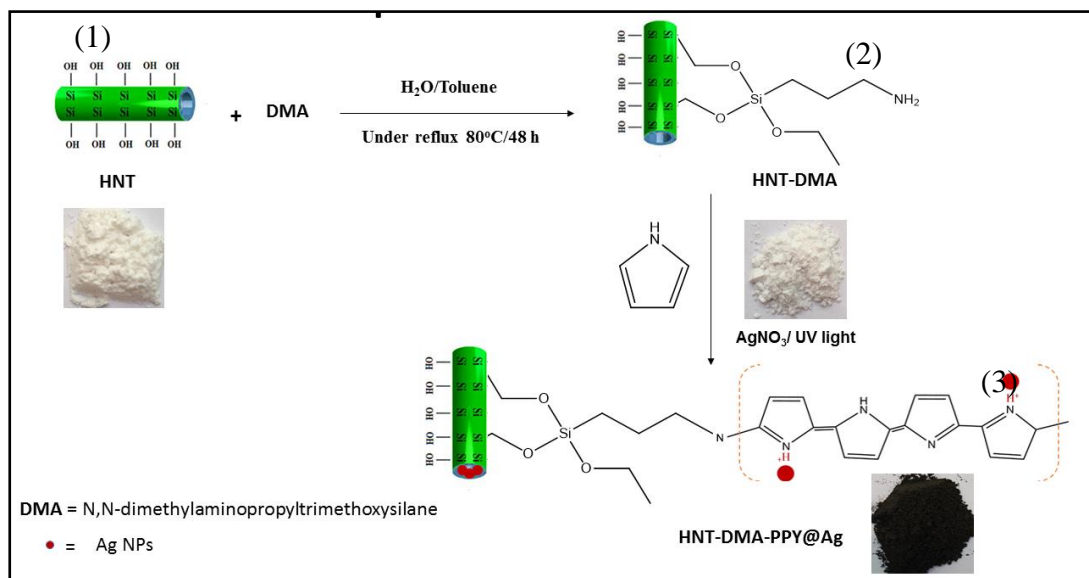
Figure 8-1 Sequential modification steps of HNT by DMA coupling agent, followed by in-situ photopolymerization of Py. The digital photographs show HNT (1), silanized halloysite (2), and HNT-DMA-PPy@Ag (3).

8.5. Morphology of materials:

Figure 8-2 (a) and 8-2 (f) shows the TEM images of the PPy@Ag coated HNT and HNT, respectively. It was observed that the surface morphology of HNTs was altered as well after coating with PPy. Figure 8-2 (f) exhibits the nano clay's tubular structures, with an average diameter of 30 nm and smooth surface morphology. Figure 8-2 (a-e) shows that after surface modification followed by in situ photopolymerizations, PPy@Ag particles are located on the HNTs' surfaces as well as wrapped inside and at the surface of the HNT tubes [166, 167], as shown in the magnified Figure 8-2 (b, d, and e). The tube diameter was observed to increase up 100 nm (Figure 8-2(e)), and an

increase in surface roughness of PPy-modified HNTs was observed.
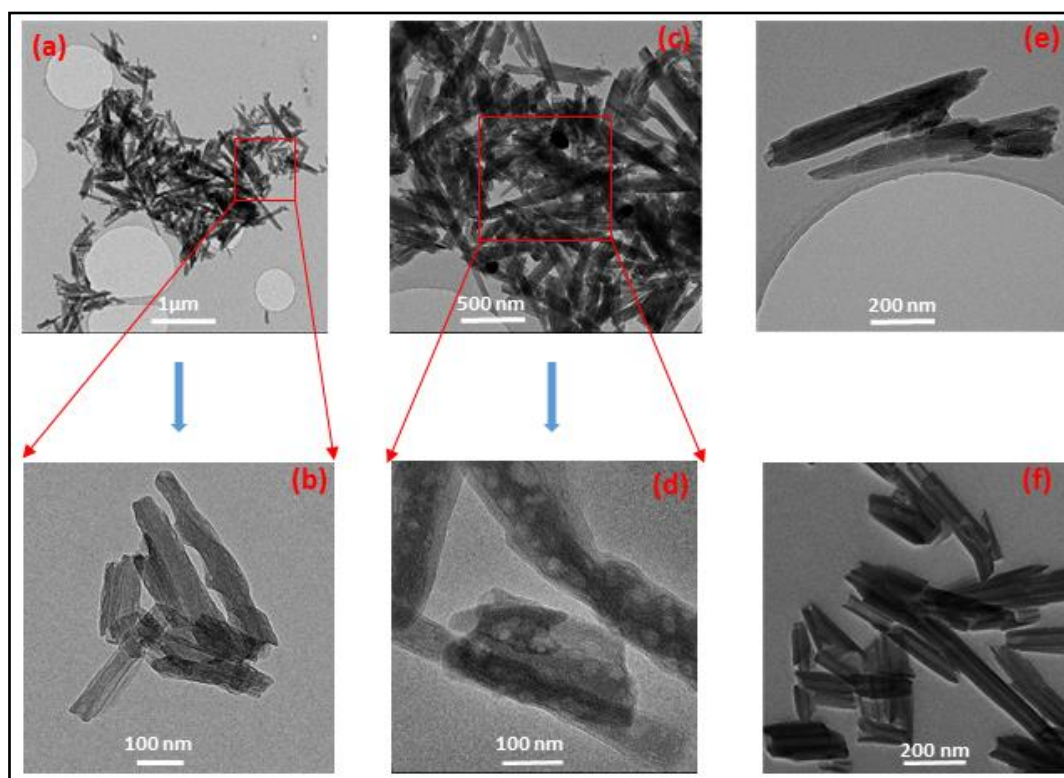
Figure 8-2 TEM images of HNT-DMA-PPy@Ag nanocomposites (a–e) and unmodified HNT (f).

8.6.   Morphology of the sensing film:

The AFM analysis was performed to study the surface roughness and morphology of the HNT-DMA-PPy@Ag nanocomposite sensing films. Figure 8-4(a)-(c) shows the AFM image of the HNT-DMA-PPy@Ag nanocomposites film with (0.25 wt%, 0.5 wt%, and 1 wt %) of the hybrid composite film, respectively. It can be observed that as the concentration of PPy@Ag in the nanocomposite increases, the roughness of the sensing film increases as well. The composite film's developed rough structure enhances the water molecule's capture over the composite film's surface, which will increase the sensitivity of the HNT-DMA-PPy@Ag based humidity sensors. The AFM

image (figure 8-4b) of HNT-DMA-PPy@Ag (0.5 wt%) shows a relatively uniformly distributed rough surface as compared to the other samples.
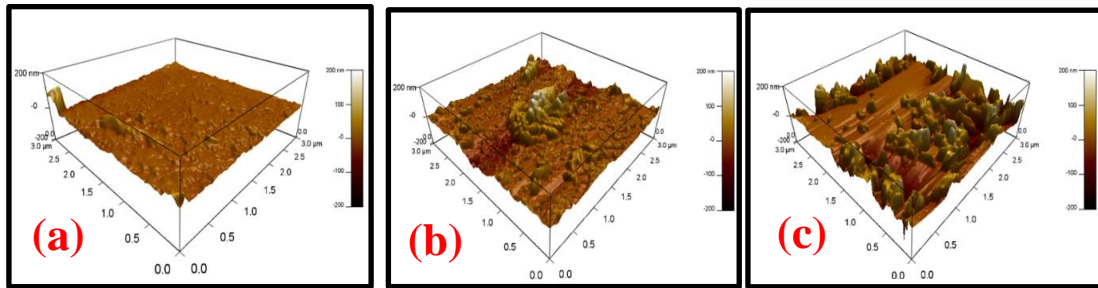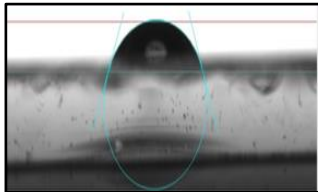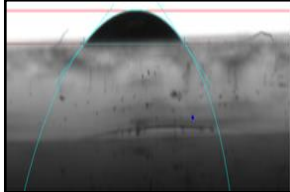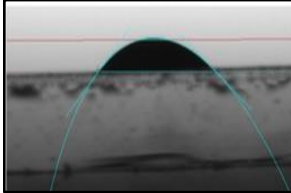
Figure 8-3. The AFM image of HNT-DMA-PPy@Ag nanocomposite film (a) 0.25 wt% of PPy@Ag (b) 0.5 wt% of PPy@Ag, and (c) 1 wt% of PPy@Ag.

8.7. The hydrophilicity of the sensing film:

The film's hydrophilicity indicates that a sensing film's capacity towards the absorption of the water molecules. The contact angle of water drops on the sensing film's surface measured by the sessile drop method. Table 8-1 shows the contact angle measurements of the HNT-DMA-PPy@Ag (0.25 wt%, 0.5 wt%, and 1 wt%) based sensing film. The contact angle of HNT-DMA-PPy@Ag nanocomposite with 0.25 wt% of PPy@Ag is 68.2°, which shows its hydrophilic nature. The contact angle of HNT-DMA-PPy@Ag nanocomposite with 0.5 wt% of PPy@Ag decreased to 46.6°. This decrease in contact angle shows that the addition of PPy@Ag improved the sensing film hydrophilic property. This increase in hydrophilicity enhances the water vapor absorption over the sensing film's surface, increasing the sensors' sensitivity at lower humidity levels. With the rise in the concentration of PPy@Ag (1 wt%), the sensing film becomes highly hydrophilic, and the contact angle decreases to 37°. The highly hydrophilic surface entraps more water vapors; thus, the sensing film's sensitivity further increased. However, in a highly hydrophilic surface, water molecules adsorbed on the sensing film and formed a strongly H-bonding with the sensing film surface, which will slow the

desorption process [168].

Table 8-1. Contact angle measurements of HNT-DMA-PPy@Ag film (0.25 wt%, 0.5 wt%, and 1 wt%).

Sample Type	0.25 w/W % HNT-DMA-PPy@Ag film	0.5 w/W % HNT-DMA-PPy@Ag film	1 w/W % HNT-DMA-PPy@Ag film
Contact angle Image			
Contact angle	68.2°	46.6°	37°

8.8.   Potential Humidity sensor application:

Photopolymerization of pyrrole in the presence of modified HNT is interesting for three main reasons: it investigates the propensity of HNT clay as a natural material with high surface area, low cost, used hereafter as bio-based micro-platforms for the in situ photopolymerizations of pyrrole, the reaction was ultrafast and particularly yielded polypyrrole with anchored silver NPs. Given the anchored PPY/Ag NPs anchored in the final HNT-DMA-PPy@Ag nanocomposite, as it is possible to interrogate the performances of this HNT-DMA-PPy@Ag in the humidity sensing filed. The humidity sensing response of the fabricated HNT-DMA-PPy@Ag nanocomposite impedance sensors characterized inside the controlled humidity chamber over the wide RH range (10 %RH-90 %RH). Figure 8-5 shows the impedance response of the HNT-DMA-PPy@Ag nanocomposite sensors with different concentrations of PPy@Ag. The impedance of the humidity sensor decreases with an increase in humidity level. As the

humidity level increases, a higher concentration of water molecules formed on the surface of the sensing film; hence more water molecules adsorbed on the sensing film, which increases the conductivity of the nanocomposite film. We have measured the humidity response of a pure HNT based humidity sensor. The HNT based humidity sensors show very low sensitivity at lower humidity levels (20-60%RH). The incorporation of PPy@Ag within HNT enhances the humidity sensor's sensitivity at a lower humidity level as well. Figures 8-5(a-c) show the hysteresis response of the HNT-DMA-PPy@Ag nanocomposite-based humidity sensors prepared with different concentrations of ppy@Ag (0.25 wt%, 0.5 wt%, and 1 wt%). Hysteresis is an important parameter to analyze the sensor's performance. The Hysteresis effect can be described as the maximum difference in impedance when the sensor is exposed to change in relative humidity level from lower humidity level to higher humidity level (absorption process) and from higher humidity level to lower humidity level (desorption process). It can be observed from figure 8a at a lower concentration of the PPy@Ag (0.25 wt%) the sensor shows lower sensitivity with respect to change in humidity level. As the concentration of PPy@Ag increases to 0.5 wt%, the impedance sensor's sensitivity enhances due to an increase in the sensing film's hydrophilicity, which enables it to operate at lower humidity levels as well. Further increasing the concentrations of PPy@Ag (1 wt%), sensing film becomes a super hydrophilic surface shown in contact angle measurement analysis. This increase in hydrophilicity increases the sensor's sensitivity; it also slows down the desorption process of the impedance sensors while decreasing the humidity level inside the humidity chamber, which in result, increases the hysteresis loss. The HNT-DMA-PPy@Ag (0.5 wt%) nanocomposite-based impedance humidity sensors show more regular response and lower hysteresis loss as compared to the other concentrations of PPy@Ag (0.25 wt% and 1 wt%). The

maximum hysteresis loss of the HNT-DMA-PPy@Ag (0.5 wt%) based humidity sensor was calculated to be 4.5% at 80 %RH levels and the minimum hysteresis loss estimated to be 0.05% at 20%RH levels.
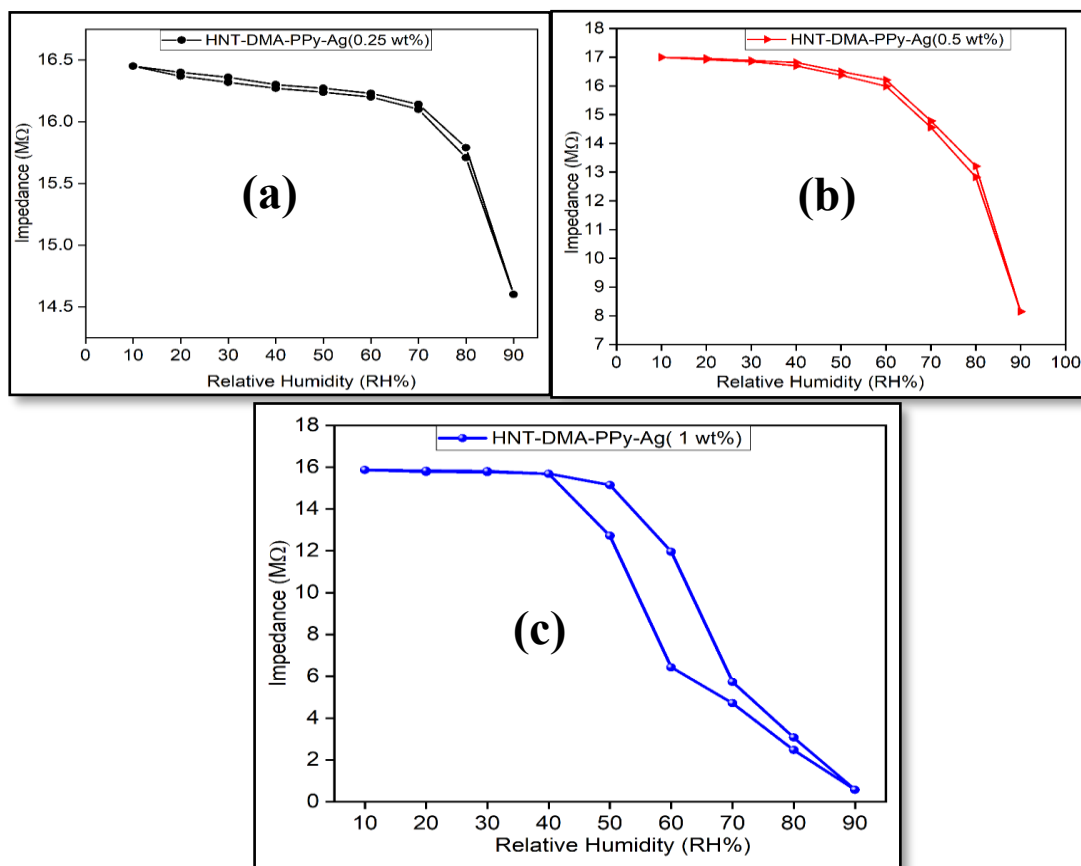
Figure 8-4. Impedance vs. Relative Humidity level for fabricated HNT-DMA-PPy@Ag nanocomposite humidity sensors operating temperature is 25°C at 10 kHz(a) Hysteresis response of HNT-DMA-PPy@Ag (0.25 wt%) (b) Hysteresis response of HNT-DMA-PPy@Ag (0.5 wt%) (c) Hysteresis response of HNT-DMA-PPy@Ag (1 wt%).

Figure 8-6 shows the stable and repeatable response and recovery curve of HNT-DMA-PPy@Ag (0.5 wt%) based impedance sensors. The HNT-DMA-PPy@Ag (0.5 wt%) response and recovery time-based impedance sensor was evaluated to be 30 s and 35 s respectively at room temperature 25°C. Table 8-2 shows the comparison of our work with previously reported PPy@Ag sensors. Our newly synthesized material has

significantly improved the response and recovery times compared to the previous study on the PPy systems.
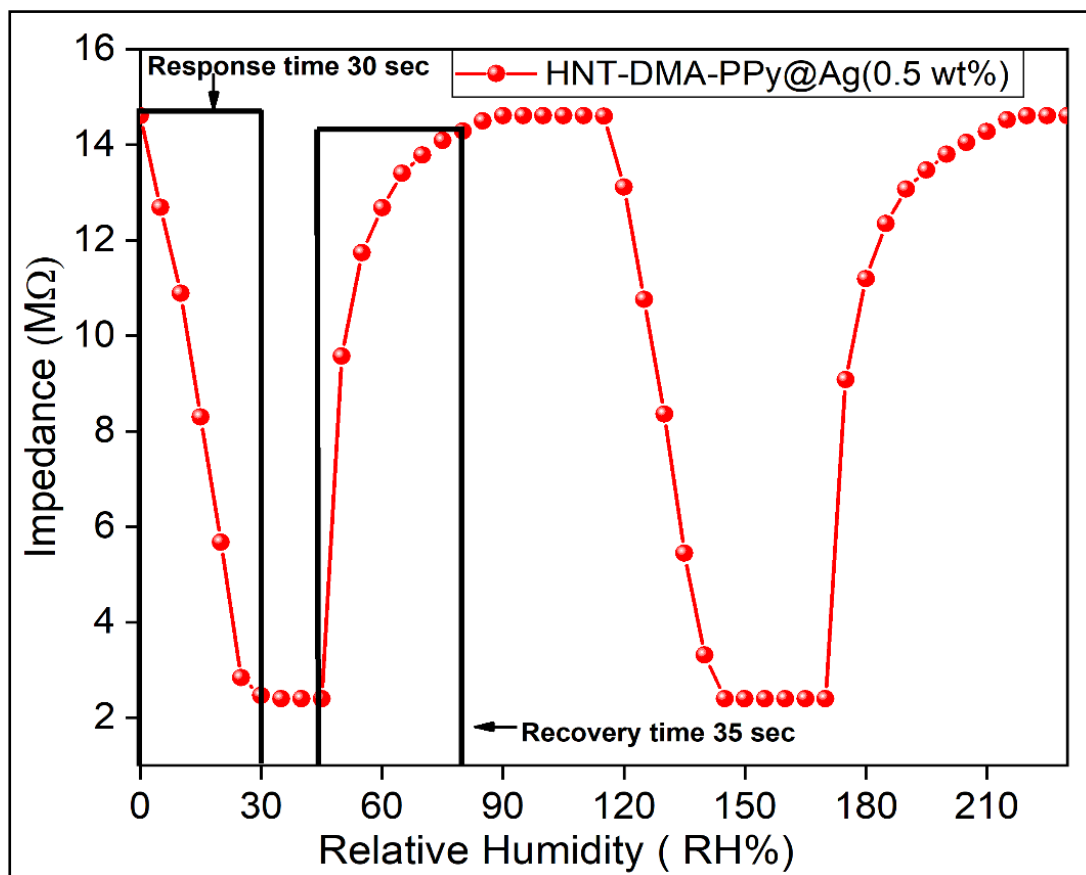
Figure 8-5. The response and recovery cycle (40- 95 %RH) of HNT-DMA-PPY@Ag (0.5 wt%) nanocomposite-based impedance sensor.

Table 8-2. Summary of the polypyrrole–NPs based Humidity sensors.

Material	Experimental details	Sensing Range (%RH)	Response/ Recovery time (s)	Ref
Cellulose–PPy nanocomposite	Chemical oxidative polymerization. Time=30 min at RT CuCl2/Py: 10 mL/5 vol% Regenerated cellulose films emerged infiltrate of PPy	30 – 90	~ 418	[169]

Material	Experimental details	Sensing Range (%RH)	Response/ Recovery time (s)	Ref
TiO₂ NPs/PPy/PMAPTAC)	Photopolymerization Time=20 min under UV light at RT AgNO₃/Pyrrole/TiO₂ NP PMAPTAC /AIBN PET substrate	11 – 90	30- 45	[170]
PPy-ZnO nanocomposite	Chemical oxidative polymerization. Time= 60 min at 70 °C PPy-ZnO NP PPy/ZnO: 50 mg / 11.8 mg	11 – 75	180 – 60	[171]
HNT-DMA-PPy@Ag	In situ photopolymerization Time= 20 min at RT HNT/AgNO₃/ Py= 1g/0.1M/0.5 M	10 – 90	30-35	This work

8.9.   Conclusion and summary:

Halloysite-polypyrrole–silver nanocomposite was successfully prepared via in situ photopolymerizations of pyrrole in the presence of silanized halloysite and silver nitrate as a photo-initiator. We have modified the halloysite Nano-clay (HNT) using hydrogen donor silane and coupling agent (DMA) to provide anchoring sites for the polypyrrole/silver composite (PPy@Ag). Both PPy and Ag mass loading were estimated to 21 and 26 wt%, respectively. The anchored Ag particles were found in the metallic state, and the resulting HNT-DMA-PPy@Ag nanocomposite was black because of the PPy rich modified surface. The resulting PPy@Ag-modified silanized HNT was finally evaluated for impedance humidity sensing using (0.25 wt%, 0.5 wt%, and 1 wt%) HNT-DMA-PPy@Ag nanocomposites. We achieved improved hysteresis and stable response with (0.5 wt%) HNT-DMA-PPy@Ag of the added nanocomposite.

The HNT-DMA-PPy@Ag (0.5 wt%) nanocomposite-based impedance sensors showed high sensitivity, stable response, and low hysteresis as compared to other ratios of PPy@Ag (0.25 wt%, 1 wt%). The response and recovery time of HNT-DMA-PPy@Ag (0.5 wt%) impedance sensors calculated to be 30 s and 35 s, respectively. From the above, we highlight a new surface modification option of low cost and naturally abundant halloysite, through in situ photopolymerizations of pyrrole, to design reactive and functional bio-based hybrid materials of interest, namely in the humidity sensing filed.

CHAPTER 9: TO INVESTIGATE THE GRAPHENE QUANTUM DOTS (GQDS), FOR HUMIDITY SENSING APPLICATIONS.

9.1. Introduction:

In this work, we aim to prepare graphene quantum dots (GQDs) from graphitic waste. The resulting GQDs will be evaluated for the potential application for resistive humidity sensors. Recently, carbon-based humidity sensors [172] have managed to capture substantial attention by their economical, easy-processing, and flexibility-accommodating attributes. Among the different allotropes of carbon, graphene has attracted many researchers' attention in the emergent materials field With the extraordinary chemical and physical properties such as remarkable electrical and thermal conductivity, excellent resistance to corrosion and stability, high strength, and graphene-based materials became the researcher's first choice for sensor fabrication. Different dopants added to the graphene to support the alienation of adsorbed water into hydrogen and hydroxyl ions. Improvement in humidity response measurements of the sensors has been observed using the quantum dots (QDs), particularly in terms of the devices' sensitivity towards change in different relative humidity. Quantum dots constitute a new class of nanomaterials, between the molecular and bulk forms of material; because of their fluorescent properties, small size, and surface defect, quantum dots display outstanding optical and electrical properties, higher than those present in bulk material However, quantum dots materials were very toxic [173] and relatively expensive. Therefore, researchers are more interested nowadays in developing suitable low cost and non-toxic alternatives, namely carbon and graphene quantum dots (GQDs). The GQDs latter's attracted many researchers because of their unique and outstanding properties such as easy preparation, low cost, and toxicity

photoluminescence, and bandgaps [174, 175]. This work describes a cost-effective and facile way to prepare highly photoluminescent GQDs, using graphite waste as a carbon source. The morphology and physio-chemical properties of the obtained GQDs were assessed by X-ray photoelectron (XPS), Raman, Fourier-transform infrared (FTIR), X-ray diffraction (XRD), atomic force microscopy (AFM), and electron microscopy (SEM and TEM). The optical properties were explored using fluorescence and UV/Vis spectroscopy (UV/Vis). The hydrophilicity of GQDs based sensing film is studied by the contact angle measurement method. Interestingly, it is observed that the concentrations of GQDs can alter the wettability of the sensing film. The resulting GQDs based sensors were evaluated as a novel low-cost impedance humidity sensor.

9.2.   Synthesis and purification of GQDs:

4g of graphite waste in powder form was first dissolved in H2SO4/HNO3 (200/60 ml) for 12 h and at 120 °C; after that, diluted and neutralized using ammonia as following, 10 ml of the material was dissolved in water (0.1 mg/mL) under vigorous stirring, then mixed with 3ml of ammonia and sonicated for 20 min; the resulting material was then heated at 180̊ C for 12 h using an autoclave. The supernatant was then filtered then dialyzed (3500 Da MWCO) membranes, yielding a deep yellow supernatant N-GQDs.

9.3. Synthesis and purification of GQDs from graphite waste

Graphite wastes were collected from the Qatalum Qatar industry then grinded to obtain a fine powder. The latter was then dispersed into concentrated H_2SO_4/HNO_3 solution under sonication, then heated under constant stirring at $120°C$ for 12 h. After cooling at room temperature, the resulting mixture was, filtered, diluted, and then dialyzed. A GQDs solution with yellowish color was acquired, displaying green emission under UV light (360 nm). The as-prepared GQDs material was then treated with ammonia for 20min using a hydrothermal process to obtain N and S co-doped GQDs, yielding a deep yellow solution, with a blue-green emission when excited at 365 nm U.V. light, as shown in figure 9-1.
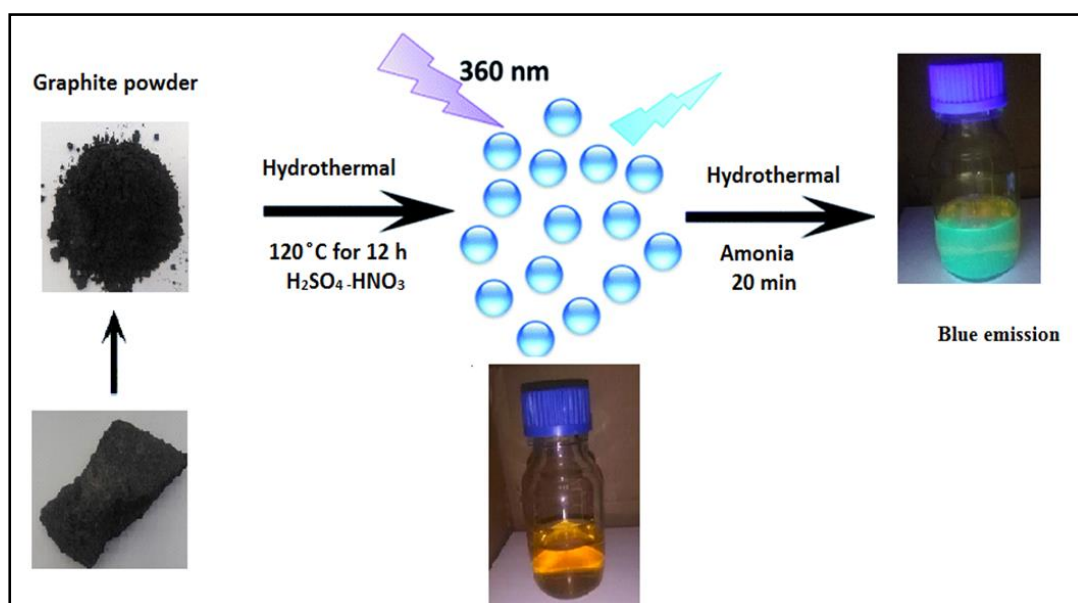
Figure 9-1. Schematic illustration summarizing the preparation of N and S co-doped GQDs from graphite waste.

Preparation of humidity sensor based GQDs:

Nanocomposite using three different concentrations of GQDs (2.5, 5, and 10 wt%) prepared by dispersing in DMF. The spin coating technique is used to deposit the GQDs

solution on the ITO/glass electrode. During the deposition of sensing film, an optimization process has been done for the rotation speed and the rotation time to form an even equilateral spread of the solution. The rotation speed and rotation time were optimized to 5000 rpm and 50 seconds. Figure 9-2 (a) shows a graphical presentation of the preparation process of the GQDs based humidity sensor. The humidity sensing response of GQDs based impedance sensors was carried out in a controlled humidity chamber. The humidifier (model HM3000) was used to increase the humidity level inside the sealed humidity chamber. Figure 9-2 (b) demonstrates the humidity sensing measurement setup used in this study.
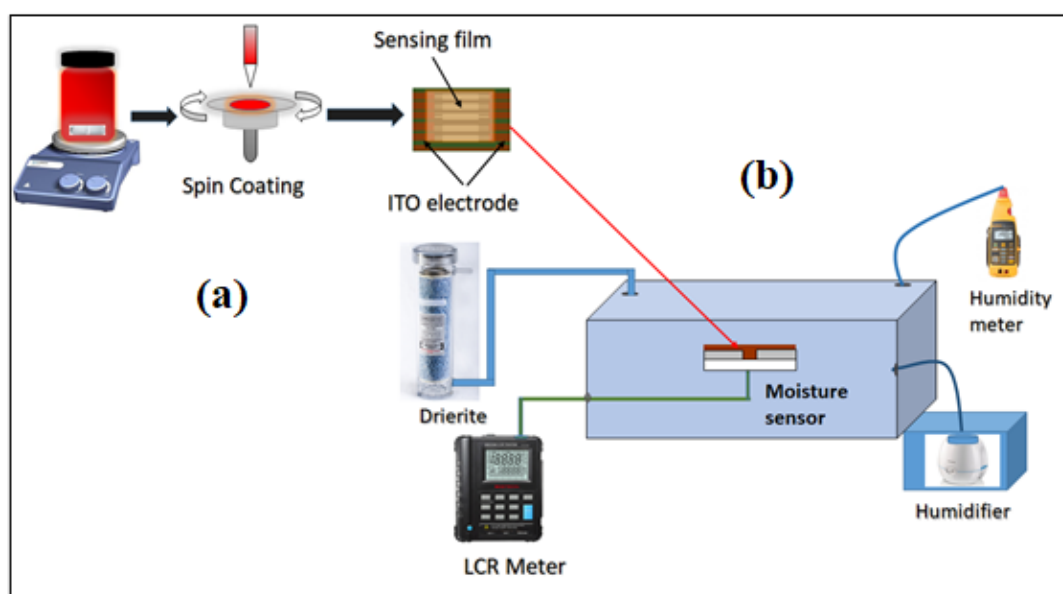
Figure 9-2. (a) Graphical illustration of GQDs based humidity sensor prepared by the spin coating method. (b) A humidity sensor setup was used during this work.

9.4.   Structure Analysis of Graphite waste and the prepared N-GQDs:

The Raman spectra of Graphite waste and N-GQDs are presented in figure 9-3(a). For N-GQDs, the G-band appears at 1593 cm^{-1} and the D-band at 1363 cm^{-1}. The ID/IG value represents a measure of disorder in graphene structure, for graphite waste is 1.36, while for graphite waste, this ratio is 1.06, also suggesting, more disordered carbon

structure because of the nitrogen doping effect, blue shifts of D and G bands can be seen, which is consistent with the results reported before [176]. The FTIR spectra of pristine and the as-prepared N-GQDs were displayed in figure 9-3(b) for graphite and their derivate N-GQDS respectively. One can note two small peaks at 2919 and 2858 cm^{-1}, assigned to –CH$_2$ groups vibration, the band at 3442 cm^{-1} is assigned to –OH group, the peaks at 1608 and 1764 cm^{-1} assigned to C=O groups stretching vibration in carboxylic moiety, the 1440 cm^{-1} peak is due to C–H stretching vibration, while the 1128 cm^{-1} peak could be attributed to C–O stretching vibration. Peaks situated around 1384 and 3153 cm^{-1} are assigned to C-N and N–H stretching vibrations, respectively [177].
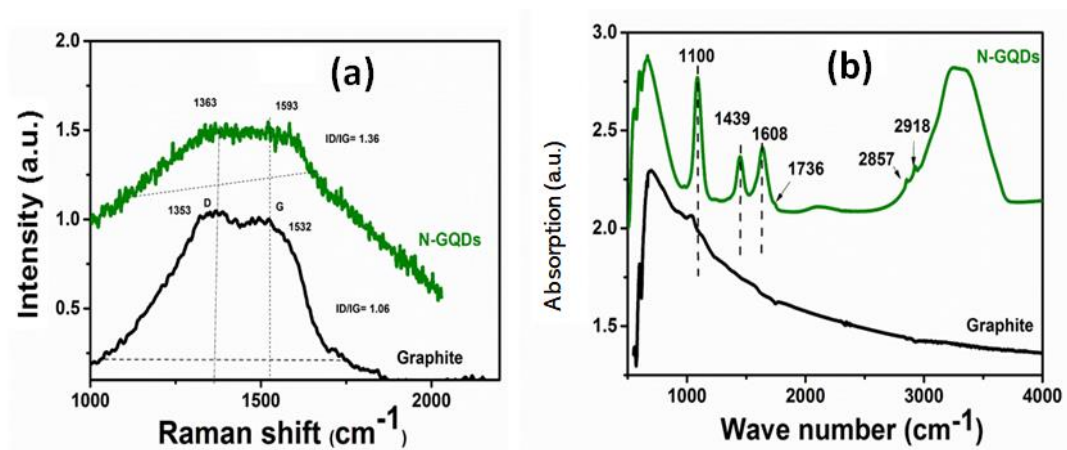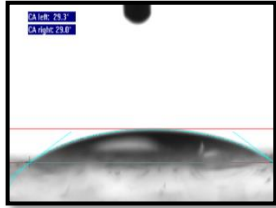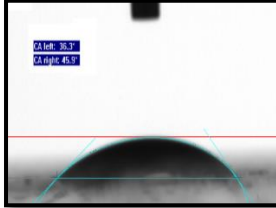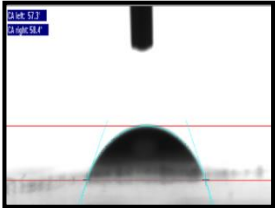
Figure 9-3. (a) Raman spectra (a) and (b) FTIR spectra of graphite waste and N-GQDs derivate.

9.5.   Contact Angle measurements:

The hydrophilicity of the film indicates that the sensing film adsorbs water drops on the sensing film surface. The contact angle of water drops on the sensing film's surface measured by the sessile drop method. Table 9-1 shows the contact angle measurements of the N-GQDs based sensing film with different concentration N-GQDs. The contact angle of N-GQDs (2.5 mg) is 29.15° shows, obviously its hydrophilic nature. As the

concentration of GQDs increases, the hydrophilicity of the sensing film decreases. The contact angle of N-GQDs (5 mg) sensing film increase to 41.1°. As the concentration, N-GQDs increase to 10 mg, its contact angle increases to 57.85°. The contact angle of 10 mg GQDs film shows that the sensing film surface is in between super hydrophilic and hydrophobic surfaces. As the latter is combining both hydrophilic and hydrophobic properties, it has enhanced the sensitivity of humidity sensors and reduces the hysteresis loss compared to other used concentrations of N-GQDs. As we further increase the concentration of GQDs (15 mg), the contact angle measurement shows that the sensing film surface becomes more hydrophobic.

Table 9-1. Contact angle measurements Graphene Quantum dots 2.5 mg, 5 mg, and 10 mg.

Sample	GQDs (2. 5mg)	GQDS (5 mg)	GQDs (10 mg)
Contact angle image			
Contact angle	29.15°	41.1°	57.85°

9.6.   Potential Humidity sensor application:

The N-GQDs based impedance humidity sensors were prepared with different concentrations of N-GQDs (2.5 mg, 5 mg, and 10 mg). The performance of the N-GQDs based impedance humidity sensors was thoroughly investigated. Figure 9-4 shows the impedance response of the N-GQDs based resistive humidity sensors, with

respect to change in humidity level 10 %RH- 90 %RH. As the humidity level increases within the humidity chamber, more water molecules formed on the sensing film's surface; hence, the conductivity of the sensing film also increases. The as-made GQDs with graphene-like structures are rich in oxygen; therefore, water molecules and oxygen radicals would form a strong hydrogen bond; this will increase the hydrophilicity and proton conductivity of the sensing film [178]. Figures 9-4 (a-c) show the hysteresis response of the 2.5 mg GQDs, 5 mg GQDs, and 10 mg GQDs based impedance humidity sensors. Hysteresis loss is an important parameter to analyze the sensor's performance and sensor stability. The Hysteresis loss can be defined as the maximum change in impedance when the sensor is exposed to change in relative humidity level from lower humidity level to higher humidity level (absorption process) and higher humidity level to lower humidity level (desorption process). It was observed in figure 9-4 that at a lower concentration of GQDs (2.5 mg), the impedance humidity sensor shows a higher hysteresis loss. At lower concentrations of GQDs (2.5 mg), sensing film is super hydrophilic; hence the desorption process is slow; therefore, it has higher hysteresis loss. As the concentration of GQDs increases, the sensing film becomes less hydrophilic; thus, the desorption process becomes relatively faster, which reduces the hysteresis loss. The maximum hysteresis of the GQDs (10 mg) based impedance humidity sensors was found to be 2.2% at 30 %RH.
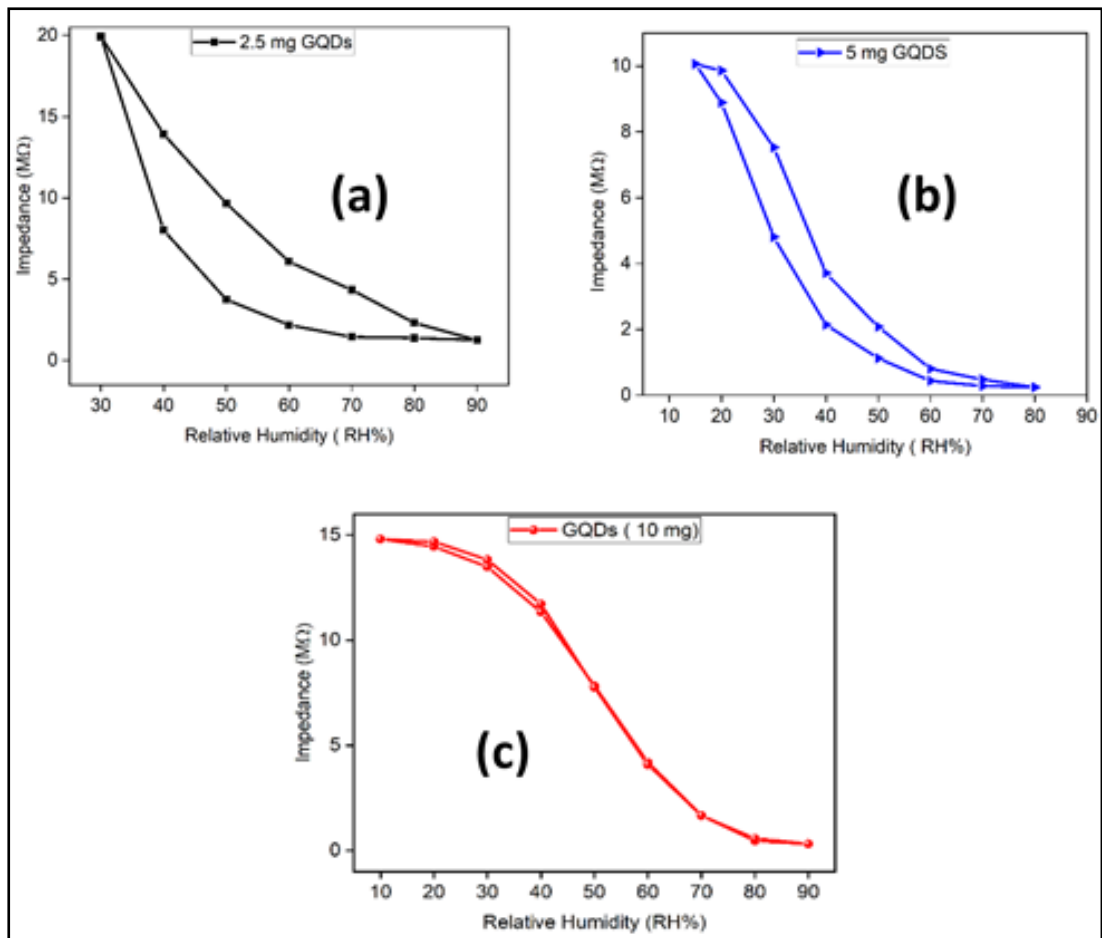
Figure 9-4. (a) Hysteresis response of Graphene Quantum dots based resistive humidity sensors (a) 2.5 mg GQDS (b) 5 mg GQDs (c) 10 mg GQDs.

To evaluate the performance of the sensors, response, and recovery times are also considered as essential parameters. Figure 9-5 shows the response and recovery curve of the GQDs (10 mg) based impedance humidity sensor; the curve shows a repeatable and stable response. The response and recovery times of the N-GQDs (10 mg) impedance humidity sensors calculate to be 15 s and 55 s, respectively.
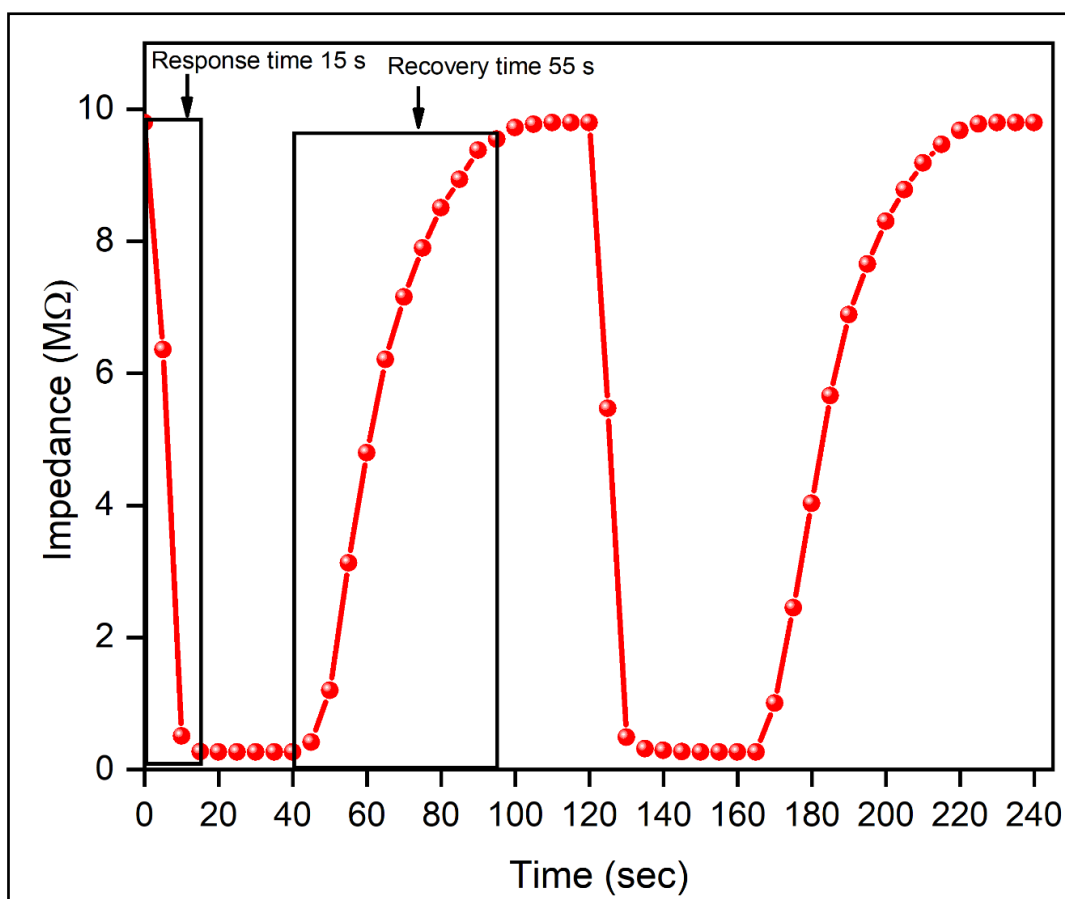
Figure 9-5. Response and recovery cycles (40- 90 %RH) of GQDs (10 mg) based resistive humidity sensor.

9.7.   Conclusion:

In conclusion, GQDs was successfully prepared from graphite waste via a hydrothermal process in the presence of ammonia. The as-made GQDs with graphene-like structures are fluorescent, rich in oxygen, nitrogen, and sulfur groups, have a uniform size and excellent water solubility. The latter GQDs were used to prepare a resistive humidity sensor using of GQDs. We achieved improved hysteresis (maximum 2.2% at 30 %RH) and stable response. The response and recovery time of the GQDs (10 wt%) impedance sensors calculated to be 15 s and 55 s, respectively. This work offers a new way of producing high-quality GQDs from graphite waste to fabricate solid-state materials as an efficient humidity sensor.

CHAPTER 10:   Summary and Future work:

Summary

Capacitive and resistive-based humidity sensors were fabricated, and their humidity sensing characteristics were studied. In this quest, different techniques were employed such as incorporation of nanoparticles within polymers, blending of polymers, formation of hybrid material using polymer with inorganic material aiming to improve the sensor's morphology and sensing characteristics. Also, graphene quantum dots (GQDs) from graphitic waste were prepared and investigated their potential for humidity sensing.

In the first part, sustainable and renewable resources for humidity sensing applications were investigated. The impact of TiO_2 ceramic nanoparticles on the thermal stability, morphology, molecular mass, structure, and electrical properties of the polylactic acid-Titanium dioxide (PLA-TiO_2) composites-based humidity sensor was studied. The modification in the sensing film composition was done to enhance the porosity over the surface of PLA-TiO_2 nanocomposites. Results confirmed that the PLA-TiO_2 nano-sensing films, having modified surface roughness, exhibited superior morphological and electrical performance features when compared to PLA-TiO_2 pristine samples. However, it is observed from the electrical response that at a higher humidity level (above 70 %RH), the sensor shows nonlinear behavior. Also, the maximum hysteresis loss of the sensor was around 12%. Therefore, we need to improve the capacitive humidity sensor linearity for higher humidity levels and reduce the sensor's hysteresis loss [179].

In the second part, we investigated the hydrophobic polymers for humidity sensing applications. We modified the hydrophobic PVDF polymeric film to a hydrophilic film

surface to improve sensing properties. The nanocomposite of the PVDF has been prepared using TiO_2 nanoparticles. Surface etching technique has been used to change the surface morphology of the nanocomposite films. The hydrophilic PVDF-TiO_2 nanocomposite sensing film-based capacitive sensors showed improved morphological and humidity sensing response as compared to the hydrophobic PVDF alone film. The hydrophilic PVDF-TiO_2 nanocomposite electrical response showed that the PVDF-TiO_2 (2.5 wt%- 0.5 wt%) based capacitive humidity sensors demonstrated linear response and increased sensitivity as compared to the PVDF-TiO_2 (5 wt%- 0.5 wt%) sensors over the whole investigated RH range. The optimized sensors showed a ~6% average hysteresis loss [180]. However, the hysteresis loss was still relatively high, which needs to be reduced. Therefore, further investigation of PVDF polymer is required to improve this aspect.

In the third part, we studied how piezoelectric nanoparticles $BaTiO_3$ affects the humidity sensing properties of the polyvinylidene fluoride (PVDF)-$BaTiO_3$ composite films in terms of dielectric response, thermal stability, and hydrophilicity. Different concentration (0.5,1, 2 wt%) of $BaTiO_3$ nanoparticles were incorporated within the PVDF. PVDF-$BaTiO_3$ (2.5 wt%-1 wt%)-based capacitive sensors showed linear and stable capacitive response and low hysteresis compared to the PVDF-$BaTiO_3$ composites with other concentrations. The maximum hysteresis of the capacitive PVDF-$BaTiO_3$ (2.5 wt%- 1 wt%) humidity sensor is ~2.5%. The response and recovery times of the PVDF-$BaTiO_3$ (2.5 wt%-1 wt%)-based capacitive sensors were 40 s and 25 s, respectively, which are significantly lower than those for the reported PVDF composite-based sensors.

In the 4th phase, the objective was to study the resistive humidity sensors and specifically improve their sensitivity at lower humidity levels. We have explored the

blending of polymers, which have unique characteristics to improve the sensing film's mechanical and electrical properties. We have studied the impact of sulfonated poly (Ether Ether Ketone (SPEEK) on the humidity sensing properties, thermal stability, and hydrophilicity of polyvinylidene fluoride (PVDF)-SPEEK blend films. The PVDF-SPEEK composite solutions were prepared by mixing an optimized concentration (2.5 wt%) of PVDF with concentrations of SPEEK varied from 1wt% to 15 wt%. The impedance response of the sensing film showed that as the concentration of SPEEK increases the sensitivity of the sensing film increases at lower humidity levels. The PVDF-SPEEK (2.5 wt%-5 wt%) showed low hysteresis, high sensitivity, and stable response as compared to pure PVDF film. The response and recovery times of the PVDF-SPEEK (2.5 wt%- 5 wt%) were found to be 25 s and 40 s, respectively.

In the 5th phase, halloysite-polypyrrole-silver nanocomposite has been prepared via in-situ photopolymerization of pyrrole in the presence of silanized halloysite and silver nitrate as a photo-initiator. The resulting PPy@Ag-modified silanized HNT has been evaluated for the potential application for resistive humidity sensing. The HNT-DMA-PPy@Ag (0.5 wt%) nanocomposite-based resistive sensors showed good sensitivity and lowered the sensor's hysteresis as compared to the other ratios of the composite. The maximum calculated hysteresis of the HNT-DMA-PPy@Ag (0.5 wt%) based humidity sensor was around 4.5% at 80 %RH. The response and recovery time of HNT-DMA-PPy@Ag (0.5 wt%) nanocomposite-based resistive sensors were found to be 30 s and 35 s, respectively. The interesting humidity-dependent resistive properties of this novel composite make it promising in humidity sensing.

In the last phase, graphene quantum dots (GQDs) were prepared from Graphitic waste. The GQDs (10 mg/ml) based impedance sensors showed good sensitivity and lowered the sensor's hysteresis as compared to the other studied ratios (2.5 and 5 wt%). The

maximum calculated hysteresis of the GQDs (10 wt%) based sensor was around 2.2% at 30 %RH and the minimum calculated hysteresis of the GQDs (10 mg/ml) based sensor was approximately 0.79 % at 60 %RH. The response and recovery times were found to be 15 s and 55 s, respectively. The interesting humidity-dependent resistive properties of these prepared GQDs make them promise for potential applications in humidity sensing and beyond.

The research presented in this thesis was deliberately dedicated for improving devices and techniques in humidity sensing and related areas. The results achieved hold promises in fostering a great deal faster commercialization of such sensors.

Future Work

Future work can be pursued by applying these novels and improved capacitive and resistive sensors for natural gas flow sensing applications. We have developed gas flow setup at our lab, our idea is to deploy these sensors on the gas flow setup and study the humidity sensitivity of these developed capacitive and impedance sensors under gas flow environment. However, the environment in the oil & gas industry is particularly severe. The desired sensor technology must be able to handle the following conditions/requirements.

1. In the natural gas flow environment, extreme conditions include high pressure (~ several thousand psi), high velocity (>10 m/s) and high temperature, the developed sensors should be able to tolerate these harsh environments.

2. The gas flow consists of gas, hydrocarbon liquid, water vapor, water, (possibly) saline water and metals and is extremely inhomogeneous.

3. Corrosive or hazardous substances, e.g. H_2S gas present in natural gas flow so need to develop sensors which can monitor these hazardous gases and should have higher sensitivity and selectivity.

4. In such an extremely noisy environment, sensor technology must be capable of detecting small concentration of information.

5. Sensing measurement must be collected and recorded in real-time mode and measurement needs to be carried out constantly.

REFERENCES

[1]   N. Yamazoe and Y. Shimizu, "Humidity sensors: principles and applications," *Sensors and Actuators,* vol. 10, no. 3-4, pp. 379-398, 1986.

[2]   E. Traversa, "Ceramic sensors for humidity detection: the state-of-the-art and future developments," *Sensors and Actuators B: Chemical,* vol. 23, no. 2-3, pp. 135-156, 1995.

[3]   G. Zhou *et al.*, "Highly Sensitive Wearable Textile-Based Humidity Sensor Made of High-Strength, Single-Walled Carbon Nanotube/Poly (vinyl alcohol) Filaments," *ACS Applied Materials & Interfaces,* vol. 9, no. 5, pp. 4788-4797, 2017.

[4]   X. Zhuang, Y. Mai, D. Wu, F. Zhang, and X. Feng, "Two-dimensional soft nanomaterials: a fascinating world of materials," *Advanced Materials,* vol. 27, no. 3, pp. 403-427, 2015.

[5]   P. Wang, Y. Wang, and L. Tong, "Functionalized polymer nanofibers: a versatile platform for manipulating light at the nanoscale," *Light: Science & Applications,* vol. 2, no. 10, p. e102, 2013.

[6]   S. Papavinasam, *Corrosion control in the oil and gas industry*. Elsevier, 2013.

[7]   N. Li, X.-D. Chen, X.-P. Chen, X. Ding, and X. Zhao, "Ultra-high sensitivity humidity sensor based on MoS2/Ag composite films," *IEEE Electron Device Letters,* 2017.

[8]   Y. Li, C. Deng, and M. Yang, "Facilely prepared composites of polyelectrolytes and graphene as the sensing materials for the detection of very low humidity," *Sensors and Actuators B: Chemical,* vol. 194, pp. 51-58, 2014.

[9]   S. Korposh, R. Selyanchyn, and S.-W. Lee, "Nano-assembled thin film gas sensors. IV. Mass-sensitive monitoring of humidity using quartz crystal microbalance (QCM) electrodes," *Sensors and Actuators B: Chemical,* vol. 147, no. 2, pp. 599-606, 2010.

[10]   D. J. Wales, R. M. Parker, J. C. Gates, M. C. Grossel, and P. G. Smith, "An investigation into relative humidity measurement using an aluminosilicate sol–gel thin film as the active layer in an integrated optical Bragg grating refractometer," *Sensors and Actuators B: Chemical,* vol. 188, pp. 857-866,

2013.

[11]   G. Verver *et al.*, "Performance of the Vaisala RS80A/H and RS90 Humicap sensors and the Meteolabor "Snow White" chilled-mirror hygrometer in Paramaribo, Suriname," vol. 23, no. 11, pp. 1506-1518, 2006.

[12]   T. V. J. J. o. N. G. S. Løkken and Engineering, "Comparison of hygrometers for monitoring of water vapour in natural gas," vol. 6, pp. 24-36, 2012.

[13]   Y. Sabri *et al.*, "QCM based mercury vapor sensor modified with polypyrrole supported palladium," *Sensors and Actuators B: Chemical,* vol. 160, no. 1, pp. 616-622, 2011.

[14]   Y. Yao, X. Huang, Q. Chen, Z. Zhang, and W. Ling, "High Sensitivity and High Stability QCM Humidity Sensors Based on Polydopamine Coated Cellulose Nanocrystals/Graphene Oxide Nanocomposite," *Nanomaterials,* vol. 10, no. 11, p. 2210, 2020.

[15]   Y. Zhang, K. Yu, R. Xu, D. Jiang, L. Luo, and Z. Zhu, "Quartz crystal microbalance coated with carbon nanotube films used as humidity sensor," *Sensors and Actuators A: Physical,* vol. 120, no. 1, pp. 142-146, 2005.

[16]   H. Chen, D. Zhang, Q. Pan, and X. Song, "Highly sensitive QCM humidity sensor based on MOFs-derived SnO2/chitosan hybrid film," *IEEE Sensors Journal,* 2020.

[17]   K. N. Chappanda, O. Shekhah, O. Yassine, S. P. Patole, M. Eddaoudi, and K. N. Salama, "The quest for highly sensitive QCM humidity sensors: The coating of CNT/MOF composite sensing films as case study," *Sensors and Actuators B: Chemical,* vol. 257, pp. 609-619, 2018.

[18]   Y. Yao, X. Chen, X. Li, X. Chen, and N. Li, "Investigation of the stability of QCM humidity sensor using graphene oxide as sensing films," *Sensors and Actuators B: Chemical,* vol. 191, pp. 779-783, 2014.

[19]   H. Fang *et al.*, "Cu (OH) 2 nanowires/graphene oxide composites based QCM humidity sensor with fast-response for real-time respiration monitoring," *Sensors and Actuators B: Chemical,* vol. 304, p. 127313, 2020.

[20]   K. Qi, Y. Xie, R. Wang, S.-y. Liu, and Z. Zhao, "Electroless plating Ni-P

cocatalyst decorated g-C3N4 with enhanced photocatalytic water splitting for H2 generation," *Applied Surface Science,* vol. 466, pp. 847-853, 2019.

[21] S. Leivo, J. Leppänen, and V. Oyj–Finland, "Transformer's moisture assessment with online monitoring," in *Presented at 23rd International Conference on Electricity Distribution*, 2015.

[22] Y. Zhang *et al.*, "Enhanced humidity sensing properties of SmFeO3-modified MoS2 nanocomposites based on the synergistic effect," *Sensors and Actuators B: Chemical,* vol. 272, pp. 459-467, 2018.

[23] H. Parangusan, J. Bhadra, Z. Ahmad, S. Mallick, F. Touati, and N. J. T. Al-Thani, "Capacitive type humidity sensor based on PANI decorated Cu–ZnS porous microspheres," vol. 219, p. 121361, 2020.

[24] Z. Chen and C. Lu, "Humidity sensors: a review of materials and mechanisms," *Sensor letters,* vol. 3, no. 4, pp. 274-295, 2005.

[25] M. Pan, J. Sheng, J. Liu, Z. Shi, and L. Jiu, "Design and Verification of Humidity Sensors Based on Magnesium Oxide Micro-Arc Oxidation Film Layers," *Sensors,* vol. 20, no. 6, p. 1736, 2020.

[26] T. Blank, L. Eksperiandova, and K. Belikov, "Recent trends of ceramic humidity sensors development: A review," *Sensors and Actuators B: Chemical,* vol. 228, pp. 416-442, 2016.

[27] M. Pelino, C. Cantalini, and M. Faccio, "Principles and applications of ceramic humidity sensors," *Active and passive electronic components,* vol. 16, 1994.

[28] B. Cheng, B. Tian, C. Xie, Y. Xiao, and S. Lei, "Highly sensitive humidity sensor based on amorphous Al 2 O 3 nanotubes," *Journal of Materials Chemistry,* vol. 21, no. 6, pp. 1907-1912, 2011.

[29] Z. Wang, L. Shi, F. Wu, S. Yuan, Y. Zhao, and M. Zhang, "The sol–gel template synthesis of porous TiO2 for a high performance humidity sensor," *Nanotechnology,* vol. 22, no. 27, p. 275502, 2011.

[30] S.-P. Chang *et al.*, "A ZnO nanowire-based humidity sensor," *Superlattices and Microstructures,* vol. 47, no. 6, pp. 772-778, 2010.

[31] H. U. Khan *et al.*, "The efficacy of polyvinylpyrrolidone (PVP)/CuO nanocomposite as an appropriate room temperature humidity sensing material: fabrication of highly sensitive capacitive resistive type humidity sensor," *JOURNAL OF MATERIALS SCIENCE-MATERIALS IN ELECTRONICS,* vol. 31, no. 10, pp. 7698-7707, 2020.

[32] M. I. Azmer, Q. Zafar, Z. Ahmad, and K. Sulaiman, "Humidity sensor based on electrospun MEH-PPV: PVP microstructured composite," *RSC advances,* vol. 6, no. 42, pp. 35387-35393, 2016.

[33] Q.-N. Zhao *et al.*, "A review on Ti 3 C 2 T x-based nanomaterials: synthesis and applications in gas and humidity sensors," *Rare Metals,* pp. 1-18, 2020.

[34] M. Arularasu, M. Harb, R. Vignesh, T. Rajendran, and R. Sundaram, "PVDF/ZnO hybrid nanocomposite applied as a resistive humidity sensor," *Surfaces and Interfaces,* vol. 21, p. 100780, 2020.

[35] I. Fratoddi, A. Bearzotti, I. Venditti, C. Cametti, and M. Russo, "Role of nanostructured polymers on the improvement of electrical response-based relative humidity sensors," *Sensors and Actuators B: Chemical,* vol. 225, pp. 96-108, 2016.

[36] K. H. Choi, M. Sajid, S. Aziz, and B.-S. Yang, "Wide range high speed relative humidity sensor based on PEDOT: PSS–PVA composite on an IDT printed on piezoelectric substrate," *Sensors and Actuators A: Physical,* vol. 228, pp. 40-49, 2015.

[37] Z. Duan, M. Xu, T. Li, Y. Zhang, and H. Zou, "Super-fast response humidity sensor based on La0. 7Sr0. 3MnO3 nanocrystals prepared by PVP-assisted sol-gel method," *Sensors and Actuators B: Chemical,* vol. 258, pp. 527-534, 2018.

[38] N. Agmon, "The grotthuss mechanism," *Chemical Physics Letters,* vol. 244, no. 5-6, pp. 456-462, 1995.

[39] C.-W. Lee *et al.*, "Polymeric humidity sensor using organic/inorganic hybrid polyelectrolytes," vol. 109, no. 2, pp. 315-322, 2005.

[40] M. V. Fuke, A. Vijayan, M. Kulkarni, R. Hawaldar, and R. J. T. Aiyer, "Evaluation of Co-Polyaniline nanocomposite thin films as humidity sensor," vol. 76, no. 5, pp. 1035-1040, 2008.

[41] J.-H. Kim, S.-M. Hong, B.-M. Moon, and K. J. M. t. Kim, "High-performance capacitive humidity sensor with novel electrode and polyimide layer based on MEMS technology," vol. 16, no. 12, pp. 2017-2021, 2010.

[42] Q. Lin, Y. Li, M. J. S. Yang, and A. B. Chemical, "Polyaniline nanofiber humidity sensor prepared by electrospinning," vol. 161, no. 1, pp. 967-972, 2012.

[43] Z. Zhuang, Y. Li, D. Qi, C. Zhao, H. J. S. Na, and A. B. Chemical, "Novel polymeric humidity sensors based on sulfonated poly (ether ether ketone) s: Influence of sulfonation degree on sensing properties," vol. 242, pp. 801-809, 2017.

[44] U. Lange, N. V. Roznyatovskaya, and V. M. Mirsky, "Conducting polymers in chemical sensors and arrays (invited review)," 2008.

[45] D. Khokhar, S. Jadoun, R. Arif, and S. Jabin, "Functionalization of conducting polymers and their applications in optoelectronics," *Polymer-Plastics Technology and Materials,* pp. 1-23, 2020.

[46] R. Baughman and L. Shacklette, "Application of dopant-induced structure-property changes of conducting," in *Science and Applications of Conducting Polymers, Papers from the Sixth European Industrial Workshop*, 2020: CRC Press, p. 47.

[47] M. El Rhazi, S. Majid, M. Elbasri, F. E. Salih, L. Oularbi, and K. Lafdi, "Recent progress in nanocomposites based on conducting polymer: application as electrochemical sensors," *International Nano Letters,* vol. 8, no. 2, pp. 79-99, 2018.

[48] L. Kabir, A. R. Mandal, and S. Mandal, "Humidity-sensing properties of conducting polypyrrole-silver nanocomposites," *Journal of Experimental Nanoscience,* vol. 3, no. 4, pp. 297-305, 2008.

[49] M. Matsuguchi, S. Umeda, Y. Sadaoka, and Y. Sakai, "Characterization of polymers for a capacitive-type humidity sensor based on water sorption behavior," *Sensors and Actuators B: Chemical,* vol. 49, no. 3, pp. 179-185, 1998.

[50] C. Lv *et al.*, "Recent advances in graphene-based humidity sensors," *Nanomaterials,* vol. 9, no. 3, p. 422, 2019.

[51]   D. Denton, D. Day, D. F. Priore, S. Senturia, E. Anolick, and D. Scheider, "Moisture diffusion in poltimide films in integrated circuits," *Journal of electronic materials,* vol. 14, no. 2, pp. 119-136, 1985.

[52]   M. Matsuguchi, Y. Sadaoka, Y. Nuwa, M. Shinmoto, Y. Sakai, and T. Kuroiwa, "Capacitive-Type Humidity Sensors Using Polymerized Vinyl Carboxylate," *Journal of the Electrochemical Society,* vol. 141, no. 3, p. 614, 1994.

[53]   T. Kuroiwa, T. Miyagishi, A. Ito, M. Matsuguchi, Y. Sadaoka, and Y. Sakai, "A thin-film polysulfone-based capacitive-type relative-humidity sensor," *Sensors and Actuators B: Chemical,* vol. 25, no. 1-3, pp. 692-695, 1995.

[54]   J. M. M. Pérez and C. Freyre, "A poly (ethyleneterephthalate)-based humidity sensor," *Sensors and Actuators B: Chemical,* vol. 42, no. 1, pp. 27-30, 1997.

[55]   M. Dokmeci and K. Najafi, "A high-sensitivity polyimide capacitive relative humidity sensor for monitoring anodically bonded hermetic micropackages," *Journal of Microelectromechanical Systems,* vol. 10, no. 2, pp. 197-204, 2001.

[56]   A. Ralston, M. Buncick, D. Denton, T. Boltshauser, J. Funk, and H. Baltes, "Effects of aging on polyimide: a model for dielectric behavior (of relative humidity sensors)," in *TRANSDUCERS'91: 1991 International Conference on Solid-State Sensors and Actuators. Digest of Technical Papers*, 1991: IEEE, pp. 759-763.

[57]   H. Lee, S. Lee, S. Jung, and J. Lee, "Nano-grass polyimide-based humidity sensors," *Sensors and Actuators B: Chemical,* vol. 154, no. 1, pp. 2-8, 2011.

[58]   B. V. Schmidt, "Hydrophilic Polymers," ed: Multidisciplinary Digital Publishing Institute, 2019.

[59]   C.-W. Lee, Y. Kim, S.-W. Joo, and M.-S. Gong, "Resistive humidity sensor using polyelectrolytes based on new-type mutually cross-linkable copolymers," *Sensors and Actuators B: Chemical,* vol. 88, no. 1, pp. 21-29, 2003.

[60]   T. M. Koshy, D. Gowda, S. Tom, G. Karunakar, A. Srivastava, and A. Moin, "Polymer Grafting–An Overview," *American Journal of Pharmtech Research,* vol. 6, no. 2, pp. 1-13, 2016.

[61]   L. Liang, X. Feng, J. Liu, and P. C. Rieke, "Preparation of composite-

crosslinked poly (N-isopropylacrylamide) gel layer and characteristics of reverse hydrophilic–hydrophobic surface," *Journal of applied polymer science,* vol. 72, no. 1, pp. 1-11, 1999.

[62]   Y. Li, Y. Chen, C. Zhang, T. Xue, and M. Yang, "A humidity sensor based on interpenetrating polymer network prepared from poly (dimethylaminoethyl methacrylate) and poly (glycidyl methacrylate)," *Sensors and Actuators B: Chemical,* vol. 125, no. 1, pp. 131-137, 2007.

[63]   Y. Li, M. Yang, and Y. She, "Humidity sensors using in situ synthesized sodium polystyrenesulfonate/ZnO nanocomposites," *Talanta,* vol. 62, no. 4, pp. 707-712, 2004.

[64]   M.-S. Gong, S.-W. Joo, and B.-K. Choi, "Humidity sensor using mutually reactive copolymers containing quaternary ammonium salt and reactive function," *Sensors and Actuators B: Chemical,* vol. 86, no. 1, pp. 81-87, 2002.

[65]   P.-G. Su and C.-L. Uen, "In situ copolymerization of copolymer of methyl methacrylate and [3-(methacrylamino) propyl] trimethyl ammonium chloride on an alumina substrate for humidity sensing," *Sensors and Actuators B: Chemical,* vol. 107, no. 1, pp. 317-322, 2005.

[66]   W. Geng *et al.*, "Remarkable humidity-responsive sensor based on poly (N, N-diethylaminoethyl methacrylate)-b-polystyrene block copolymers," vol. 226, pp. 471-477, 2016.

[67]   P.-G. Su, C.-L. J. S. Uen, and A. B. Chemical, "In situ copolymerization of copolymer of methyl methacrylate and [3-(methacrylamino) propyl] trimethyl ammonium chloride on an alumina substrate for humidity sensing," vol. 107, no. 1, pp. 317-322, 2005.

[68]   P.-G. Su, H.-C. Hsu, C.-Y. J. S. Liu, and A. B. Chemical, "Layer-by-layer anchoring of copolymer of methyl methacrylate and [3-(methacrylamino) propyl] trimethyl ammonium chloride to gold surface on flexible substrate for sensing humidity," vol. 178, pp. 289-295, 2013.

[69]   P. Pattananuwat, M. Tagaya, T. J. S. Kobayashi, and A. B. Chemical, "A novel highly sensitive humidity sensor based on poly (pyrrole-co-formyl pyrrole) copolymer film: AC and DC impedance analysis," vol. 209, pp. 186-193, 2015.

[70]   D. Ballantine, A. Glines, G. Adler, and D. Metz, "Graft copolymerization by

pre-irradiation technique," *Journal of Polymer Science,* vol. 34, no. 127, pp. 419-438, 1959.

[71]   Y. Sakai, Y. Sadaoka, and K. Ikeuchi, "Humidity sensors composed of grafted copolymers," *Sensors and Actuators,* vol. 9, no. 2, pp. 125-131, 1986.

[72]   K.-S. Chen *et al.*, "Novel stable humidity layers prepared by surface graft polymerization of anionic monomers mixing with phenol-formaldehyde," *Biomedical Engineering: Applications, Basis and Communications,* vol. 21, no. 06, pp. 371-374, 2009.

[73]   M. Matsuguchi, M. Shinmoto, Y. Sadaoka, T. Kuroiwa, and Y. Sakai, "Effect of cross-linking degree of PVCA film on the characteristics of capacitive-type humidity sensor," in *Proceedings of the International Solid-State Sensors and Actuators Conference-TRANSDUCERS'95*, 1995, vol. 2: IEEE, pp. 825-828.

[74]   Y. SAKAI and M. MATSUGUCHI, "Humidity sensors using chemically modified polymer thin films," *Electrochemistry,* vol. 67, no. 10, pp. 950-956, 1999.

[75]   C.-W. Lee, D.-H. Nam, Y.-S. Han, K.-C. Chung, and M.-S. Gong, "Humidity sensors fabricated with polyelectrolyte membrane using an ink-jet printing technique and their electrical properties," *Sensors and Actuators B: Chemical,* vol. 109, no. 2, pp. 334-340, 2005.

[76]   E. P. Giannelis, "Polymer-layered silicate nanocomposites: synthesis, properties and applications," 1998.

[77]   J. Zheng, R. Ozisik, and R. W. Siegel, "Disruption of self-assembly and altered mechanical behavior in polyurethane/zinc oxide nanocomposites," *Polymer,* vol. 46, no. 24, pp. 10873-10882, 2005.

[78]   H. Ragab and A. Rajeh, "Structural, thermal, optical and conductive properties of PAM/PVA polymer composite doped with Ag nanoparticles for electrochemical application," *Journal of Materials Science: Materials in Electronics,* vol. 31, no. 19, pp. 16780-16792, 2020.

[79]   S. C. J. M. S. Tjong and E. R. Reports, "Structural and mechanical properties of polymer nanocomposites," vol. 53, no. 3-4, pp. 73-197, 2006.

[80] P.-G. Su and L.-N. Huang, "Humidity sensors based on TiO2 nanoparticles/polypyrrole composite thin films," *Sensors and Actuators B: Chemical,* vol. 123, no. 1, pp. 501-507, 2007.

[81] S. Taccola *et al.*, "Characterization of free-standing PEDOT: PSS/iron oxide nanoparticle composite thin films and application as conformable humidity sensors," *ACS applied materials & interfaces,* vol. 5, no. 13, pp. 6324-6332, 2013.

[82] P.-G. Su, L.-N. J. S. Huang, and A. B. Chemical, "Humidity sensors based on TiO2 nanoparticles/polypyrrole composite thin films," vol. 123, no. 1, pp. 501-507, 2007.

[83] W. Yao, X. Chen, J. J. S. Zhang, and A. B. Chemical, "A capacitive humidity sensor based on gold–PVA core–shell nanocomposites," vol. 145, no. 1, pp. 327-333, 2010.

[84] S. Taccola *et al.*, "Characterization of free-standing PEDOT: PSS/iron oxide nanoparticle composite thin films and application as conformable humidity sensors," vol. 5, no. 13, pp. 6324-6332, 2013.

[85] D. Zhang, J. Tong, B. Xia, Q. J. S. Xue, and A. B. Chemical, "Ultrahigh performance humidity sensor based on layer-by-layer self-assembly of graphene oxide/polyelectrolyte nanocomposite film," vol. 203, pp. 263-270, 2014.

[86] G. Markovic and P. Visakh, "Polymer blends: state of art," in *Recent Developments in Polymer Macro, Micro and Nano Blends*: Elsevier, 2017, pp. 1-15.

[87] A. Marra, C. Silvestre, A. P. Kujundziski, D. Chamovska, and D. Duraccio, "Preparation and characterization of nanocomposites based on PLA and TiO2 nanoparticles functionalized with fluorocarbons," *Polymer Bulletin,* vol. 74, no. 8, pp. 3027-3041, 2017.

[88] R. Auras, B. Harte, and S. Selke, "An overview of polylactides as packaging materials," *Macromolecular bioscience,* vol. 4, no. 9, pp. 835-864, 2004.

[89] X. Wang *et al.*, "Flame retardancy and thermal degradation of intumescent flame retardant poly (lactic acid)/starch biocomposites," *Industrial & Engineering Chemistry Research,* vol. 50, no. 2, pp. 713-720, 2010.

[90]   E. Aksel and J. L. Jones, "Advances in lead-free piezoelectric materials for sensors and actuators," *Sensors,* vol. 10, no. 3, pp. 1935-1954, 2010.

[91]   Y. He *et al.*, "Humidity sensing properties of BaTiO 3 nanofiber prepared via electrospinning," *Sensors and Actuators B: Chemical,* vol. 146, no. 1, pp. 98-102, 2010.

[92]   L. Gu, D. Zhou, and J. C. Cao, "Piezoelectric Active Humidity Sensors Based on Lead-Free NaNbO3 Piezoelectric Nanofibers," *Sensors,* vol. 16, no. 6, p. 833, 2016.

[93]   J. Wang, Q. Lin, R. Zhou, B. J. S. Xu, and A. B. Chemical, "Humidity sensors based on composite material of nano-BaTiO3 and polymer RMX," vol. 81, no. 2-3, pp. 248-253, 2002.

[94]   J. Wang, B. K. Xu, S. P. Ruan, S. P. J. M. C. Wang, and physics, "Preparation and electrical properties of humidity sensing films of BaTiO3/polystrene sulfonic sodium," vol. 78, no. 3, pp. 746-750, 2003.

[95]   B. J. S. Ertug and Materials, "Electrical Conductivity and Hysteresis Characteristic of BaTiO3-Based Sensors with Polymethyl metacrylate (PMMA) Pore Former," vol. 25, no. 5, pp. 309-321, 2013.

[96]   F.-S. Tsai, S.-J. J. S. Wang, and A. B. Chemical, "Enhanced sensing performance of relative humidity sensors using laterally grown ZnO nanosheets," vol. 193, pp. 280-287, 2014.

[97]   X. Yu, X. Chen, X. Ding, X. Chen, X. Yu, and X. Zhao, "High-sensitivity and low-hysteresis humidity sensor based on hydrothermally reduced graphene oxide/nanodiamond," *Sensors and Actuators B: Chemical,* vol. 283, pp. 761-768, 2019.

[98]   J.-M. Tulliani, B. Inserra, and D. Ziegler, "Carbon-based materials for humidity sensing: a short review," *Micromachines,* vol. 10, no. 4, p. 232, 2019.

[99]   J. Dai, T. Zhang, H. Zhao, and T. Fei, "Preparation of organic-inorganic hybrid polymers and their humidity sensing properties," *Sensors Actuators B: Chem.,* vol. 242, pp. 1108-1114, 4// 2017.

[100]   M. S. Mauter and M. Elimelech, "Environmental applications of carbon-based

nanomaterials," *Environmental Science & Technology,* vol. 42, no. 16, pp. 5843-5859, 2008.

[101] D. Zhang, X. Zong, and Z. Wu, "Fabrication of tin disulfide/graphene oxide nanoflower on flexible substrate for ultrasensitive humidity sensing with ultralow hysteresis and good reversibility," *Sensors and Actuators B: Chemical,* vol. 287, pp. 398-407, 2019.

[102] Y. S. Zhao, H. Fu, A. Peng, Y. Ma, D. Xiao, and J. Yao, "Low-dimensional nanomaterials based on small organic molecules: preparation and optoelectronic properties," *Advanced Materials,* vol. 20, no. 15, pp. 2859-2876, 2008.

[103] X. Zhao, W. Gao, H. Zhang, X. Qiu, and Y. Luo, "Graphene quantum dots in biomedical applications: recent advances and future challenges," in *Handbook of Nanomaterials in Analytical Chemistry*: Elsevier, 2020, pp. 493-505.

[104] R. Aacharya and H. Chhipa, "Nanocarbon fertilizers: Implications of carbon nanomaterials in sustainable agriculture production," in *Carbon Nanomaterials for Agri-Food and Environmental Applications*: Elsevier, 2020, pp. 297-321.

[105] L. Cao *et al.*, "Carbon dots for energy conversion applications," *Journal of Applied Physics,* vol. 125, no. 22, p. 220903, 2019.

[106] H. Ouarrad, F.-Z. Ramadan, and L. Drissi, "Size engineering optoelectronic features of C, Si and CSi hybrid diamond-shaped quantum dots," *RSC Advances,* vol. 9, no. 49, pp. 28609-28617, 2019.

[107] S. Shen, B. Huang, X. Guo, and H. Wang, "A dual-responsive fluorescent sensor for Hg 2+ and thiols based on N-doped silicon quantum dots and its application in cell imaging," *Journal of Materials Chemistry B,* vol. 7, no. 44, pp. 7033-7041, 2019.

[108] H. Elmizadeh, M. Soleimani, F. Faridbod, and G. Bardajee, "Fabrication of a nanomaterial-based fluorescence sensor constructed from ligand capped CdTe quantum dots for ultrasensitive and rapid detection of silver ions in aqueous samples," *Spectrochimica Acta Part A: Molecular and Biomolecular Spectroscopy,* vol. 211, pp. 291-298, 2019.

[109] M. Bilal, E. Oh, R. Liu, J. C. Breger, I. L. Medintz, and Y. Cohen, "Bayesian Network Resource for Meta-Analysis: Cellular Toxicity of Quantum Dots," *Small,* vol. 15, no. 34, p. 1900510, 2019.

[110] J. C. Kays, A. M. Saeboe, R. Toufanian, D. E. Kurant, and A. M. Dennis, "Shell-Free Copper Indium Sulfide Quantum Dots Induce Toxicity in Vitro and in Vivo," *Nano Letters,* vol. 20, no. 3, pp. 1980-1991, 2020.

[111] M. Wu *et al.*, "Preparation of functionalized water-soluble photoluminescent carbon quantum dots from petroleum coke," *Carbon,* vol. 78, pp. 480-489, 2014.

[112] V. Ruiz, I. Fernández, P. Carrasco, G. Cabañero, H. J. Grande, and J. Herrán, "Graphene quantum dots as a novel sensing material for low-cost resistive and fast-response humidity sensors," *Sensors and Actuators B: Chemical,* vol. 218, pp. 73-77, 2015.

[113] S. Iravani and R. S. Varma, "Green synthesis, biomedical and biotechnological applications of carbon and graphene quantum dots. A review," *Environmental Chemistry Letters,* pp. 1-25, 2020.

[114] S. Lai, Y. Jin, L. Shi, R. Zhou, Y. Zhou, and D. An, "Mechanisms behind excitation-and concentration-dependent multicolor photoluminescence in graphene quantum dots," *Nanoscale,* vol. 12, no. 2, pp. 591-601, 2020.

[115] X. Yan, B. Li, X. Cui, Q. Wei, K. Tajima, and L.-s. Li, "Independent tuning of the band gap and redox potential of graphene quantum dots," *The journal of physical chemistry letters,* vol. 2, no. 10, pp. 1119-1124, 2011.

[116] C. Hu *et al.*, "One-step preparation of nitrogen-doped graphene quantum dots from oxidized debris of graphene oxide," *Journal of Materials Chemistry B,* vol. 1, no. 1, pp. 39-42, 2013.

[117] Y. Zhang, M. Park, H. Y. Kim, B. Ding, and S.-J. Park, "A facile ultrasonic-assisted fabrication of nitrogen-doped carbon dots/BiOBr up-conversion nanocomposites for visible light photocatalytic enhancements," *Scientific reports,* vol. 7, no. 1, pp. 1-12, 2017.

[118] W. Li *et al.*, "Three minute ultrarapid microwave-assisted synthesis of bright fluorescent graphene quantum dots for live cell staining and white LEDs," *ACS Applied Nano Materials,* vol. 1, no. 4, pp. 1623-1630, 2018.

[119] S. Kang *et al.*, "Pulsed laser ablation based synthetic route for nitrogen-doped graphene quantum dots using graphite flakes," *Applied Surface Science,* vol. 506, p. 144998, 2020.

[120] D. B. Shinde and V. K. Pillai, "Electrochemical preparation of luminescent graphene quantum dots from multiwalled carbon nanotubes," *Chemistry–A European Journal,* vol. 18, no. 39, pp. 12522-12528, 2012.

[121] L. Li, D. Liu, K. Wang, H. Mao, and T. You, "Quantitative detection of nitrite with N-doped graphene quantum dots decorated N-doped carbon nanofibers composite-based electrochemical sensor," *Sensors and Actuators B: Chemical,* vol. 252, pp. 17-23, 2017.

[122] A. Pourjavadi, H. Abdolmaleki, M. Doroudian, and S. H. Hosseini, "Novel synthesis route for preparation of porous nitrogen-doped carbons from lignocellulosic wastes for high performance supercapacitors," *Journal of Alloys and Compounds,* vol. 827, p. 154116, 2020.

[123] Z. Taleat, A. Khoshroo, and M. J. M. A. Mazloum-Ardakani, "Screen-printed electrodes for biosensing: a review (2008–2013)," vol. 181, no. 9-10, pp. 865-891, 2014.

[124] T. Kavc, W. Kern, M. F. Ebel, R. Svagera, and P. J. C. o. m. Pölt, "Surface modification of polyethylene by photochemical introduction of sulfonic acid groups," vol. 12, no. 4, pp. 1053-1059, 2000.

[125] B. Smitha, S. Sridhar, and A. J. J. o. M. S. Khan, "Synthesis and characterization of proton conducting polymer membranes for fuel cells," vol. 225, no. 1-2, pp. 63-76, 2003.

[126] J. Zhang, J. Lou, S. Ilias, P. Krishnamachari, and J. Yan, "Thermal properties of poly (lactic acid) fumed silica nanocomposites: experiments and molecular dynamics simulations," *Polymer,* vol. 49, no. 9, pp. 2381-2386, 2008.

[127] M. Jonoobi, J. Harun, A. P. Mathew, and K. Oksman, "Mechanical properties of cellulose nanofiber (CNF) reinforced polylactic acid (PLA) prepared by twin screw extrusion," *Composites Science and Technology,* vol. 70, no. 12, pp. 1742-1747, 2010.

[128] X. Chen and S. S. Mao, "Titanium dioxide nanomaterials: synthesis, properties, modifications, and applications," *Chemical reviews,* vol. 107, no. 7, pp. 2891-2959, 2007.

[129] Y.-B. Luo, W.-D. Li, X.-L. Wang, D.-Y. Xu, and Y.-Z. Wang, "Preparation and properties of nanocomposites based on poly (lactic acid) and functionalized TiO

2," *Acta Materialia,* vol. 57, no. 11, pp. 3182-3191, 2009.

[130]   H. Zhang *et al.*, "Preparation, characterization and properties of PLA/TiO 2 nanocomposites based on a novel vane extruder," *RSC Advances,* vol. 5, no. 6, pp. 4639-4647, 2015.

[131]   A. Marra, C. Silvestre, A. P. Kujundziski, D. Chamovska, and D. Duraccio, "Preparation and characterization of nanocomposites based on PLA and TiO2 nanoparticles functionalized with fluorocarbons," *Polymer Bulletin,* pp. 1-15.

[132]   N. Nakayama and T. Hayashi, "Preparation and characterization of poly (L-lactic acid)/TiO2 nanoparticle nanocomposite films with high transparency and efficient photodegradability," *Polymer degradation and stability,* vol. 92, no. 7, pp. 1255-1264, 2007.

[133]   Y. Li and X. S. Sun, "Preparation and characterization of polymer− inorganic nanocomposites by in situ melt polycondensation of l-lactic acid and surface-hydroxylated MgO," *Biomacromolecules,* vol. 11, no. 7, pp. 1847-1855, 2010.

[134]   K. Thamaphat, P. Limsuwan, and B. Ngotawor
nchai, "Phase characterization of TiO2 powder by XRD and TEM," *Kasetsart J.(Nat. Sci.),* vol. 42, no. 5, pp. 357-361, 2008.

[135]   F. Aziz *et al.*, "Influence of humidity conditions on the capacitive and resistive response of an Al/VOPc/Pt co-planar humidity sensor," *Measurement Science and Technology,* vol. 23, no. 1, p. 014001, 2011.

[136]   L. Y. Yu, H. M. Shen, and Z. L. J. J. o. a. p. s. Xu, "PVDF–TiO2 composite hollow fiber ultrafiltration membranes prepared by TiO2 sol–gel method and blending method," vol. 113, no. 3, pp. 1763-1772, 2009.

[137]   T. Lei *et al.*, "Spectroscopic evidence for a high fraction of ferroelectric phase induced in electrospun polyvinylidene fluoride fibers," vol. 3, no. 47, pp. 24952-24958, 2013.

[138]   A. M. Stephan, K. S. Nahm, M. A. Kulandainathan, G. Ravi, and J. J. E. P. J. Wilson, "Poly (vinylidene fluoride-hexafluoropropylene)(PVdF-HFP) based composite electrolytes for lithium batteries," vol. 42, no. 8, pp. 1728-1734, 2006.

[139] M. Ghadiry, M. Gholami, C. Lai, H. Ahmad, and W. J. P. o. Chong, "Ultra-sensitive humidity sensor based on optical properties of graphene oxide and nano-anatase TiO2," vol. 11, no. 4, p. e0153949, 2016.

[140] T. Zhou *et al.*, "Improving dielectric properties of BaTiO3/ferroelectric polymer composites by employing surface hydroxylated BaTiO3 nanoparticles," vol. 3, no. 7, pp. 2184-2188, 2011.

[141] C. Chanmal and J. J. E. P. L. Jog, "Dielectric relaxations in PVDF/BaTiO3 nanocomposites," vol. 2, no. 4, pp. 294-301, 2008.

[142] S. Mallick, Z. Ahmad, F. Touati, J. Bhadra, R. Shakoor, and N. J. C. I. Al-Thani, "PLA-TiO 2 nanocomposites: Thermal, morphological, structural, and humidity sensing properties," 2018.

[143] S. Thirumalai, B. P. J. J. o. M. P. Shanmugavel, and E. Energy, "Microwave assisted synthesis and characterization of barium titanate nanoparticles for multi layered ceramic capacitor applications," vol. 45, no. 3, pp. 121-127, 2011.

[144] I. Y. Abdullah, M. Yahaya, M. H. H. Jumali, and H. M. Shanshool, "Effect of annealing process on the phase formation in poly (vinylidene fluoride) thin films," in *AIP Conference Proceedings*, 2014, vol. 1614, no. 1: AIP, pp. 147-151.

[145] B. G. Soares, M. E. Leyva, G. M. Barra, and D. J. E. P. J. Khastgir, "Dielectric behavior of polyaniline synthesized by different techniques," vol. 42, no. 3, pp. 676-686, 2006.

[146] Y. Feng *et al.*, "Enhanced dielectric properties of PVDF-HFP/BaTiO 3-nanowire composites induced by interfacial polarization and wire-shape," vol. 3, no. 6, pp. 1250-1260, 2015.

[147] P. Patel, T. R. Hull, R. W. McCabe, D. Flath, J. Grasmeder, and M. Percy, "Mechanism of thermal decomposition of poly (ether ether ketone)(PEEK) from a review of decomposition studies," *Polymer Degradation and Stability,* vol. 95, no. 5, pp. 709-718, 2010.

[148] A. Fazal and A. Al-Ahmed, "Nanomaterial-incorporated sulfonated poly (ether ether ketone)(SPEEK) based proton-conducting membranes: properties and applications," in *Advanced Nanomaterials for Membrane Synthesis and its Applications*: Elsevier, 2019, pp. 227-252.

[149] R. S. Yee, K. Zhang, and B. P. Ladewig, "The effects of sulfonated poly (ether ether ketone) ion exchange preparation conditions on membrane properties," *Membranes,* vol. 3, no. 3, pp. 182-195, 2013.

[150] N. Carretta, V. Tricoli, and F. J. J. o. M. S. Picchioni, "Ionomeric membranes based on partially sulfonated poly (styrene): synthesis, proton conduction and methanol permeation," vol. 166, no. 2, pp. 189-197, 2000.

[151] C. Rubinger, C. Martins, M.-A. De Paoli, R. J. S. Rubinger, and A. B. Chemical, "Sulfonated polystyrene polymer humidity sensor: synthesis and characterization," vol. 123, no. 1, pp. 42-49, 2007.

[152] W. Goepel, T. A. Jones, M. Kleitz, I. Lundström, and T. Seiyama, *Sensors, chemical and biochemical sensors*. John Wiley & Sons, 2008.

[153] H. Farahani, R. Wagiran, and M. N. Hamidon, "Humidity sensors principle, mechanism, and fabrication technologies: a comprehensive review," *Sensors,* vol. 14, no. 5, pp. 7881-7939, 2014.

[154] G. Dönmez and H. J. I. J. Deligöz, "A comparative study on sulfonated PEEK and PVDF blend membranes for direct methanol fuel cells," vol. 2, no. 2, p. 11, 2015.

[155] D. Qi, C. Zhao, Z. Zhuang, G. Li, and H. J. E. A. Na, "Novel humidity sensitive materials derived from naphthalene-based poly (arylene ether ketone) containing sulfobutyl pendant groups," vol. 197, pp. 39-49, 2016.

[156] R. Holze and J. Stejskal, "Recent trends and progress in research into structure and properties of polyaniline and polypyrrole—Topical Issue," *Chemical Papers,* vol. 67, no. 8, pp. 769-770, 2013.

[157] R. Turcu *et al.*, "New polypyrrole-multiwall carbon nanotubes hybrid materials," vol. 8, no. 2, pp. 643-647, 2006.

[158] R. Qi *et al.*, "Humidity sensors based on MCM-41/polypyrrole hybrid film via in-situ polymerization," *Sensors and Actuators B: Chemical,* vol. 277, pp. 584-590, 2018.

[159] E. Joussein, S. Petit, J. Churchman, B. Theng, D. Righi, and B. Delvaux, "Halloysite clay minerals–a review," ed: De Gruyter, 2005.

[160] P. Yuan, D. Tan, and F. Annabi-Bergaya, "Properties and applications of halloysite nanotubes: recent research advances and future prospects," *Applied Clay Science,* vol. 112, pp. 75-93, 2015.

[161] E. S. Goda, M. Gab-Allah, B. S. Singu, and K. R. J. M. J. Yoon, "Halloysite nanotubes based electrochemical sensors: A review," 2019.

[162] M. Ghanbari, D. Emadzadeh, W. Lau, T. Matsuura, M. Davoody, and A. J. D. Ismail, "Super hydrophilic TiO2/HNT nanocomposites as a new approach for fabrication of high performance thin film nanocomposite membranes for FO application," vol. 371, pp. 104-114, 2015.

[163] M. Liu, B. Guo, M. Du, and D. J. P. j. Jia, "The role of interactions between halloysite nanotubes and 2, 2′-(1, 2-ethenediyldi-4, 1-phenylene) bisbenzoxazole in halloysite reinforced polypropylene composites," vol. 40, no. 11, pp. 1087-1093, 2008.

[164] L. Zhang, T. Wang, and P. J. A. S. S. Liu, "Polyaniline-coated halloysite nanotubes via in-situ chemical polymerization," vol. 255, no. 5, pp. 2091-2097, 2008.

[165] K. Jlassi, M. Benna-Zayani, M. M. Chehimi, and Y. Yagci, "Efficient photoinduced In situ preparation of clay/poly (glycidyl methacrylate) nanocomposites using hydrogen-donor silane," *Journal of Polymer Science Part A: Polymer Chemistry,* vol. 53, no. 6, pp. 800-808, 2015.

[166] S. Zuo *et al.*, "Preparation of polyaniline–polypyrrole binary composite nanotube using halloysite as hard-template and its characterization," *Chemical engineering journal,* vol. 228, pp. 1092-1097, 2013.

[167] C. Yang, P. Liu, and Y. Zhao, "Preparation and characterization of coaxial halloysite/polypyrrole tubular nanocomposites for electrochemical energy storage," *Electrochimica Acta,* vol. 55, no. 22, pp. 6857-6864, 2010.

[168] C. Xiao *et al.*, "Thickness and Structure of Adsorbed Water Layer and Effects on Adhesion and Friction at Nanoasperity Contact," vol. 3, no. 3, p. 55, 2019.

[169] S. K. Mahadeva, S. Yun, and J. Kim, "Flexible humidity and temperature sensor based on cellulose–polypyrrole nanocomposite," *Sensors and Actuators A: Physical,* vol. 165, no. 2, pp. 194-199, 2011.

[170] P.-G. Su and C.-P. Wang, "Flexible humidity sensor based on TiO2 nanoparticles-polypyrrole-poly-[3-(methacrylamino) propyl] trimethyl ammonium chloride composite materials," *Sensors and Actuators B: Chemical,* vol. 129, no. 2, pp. 538-543, 2008.

[171] R. Najjar and S. Nematdoust, "A resistive-type humidity sensor based on polypyrrole and ZnO nanoparticles: hybrid polymers vis-a-vis nanocomposites," *RSC advances,* vol. 6, no. 113, pp. 112129-112139, 2016.

[172] Y. Wu *et al.*, "All-Carbon based flexible humidity sensor," *Journal of Nanoscience and Nanotechnology,* vol. 19, no. 8, pp. 5310-5316, 2019.

[173] N. A. A. Anas, Y. W. Fen, N. A. S. Omar, W. M. E. M. M. Daniyal, N. S. M. Ramdzan, and S. Saleviter, "Development of graphene quantum dots-based optical sensor for toxic metal ion detection," *Sensors,* vol. 19, no. 18, p. 3850, 2019.

[174] P. Tian, L. Tang, K. Teng, and S. Lau, "Graphene quantum dots from chemistry to applications," *Materials today chemistry,* vol. 10, pp. 221-258, 2018.

[175] Z.-M. Li, T. Pi, Y.-P. Sheng, and X.-J. Zheng, "Fluorescence Detection of Glutathione Using N-Doped Graphene Quantum Dots–MnO2 Nanoarchitecture," *Journal of Applied Spectroscopy,* pp. 1-8, 2020.

[176] K. Jlassi, K. Eid, M. H. Sliem, A. M. Abdullah, M. M. Chehimi, and I. Krupa, "Rational synthesis, characterization, and application of environmentally friendly (polymer–carbon dot) hybrid composite film for fast and efficient UV-assisted Cd 2+ removal from water," *Environmental Sciences Europe,* vol. 32, no. 1, pp. 1-13, 2020.

[177] J. Jiang, Y. He, S. Li, and H. Cui, "Amino acids as the source for producing carbon nanodots: microwave assisted one-step synthesis, intrinsic photoluminescence property and intense chemiluminescence enhancement," *Chemical communications,* vol. 48, no. 77, pp. 9634-9636, 2012.

[178] L. Guo *et al.*, "Two-beam-laser interference mediated reduction, patterning and nanostructuring of graphene oxide for the production of a flexible humidity sensing device," *Carbon,* vol. 50, no. 4, pp. 1667-1673, 2012.

[179] S. Mallick, Z. Ahmad, F. Touati, J. Bhadra, R. Shakoor, and N. J. C. I. Al-Thani,

"PLA-TiO2 nanocomposites: Thermal, morphological, structural, and humidity sensing properties," vol. 44, no. 14, pp. 16507-16513, 2018.

[180] S. Mallick, Z. Ahmad, F. Touati, R. J. S. Shakoor, and A. B. Chemical, "Improvement of humidity sensing properties of PVDF-TiO2 nanocomposite films using acetone etching," vol. 288, pp. 408-413, 2019.